IDA

INSTITUTE FOR DEFENSE ANALYSES

Evaluation of the Multi-Sensor Towed Array Detection System (MTADS) Performance at the Marine Corps Air Ground Combat Center (MCAGCC), Twentynine Palms, California

Thomas W. Altshuler
Marc Mander

September 1998

Approved for public release;
distribution unlimited.

IDA Document D-2161
Log: H 98-001681

20000712 044

DTIC QUALITY INSPECTED 4

This work was conducted under contract DASW01 94 C 0054, Task T-AM2-1528, for the Deputy Under Secretary of Defense (Environmental Security). The publication of this IDA document does not indicate endorsement by the Department of Defense, nor should the contents be construed as reflecting the official position of that Agency.

© 1998, 2000 Institute for Defense Analyses, 1801 N. Beauregard Street, Alexandria, Virginia 22311-1772 • (703) 845-2000.

This material may be reproduced by or for the U.S. Government pursuant to the copyright license under the clause at DFARS 252.227-7013 (10/88).

INSTITUTE FOR DEFENSE ANALYSES

IDA Document D-2161

Evaluation of the Multi-Sensor Towed Array Detection System (MTADS) Performance at the Marine Corps Air Ground Combat Center (MCAGCC), Twentynine Palms, California

Thomas W. Altshuler
Marc Mander

PREFACE

This paper was prepared for the Deputy Under Secretary of Defense for Environmental Security under a task entitled "Assessment of Traditional and Emerging Approaches to the Detection and Identification of Surface and Buried Unexploded Ordnance."

We greatly appreciate the comments and assistance we received from Dr. Jim McDonald and Dr. Herbert Nelson of the Naval Research Laboratory, and from Dr. Thomas Bell, Dr. Bruce Barrow, and Dr. Nagi Khadr of AETC, Inc. Their comments and suggestions greatly improved the quality of this paper.

Preceding Page Is Blank

CONTENTS

TABLES

FIGURES

EXECUTIVE SUMMARY

INTRODUCTION

During the last 3 years, the Environmental Security Technology Certification Program (ESTCP) has sponsored the development of an advanced vehicular unexploded ordnance (UXO) detection system at the Naval Research Laboratory (NRL) called the Multi-sensor Towed Array Detection System (*MTADS*). The *MTADS* can be configured with one of three sensor arrays: magnetometer, magnetic gradiometer, and electromagnetic induction (EMI).

In December 1996, on the Magnetic Test Range (MTR) at the Marine Corps Air Ground Combat Center (MCAGCC), Twentynine Palms, California, the *MTADS* underwent its first semi-blind field test. During the test, all three sensors were used. The *MTADS* was driven over a test site in which ordnance had been emplaced. After completing the data acquisition and determining the location of potential ordnance, IDA performed an assessment to determine overall detection performance and unique characteristics of the *MTADS*. We assessed both the results of the IDA target-picking analyses and the results of a separate analysis performed by NRL. This analysis provides a comprehensive look at the overall capabilities of the *MTADS* as a tool for UXO detection and location.

This paper gives the results of IDA's and NRL's analysis and provides a performance analysis of each sensor array.

RESULTS

Detection Rate

In general, the detection rate for the magnetometer and magnetic gradiometer systems was very good (see Table ES-1 and Figure ES-1), considering the difficult magnetic background present at the MTR. The robustness of the *MTADS*-Data Acquisition System (DAS) improved these systems' performance. For the smaller, near-surface mortars, however, the magnetometer and magnetic gradiometer exhibited reduced detection performance. Also, the magnetometer did not detect many of the large, deeply

Table ES-1. Detection and False-Alarm Performance of *MTADS* from IDA and NRL Analysis with a 1-m R_{crit}

Sensor	IDA P_d	IDA *FAR* (m^{-2})	IDA P_{fa}	NRL P_d	NRL *FAR* (m^{-2})	NRL P_{fa}
Magnetometer (Full Data Set)	0.726	2.0×10^{-2}	6.5×10^{-2}	0.823	7.4×10^{-3}	2.4×10^{-2}
Magnetometer (Confidence Level 2)	0.677	7.4×10^{-3}	2.4×10^{-2}	0.790	4.9×10^{-3}	1.5×10^{-2}
Magnetic Gradiometer (Full Data Set)	0.710	8.3×10^{-3}	2.6×10^{-2}	0.774	7.7×10^{-3}	2.4×10^{-2}
Magnetic Gradiometer (Confidence Level 2)	0.532	2.6×10^{-3}	8.1×10^{-3}	0.726	4.9×10^{-3}	1.6×10^{-2}
EMI	0.823	9.5×10^{-3}	2.0×10^{-2}	0.839	4.8×10^{-3}	1.5×10^{-2}

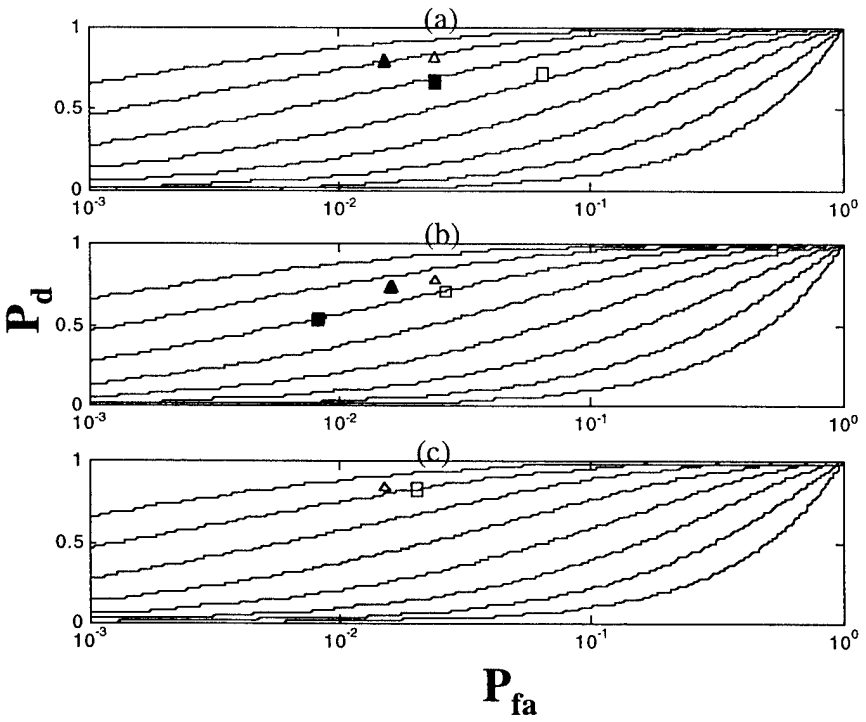

Figure ES-1. P_d versus P_{fa} for NRL Processing (Triangles) and IDA Processing (Squares). The open marks are for the full declaration set. The solid symbols result from implementing the appropriate discrimination algorithms for each data set to a confidence level of 2. (a) Magnetometer. (b) Magnetic Gradiometer. (c) EMI.

buried bombs. These items probably were missed because their spatially broad signatures were difficult to analyze using the *MTADS*-DAS, given the magnetic geological clutter at the MTR.

The detection rate for the EMI was better than that of the magnetometer or the magnetic gradiometer. The EMI system detected all the smaller near-surface ordnance, missing only the deepest ordnance. The EMI achieved this level of performance because of good location accuracy, a result of using the real-time kinematic-differential global positioning system (RTK–DGPS) as a navigation system.

Location Accuracy

All sensor modalities exhibited excellent location accuracy (see Table ES-2). Both the magnetometer and the EMI had a mean location accuracy better than 30 cm. Analysis of the magnetometer and magnetic gradiometer data showed excellent depth estimations. The EMI system (including the EMI analysis portion of the *MTADS*-DAS), however, systematically underestimated the ordnance depth.

Table ES-2. Detection Location Error and Depth Error for 1-m Critical Radius[+]

Sensor	Radial		Depth		Magnitude Depth	
	Mean Error (m)	Standard Deviation (m)	Mean Error (m)	Standard Deviation (m)	Mean Error (m)	Standard Deviation (m)
Magnetometer	0.28	0.24	0.10	0.39	0.26	0.31
Magnetic Gradiometer	0.37	0.26	0.09	0.66	0.28	0.61
EMI	0.27	0.16	–0.19	0.52	0.37	0.41

[+] Data is determined from the anomalies chosen by NRL.

False-Alarm Rate

We used the relative inclination of the magnetic dipole moment of the anomalies (calculated using the *MTADS*-DAS) as a discriminant on the magnetic data, resulting in greater than 30-percent reduction (for the IDA targets picked) in the number of false alarms for both the magnetometer (see Figure ES-2) and the magnetic gradiometer data. This technique also resulted in a small reduction of the number of detections. Because the quality of the fit magnetic moment data was poor, the magnetic gradiometer did not exhibit as large a performance increase using this technique as the magnetometer.

Conclusions

Overall, the *MTADS* exhibited excellent performance for detection of buried UXO. In addition, the quality of the data collected by the *MTADS* permits the development and implementation of advanced descrimination algorithms to help mitigate the false-alarm problem that plagues most detections systems.

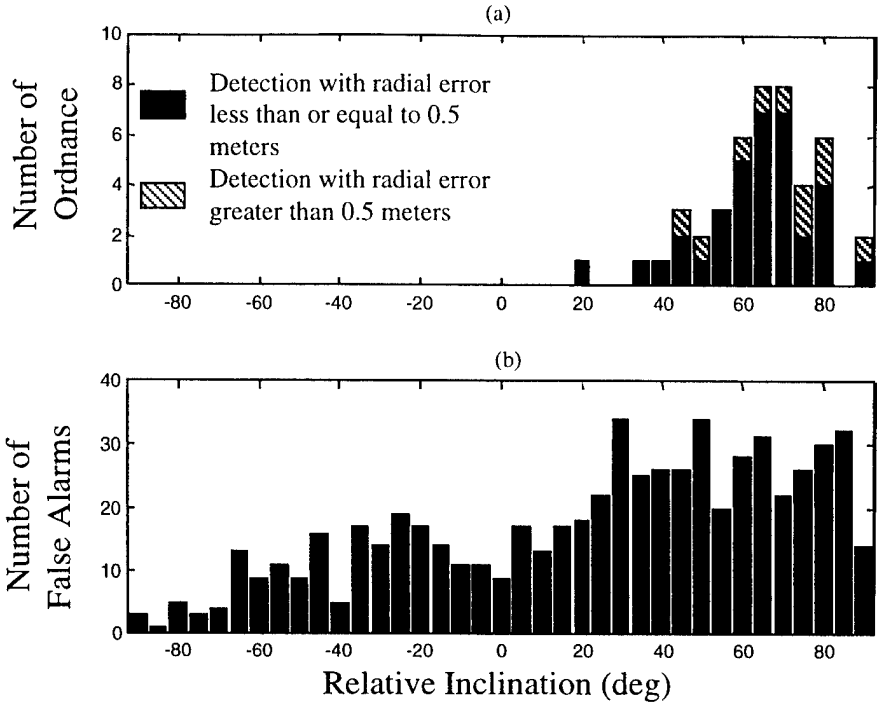

Figure ES-2. Distribution of Magnetic Moments Relative to the Geomagnetic Field as Measured by the Magnetometer. Relative inclination of 90 deg is aligned with the geomagnetic field. Relative inclination of 0 deg is orthogonal to geomagnetic field. (a) Ordnance. (b) False alarms.

1.0 INTRODUCTION

During the last 3 years the Environmental Security Technology Certification Program (ESTCP) has sponsored the development of an advanced vehicular unexploded ordnance detection (UXO) system at the Naval Research Laboratory (NRL). This vehicle, the Multi-sensor Towed Array Detection System (*MTADS*), underwent its first semi-blind field test at the Marine Corps Air Ground Combat Center (MCAGCC), Twentynine Palms, California, in December 1996. The test was conducted at the NRL Magnetic Test Range (MTR) located within the confines of the MCAGCC. The Institute for Defense Analyses (IDA) used data acquired during that semi-blind test to locate the emplaced ordnance (before release of the emplaced ordnance baseline information), i.e., to pick targets.

After completing the data acquisition and determining the location of potential ordnance, IDA performed an assessment to determine overall detection performance and unique characteristics of the *MTADS*. We assessed both the results of the IDA target-picking analyses and the results of a separate analysis performed by NRL. In this document, the focus is on the analysis tool, but since the ability to perform good analysis is dependent on the quality of data, we will also comment on the strengths and weaknesses of the *MTADS* platform.

1.1 THE *MTADS*

The *MTADS* consists of a low-magnetic tow vehicle and two carts which carry either magnetometer/magnetic gradiometer arrays or an electromagnetic induction (EMI) array. The *MTADS* is designed to minimize the noise and signal bias caused by the tow vehicle and the cart, while providing a capable and versatile detection system. Extensive development has focused on the quality of the test data, with navigation being a paramount issue. The vehicle and sensor position are determined using a real-time kinematic differential global position system (RTK-DGPS). The RTK-DGPS has been integrated with great care to ensure that all sensor time stamps are accurate and synchronized with the RTK-DGPS. The result is a location accuracy of approximately 5 cm. This high level of location accuracy provides a unique capability to co-register data collected at different times, with different sensors or sensor configurations, over the same survey site.

Software tools have been developed to provide a dynamic data acquisition system (*MTADS*-DAQ); also developed is a data analysis tool called the *MTADS* data analysis system (*MTADS*-DAS). The *MTADS*-DAS permits the user to visually process both magnetostatic and EMI data collected with the *MTADS*-DAQ. The user can preprocess any of the raw data to deal with loss of good signal from the RTK-DGPS. In addition, the *MTADS*-DAS provides a series of tool boxes that permit the user to hand pick anomalies[1] within the sensor data and determine a list of features or parameters associated with that anomaly. Those parameters provide a basis for relocation and remediation of all suspected UXO. The parameter set is dependent on the sensor being towed. For the magnetometer and magnetic gradiometer the parameter set includes magnitude of the fit magnetic moment, inclination and declination of the fit magnetic moment, depth, northing coordinate, easting coordinate, and goodness of fit (GoF).[2] For the EMI system the set includes depth, northing coordinate, easting coordinate, ferrous and nonferrous size, and GoF. Along with detection performance (this includes both detection and false-alarm rates), the fitted parameters for each declaration are analyzed.

The next step in developing a robust UXO detection system immune to the staggering false-alarm rates (*FAR*) that currently plague the UXO detection and remediation process is to implement a discrimination tool. This tool lets the user separate potentially hazardous objects—the UXO—from a large set of the naturally occurring and anthropic clutter. In this report, IDA discusses the piece of a discrimination tool under development that attempts to reduce false alarms caused by magnetic clutter (Nelson et al., 1998).

1.2 THE MCAGCC FIELD TEST

During the first 2 weeks in December 1996, an NRL team surveyed the MTR at the MCAGCC. The MTR contains 70 emplaced inert ordnance items ranging from 60-mm mortars to 2,000-lb bombs. Emplaced approximately 10 years ago, the ordnance has been used by NRL for previous UXO sensor system development. NRL has full knowledge of the original location of all emplaced items. Since this site is in an area that sees both dismounted and vehicle activity, there is the potential that some near-surface

---

1 A more recent version of the *MTADS*-DAS has a rudimentary automatic target-picking feature.

2 A measure of size (or radius of a sphere of equivalent volume) is also provided, but this is directly proportional to the fit magnetic moment magnitude.

ordnance has shifted slightly. There is no indication from the test results that any ordnance has been removed.

The site exhibits a high level of both geological and anthropic clutter. The Marines have littered the site with a broad range of waste, including spent cartridges, cans, and communication wire. Although the presence of this material complicates the detection process, it reflects real-world conditions and therefore provides a good test of the *MTADS*. The magnetic geological clutter provides a more difficult environment in which to detect UXO using the magnetometer, but it does not prevent the use of the sensor.

Additional small ordnance and rebar markers were emplaced during the test along the MTR perimeter to assess the minimum detection performance and act as fiducials, respectively. This document does not use this data and removes both the emplaced items from the baseline and any target declarations associated with these emplaced items.

1.3 TEST DATA

Three sets of test data were collected during the 2 weeks:

- Magnetic data—taken using eight total field magnetometers in a linear array with 0.25-cm spacing between magnetometers and a nominal ground-to-sensor height of 0.25 m.
- Magnetic gradiometric data—taken using eight total field magnetometers configured as four vertical magnetic gradiometers. Each magnetic gradiometer has a pair of magnetometers with 0.5-m vertical separation. The magnetic gradiometers are separated linearly by 0.5 m. The lower magnetometer in each magnetic gradiometer has a nominal distance above ground of 0.25 m.
- EMI data—taken using three modified Geonics, Ltd., EM61s nested in a 2-m linear array.

Once collected, this data was preprocessed by a member of the NRL team[3] to remove any navigational errors caused by loss of RTK-DGPS. This preprocessed data, along with the *MTADS*-DAS, was then provided to IDA for analysis. IDA used the *MTADS*-DAS to pick suspected ordnance and determine the characteristics of each

---

[3] The preprocessing was done by a subcontractor to NRL. This subcontractor, AETC, Inc., also developed and wrote the *MTADS*-DAS.

anomaly. In addition, NRL also analyzed the data and provided IDA a list of suspected ordnance items.[4]

Upon completion of the target-picking analysis of the preprocessed data and delivery of the NRL list of suspected ordnance, IDA was provided a full list of emplaced ordnance. Using this baseline knowledge, an in-depth analysis of the performance of *MTADS* at the MTR was completed. This analysis appears later in this document.

Chapter 2 provides a description of the picking process and processing used by IDA. Chapter 3 presents analyses of the detection performance for the list of target declarations picked by IDA for each of the three sensor types. Chapter 4 gives a similar assessment of detection performance for the NRL list of target declarations and compares this to the IDA targets chosen. The overall assessment is summarized in Chapter 5. In addition, an appendix provides a list of expected magnetic signatures for each of the emplaced ordnance items in the ground using the prolate spheroidal model employed by IDA (Altshuler, 1996).

---

[4] This is not a true blind test for NRL because the same personnel were responsible for the original emplacement of the ordnance. But it is apparent that an accurate attempt was made to analyze the sensor data without employing the knowledge of the baseline.

2.0 IDA TARGET-PICKING AND MAGNETIC-MOMENT ANALYSES

NRL provided IDA a full copy of the *MTADS*-DAS and the three principal data sets collected at the MTR located at the MCAGCC at Twentynine Palms. The three data sets—magnetometer, magnetic gradiometer, and EMI—had been preprocessed by AETC, Inc. (a subcontractor and member of the *MTADS* team) to remove or correct bad location information caused by loss of RTK-DGPS signal. The post-processed data was then ported to a Silicon Graphics workstation for analysis by IDA. During the initial target-picking phase, IDA had no knowledge of the baseline of targets emplaced at the MTR. Thus, the target-picking process was blind.

Since the version of the *MTADS*-DAS used for this analysis did not contain an automatic anomaly-picking feature, anomalies were selected manually by the analyst. Once a final list of potential targets was generated, IDA passed the list to NRL for assessment. At that time, NRL provided IDA with the baseline of targets emplaced at the MTR and NRL's own list of targets chosen using the *MTADS*-DAS. Using the baseline provided by NRL, IDA performed an extensive analysis of the targets chosen by each analysis team from each of the data sets. This analysis appears in Chapters 3 and 4 of this document. This chapter describes the process used by IDA to pick anomalies from the data sets and generate its list of potential ordnance.

2.1 TARGET-PICKING PROCESS

Each data set generated during the test of *MTADS* at the MTR was processed independently. For all data, the site was divided using 20-m × 20-m grid cells to simplify analysis. Point sensor data, rather than interpolated data, was viewed. To ensure that knowledge gained during the target-picking phase for one sensor was not applied during the target-picking phase of a second sensor, the data sets were divided into two groups: passive magnetic (magnetometry and magnetic gradiometry) and EMI, and a different analyst was responsible for picking the targets from each group. The picking processes used for the three data sets are described below.

2.1.1 Magnetometer Data

The magnetometer data set was processed first. Using two different threshold levels, a total of 676 anomalies were chosen. The site map was completely analyzed at the first threshold, set at 100 γ above or below the average background. Any compact feature in the image of the measured magnetic field that exceeded the threshold was chosen for fitting using the *MTADS*-DAS dipole-fitting routine. The process consisted of defining a box surrounding the anomaly to be processed, then using the magnetic-dipole-fitting routine to generate a set of fit parameters from the data within the boxed region. At the 100-γ threshold, 357 anomalies were chosen. Once the data was recorded, a lower threshold—30 γ above or below the average background—was used, and 319 additional anomalies were chosen. These thresholds were not stringent because the analyst used a color map of the magnetic field to identify potential anomalies and segment the image. Thus, it is possible that anomalies with peak values slightly below a threshold were chosen. Also note that both positive and negative threshold exceedences were chosen. If the positive and negative exceedences were spatially close, they were fit as a single segmented anomaly. Other than using a very rough shape filter (to eliminate large spatially extended features) and the threshold, no attempt was made to discriminate during the picking phase.

Once the anomaly was chosen, a magnetic-dipole-fitting routine was used to extract the anomaly features:

- location (northing and easting);
- depth;
- ferrous size, given as the radius of a solid sphere that would yield the same size anomaly;
- magnitude of the dipole moment;
- inclination and declination of the magnetic dipole moment; and
- GoF of the dipole model used to generate the other fitting parameters.

The *MTADS*-DAS permits the user to eliminate small sections from the region chosen for analysis and detrend the data to optimize the GoF. Both these features were used and the best GoF chosen as the final fit. Note that no attempt was made at either threshold to adjust the extent of the region chosen to find an optimum fit; however, at the lower threshold (±30 γ) if it was apparent to the analyst that a section of the anomaly was outside the fitting region, the region was redrawn and refit. The new fit parameters were

then optimized and used to provide a second fit for the anomaly. Both fits were analyzed and the best was chosen in post-processing.

As discussed in Chapter 3, using a single fit region at a given threshold resulted in a number of missed targets because of the large location errors, which suggests that the fit region should be adjusted during analysis to optimize the fit. For manual target picking, optimizing the fit means that multiple fits should be recorded and the final fit parameters chosen from this group.

2.1.2 Magnetic Gradiometer Data

The magnetic gradiometer data was processed in the same manner as the magnetometer data, except that three thresholds were used (±50 γ, ±30 γ, and ±15 γ). Using these three thresholds, a total of 302 anomalies were identified, with 205 chosen at ±50 γ, 75 chosen at ±30 γ, and 22 chosen at ±15 γ. This list of anomalies was used to analyze the performance of the magnetic gradiometer.

2.1.3 EMI Data

The first criterion for ranking targets was magnitude of return, so it was decided that the initial target list should include only the most intense returns. The false-color scale and threshold were varied several times to find a combination expected to produce approximately 200 target nominations. Random grid cells were sampled at each step to estimate the total number of targets that would be selected. From this procedure, the false-color scale was set at 5 to 100 mV. To be included in the target nomination list, a return was required to exhibit 80-mV color. In addition, a few other peaks that were weaker (as low as ~40 mV) but very large spatially were included in the initial threshold because it was discovered that these returns generally resulted from large, deep items. This initial screening resulted in 174 target nominations. After the entire image had been processed, the procedure was repeated using the 5–30 mV false-color scale, and 78 additional targets were added to the initial list.

Each anomaly nominated was then fit using an EMI fit routine (McDonald et al., 1997). The procedure for defining the region to fit and the fitting process are similar to those used for the magnetometer and magnetic gradiometer. The following fit parameters were determined for each anomaly:

- location (northing and easting);
- depth;

- ferrous and nonferrous size, given as the radius of a solid sphere that would yield the same size anomaly; and
- GoF of the dipole model used to generate the other fitting parameters.

2.2 MAGNETIC DIPOLE MOMENT FALSE-ALARM MITIGATION TECHNIQUE

After the generation of the target nominations for each of the data sets, the magnetic and magnetic gradiometer data were analyzed using a discrimination algorithm developed at IDA (Nelson et al., 1998). This discrimination algorithm applies a confidence rating determined by the inclination of the fitted magnetic moment relative to the geomagnetic field. The final confidence for each anomaly was also influenced by the GoF and whether the fitted depth of the anomaly was zero. Although both the depth and the GoF are reasonable and common tools for discrimination, the use of the magnetic moment direction is novel. An in-depth description of the theory underlying the magnetic moment direction discrimination will be published by IDA.

2.2.1 The Magnetic Signature of Ordnance

Previous work (Altshuler, 1996) has demonstrated that the induced magnetization of the ordnance item is dependent on the size, shape, and orientation relative to the geomagnetic field. To a lesser extent, the casing thickness also contributes to the signature. In most cases, the magnetic signature of ordnance is dominated by the dipole term, which is proportional to x^{-3}, where x is the distance from the center of volume of the ordnance to the magnetometer. Higher moments contribute to the measured signature when the stand-off distance of the sensor is approximately the length of the ordnance item. In the dipole approximation, the ith component of the induced magnetization, M_i, of the ordnance item must be calculated using the ith component of the magnetization of the prolate spheroid:

$$M_i = \frac{(\mu-1)H_{gi}}{4\pi+(\mu-1)N_i} \quad ,$$

where H_g is the geomagnetic field strength and N_i is the ith component of the demagnetization factor. In truth, ordnance is not a perfect prolate spheroid but is more generally a body of revolution. Still, the extent of the asymmetry through the central plane of the ordnance item is small, and thus the quadrupole moment resulting from this asymmetry should also be small. So the assumption that the signature is accurately described by only the dipole term is valid.

Because ordnance casings are made of ferromagnetic materials, there is a potential for the ordnance to have a permanent magnetization, called a remanent magnetization. The simple model discussed in the previous section ignores any remanent contribution to the total magnetization. In reality, the total magnetization, and thus the magnetic signature, is highly dependent on the magnetic history of each specific ordnance item. It can be argued that if the largest magnetic field the ordnance item ever encounters is the geomagnetic field, then the remanent magnetization is small compared to the induced magnetization. On the other hand, if the ordnance item is subjected to large magnetic fields relative to the geomagnetic field, it is possible that a large remanent signature could exist. Since the magnetization is dependent on the entire magnetic history, however, even ordnance exposed to large magnetic fields before deployment (i.e., firing, launching, or dropping) will experience substantial shock upon ground impact, which in turn causes the microscopic magnetic structure, the magnetic domain, to rearrange to a lower energy state, resulting in a shock demagnetization. The shock demagnetization will leave the ordnance with only a small remanent magnetization and a signature dominated by the induced magnetization. There are still a number of circumstances that can cause ordnance to have a large remanent signature after ground impact. These include lightning strikes near the ordnance.

If it is assumed that the ordnance has impacted the ground or has not been exposed to large magnetic fields, it is possible to estimate the upper bound for the remanent contribution to the ordnance magnetization. This estimate can be made by using a prolate spheroidal approximation for the shape of ordnance and modeling the magnetization process. In this model, it is assumed that the ordnance is exposed to a magnetic field parallel to the long axis, the easiest direction of magnetization, which results in the strongest effective magnetic field in the metal casing. Since the geomagnetic field is small (approximately 0.5 Oe), the magnetization process is very nearly reversible. It is the slight deviation from reversibility at these applied magnetic field levels that causes hysteresis and the resulting remanent magnetization. Back-of-the-envelope estimations of the remanent signature suggest that, in most cases, it is no more than 20 percent of the maximum induced magnetization. For this document, we will use this estimate as an upper limit for ordnance.

2.2.2 Expected Distribution of Magnetic Signatures

Assuming that the maximum remanent signature for ordnance cannot exceed 20 percent of the magnetization induced by the geomagnetic field, it is possible to limit

the orientation of the magnetic dipole relative to a small solid angle. The size of the solid angle is dependent on the aspect ratio of the ordnance item. Table 2-1 gives the inclination of the magnetization of an ordnance item relative to geomagnetic coordinates (see Figure 2-1)[1] at four remanent magnetizations (0, 10, 20, and 30 percent) and three aspect ratios (3, 4, and 5). The relative inclination is the angle between the magnetization and a plane orthogonal to the geomagnetic field. The angles are generated assuming that the remanent signature is aligned along the long axis of the ordnance item; its projection can be parallel or antiparallel to the geomagnetic field.

Table 2-1. Maximum Angle (Degrees) of Magnetization Relative to Geomagnetic Field

Aspect Ratio	No remanent magnetization	10-percent remanent	20-percent remanent	30-percent remanent
3 to 1	54.1	49.0	43.8	38.4
4 to 1	46.1	40.1	35.4	30.0
5 to 1	40.6	35.2	29.8	24.2

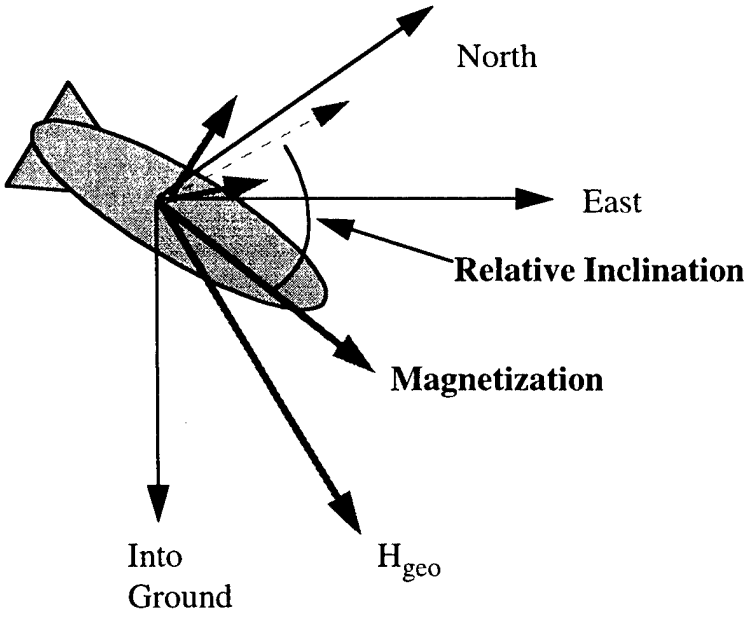

Figure 2-1. The Relative Inclination Used to Determine the Direction of Magnetization in the Geomagnetic Coordinate System

---

1 We use a relative coordinate system that is slightly different from the geophysical coordinate system. In the geophysical coordinate system, the x-axis is north, the y-axis is east, and the z-axis is into the ground. Our relative coordinate system is rotated such that the z-axis is aligned with the geomagnetic field. This results in a 90-deg relative inclination of the geomagnetic field (with no declination). Thus, if the difference between the inclination of the magnetization and the geomagnetic field is 30 deg, then the relative inclination of that magnetization is 60 deg. This results in azimuthal symmetry when doing our magnetization modeling.

Clutter, on the other hand, is not restricted in angular distribution relative to geomagnetic coordinate. This assumption is based on the substantially different magnetic histories of both naturally occurring and anthropic clutter. Most nonordnance materials have not been subject to shock demagnetization. In addition, the manufacturing processes for many nonordnance items (rebar, banding, drums, etc.) tend to form stronger remanent magnetization relative to that formed by the casting process used to manufacture ordnance. It is unlikely that the angular distribution of clutter signatures will be uniform. Instead, there will be a distribution more heavily weighted toward the pure induced angular distribution, with an extended tail that results from a strong remanent contribution to the signature.

To estimate the distribution expected for ordnance and clutter, we use a Monte Carlo technique to estimate the relative inclination distribution for a prolate spheroid with an aspect ratio of 4 to 1. We assume that the remanent magnetization could be any value between 0 and 20 percent of the maximum induced magnetization. The remanent magnetization is fixed along the semimajor axis, and the ordnance direction is allowed to take any direction covering 4π steradians. Figure 2-2(a) shows the resulting distribution. This distribution is consistent with Table 2-1.

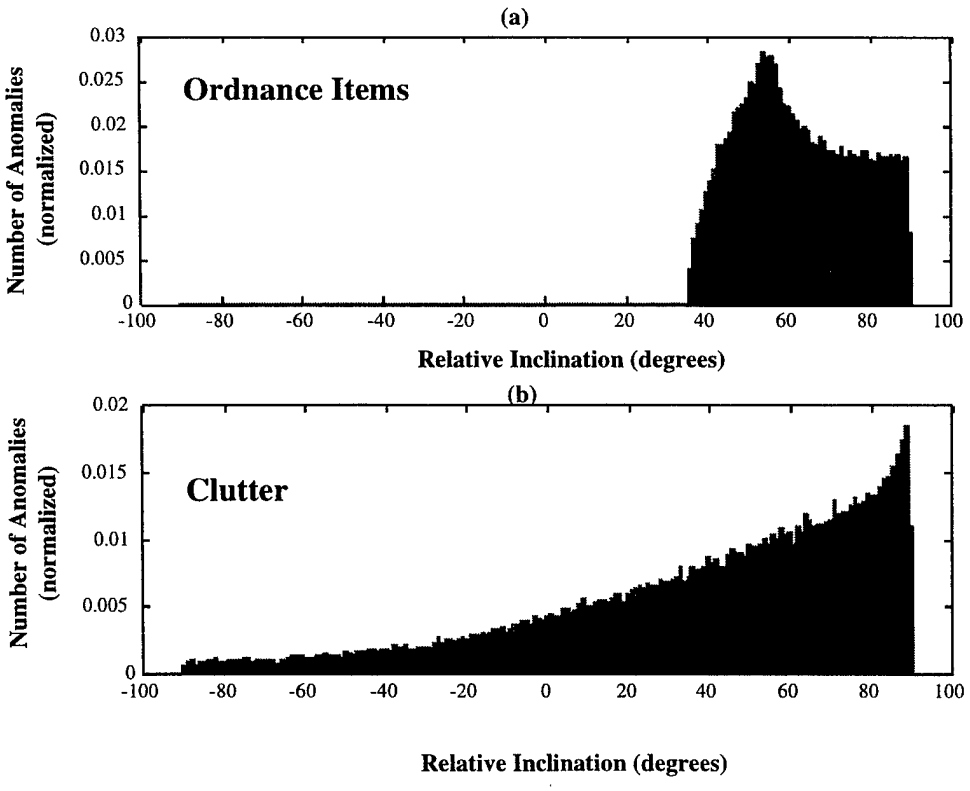

Figure 2-2. Monte Carlo Analysis of Distribution of Relative Inclinations for Ordnance and Clutter

Figure 2-2(b) shows the resulting distribution for clutter; it was calculated using the method described for the ordnance, except an aspect ratio ranging between 1 to 10 and 10 to 1 was assumed. Here, the remanent signature can take a value between 0 and 300 percent of the induced magnetization along the semimajor axis. This figure shows that clutter can exhibit relative inclination covering –90 deg to +90 deg. Thus, it is possible to use the expected relative inclination of ordnance as a discrimination technique. The relative inclination values used for the IDA-processed and NRL-processed data are described in Chapters 3 and 4, respectively.

3.0 IDA DECLARATION ANALYSIS

This chapter contains an analysis of target declarations selected by IDA using the *MTADS*-DAS. These declarations are a result of analysis of the three complete survey runs over the MTR at Twentynine Palms. For each sensor type and configuration (magnetometer, magnetic gradiometer, and EMI), detection (using the full baseline) and false-alarm performance is discussed. Since the *MTADS*-DAS provides more information than just the simple northing/easting position of the declaration, it is possible to evaluate the characteristics of the *MTADS* platform and the *MTADS*-DAS. Along with detection performance (this includes both detection rates and false-alarm rates), the fitted parameters for each declaration are analyzed. In addition, trends and common features for both detections and false alarms are presented for the magnetometer and EMI pair only. Although the magnetic gradiometer[1] data is interesting, few differences were observed between it and the magnetometer data. Therefore, we feel that a comparison using the magnetic gradiometer would be redundant.

This chapter is broken down into four sections. The first two sections present the detection and false-alarm rates and a general analysis of the IDA-developed false-alarm discrimination algorithm, which uses the fitted magnetic moment direction determined from the magnetometer and magnetic gradiometer data. The third section presents an analysis of the location accuracy relative to fitted parameters available from the *MTADS*-DAS. The final section presents an evaluation of the trends in both detection and false-alarm space for the magnetometer and EMI pair. It should be noted throughout this document that performance of the three sensor types is discussed without explicit discussion of the role of the *MTADS*-DAS. In all cases, when we refer to the performance of a specific sensor, that assessment includes the processing feature provided by the *MTADS*-DAS and also any other additional processing on the *MTADS*-DAS output.

---

1 The magnetic gradiometer and magnetometer use the same eight total field magnetometers. The difference is just the configuration of the array.

3.1 GENERAL PERFORMANCE RESULTS

Each declaration data set generated by IDA using the *MTADS*-DAS is compared with the emplaced target baseline. To match a target declaration to the baseline, we determine if the relative northing/easting position of the declaration is within the critical radius, R_{crit}, of the center of the emplaced ordnance item (in the north-east plane) (see Figure 3-1). If the declaration falls outside R_{crit}, the declaration is classified as a false alarm.

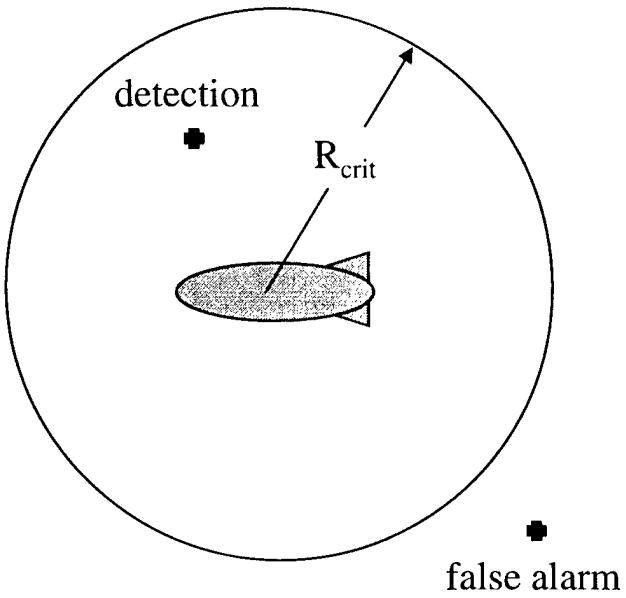

Figure 3-1. Detection of the Ordnance Item is Dependent on the Relative Location of the Declaration (Marked with a Cross) and the Center of Volume of the Ordnance Item. If the declaration is within the critical radius R_{crit}, the ordnance is detected. If the declaration is outside R_{crit}, the declaration is a false alarm. If multiple declarations are located within R_{crit}, only the closest counts as a detection. The others are classified as neither detections nor false alarms.

3.1.1 Detection and False-Alarm Rates

A total of 70 ordnance items are emplaced at the MTR. Of these items, eight are located in proximity to one another, that is, at less than 1.5 m surface distance[2] (see Table 3-1). An additional pair of ordnance items is located with a separation of 2.6 m.

---

2 Measurements of distances are broken into two types: (1) depths measured from ground level to the center of volume of the ordnance item emplace and (2) surface distances measured as the projection of the distance in the north-east plane from a point to the center of volume of the ordnance item emplaced. In this document, we refer to the first as depth and the second as location.

Table 3-1. Ordnance Item Groups

Type— Ordnance #1	Type— Ordnance #2	Surface Distance (m)	Depth Difference (m)
155-mm Projectile	155-mm Projectile	1.00	0.0
105-mm Projectile	105-mm Projectile	0.64	0.0
81-mm Mortar	81-mm Mortar	1.30	0.0
155-mm Projectile	105-mm Projectile	0.0	0.12
250-lb bomb	250-lb bomb	2.6	0.06

The ability to resolve targets is a function of depth, signal to noise, and density of sensor sampling over the targets. The two individual ordnance items constituting each of the four groups with small separation (<1.5 m) are either unresolvable by current sensor technology and processing or, at best, very stressing for the systems. Although the goal of this assessment is to analyze the performance of the *MTADS,* inclusion of the four groups in the baseline has the potential of producing statistics on the depth and location accuracy, and the magnetic moment, that will be misleading. All performance statistics presented are determined using the 62 remaining emplaced ordnance items. Any declarations that are within R_{crit} of the four groups will be discarded from both the detection and false-alarm lists.

The two 250-lb bombs separated by 2.6 m present a more complex situation. If they were shallow, they too would be resolvable by all three sensor types. But since the resolvability is dependent on depth (in this case, approximately 2 m) and separation, resolution of these as individual items is difficult. Still, we feel that it is within the capability of the sensor used on the *MTADS* to resolve these targets. Thus, we will include them as two separate targets in the baseline for this assessment.

It should be noted that in past assessments (for example, Altshuler et al., 1995), grouped sets of targets have been included in the baseline as a single item (called a *group*). The goal was to focus on performance using the probability of detection and false-alarm rate as metrics. In this document, we are evaluating a far greater set of performance parameters, as well as the software processing. Thus, the exclusion of the grouped targets does not diminish the results of the present assessment.

A final declaration set is produced for each sensor type. Detection probabilities and false-alarm rates can then be determined for the three sets of data. Table 3-2 lists P_d,

Table 3-2. Detection and False-Alarm Performance of *MTADS*

Sensor[+]	P_d	*FAR* (m^{-2}) 0.5 m	P_{fa}	P_d	*FAR* (m^{-2}) 1.0 m	P_{fa}
Magnetometer (Full Data Set)	0.581	2.1×10^{-2}	1.6×10^{-2}	0.726	2.0×10^{-2}	6.5×10^{-2}
Magnetometer (Confidence Level 2)	0.548	7.8×10^{-3}	6.1×10^{-3}	0.677	7.4×10^{-3}	2.4×10^{-2}
Magnetometer (Confidence Level 1)	0.532	5.5×10^{-3}	4.3×10^{-3}	0.645	5.2×10^{-3}	1.6×10^{-2}
Magnetometer (Confidence Level 0)	0.468	2.8×10^{-3}	2.2×10^{-3}	0.548	2.6×10^{-3}	8.4×10^{-3}
Magnetic Gradiometer (Full Data Set)	0.581	8.6×10^{-3}	7.0×10^{-3}	0.710	8.3×10^{-3}	2.6×10^{-2}
Magnetic Gradiometer (Confidence Level 2)	0.468	2.7×10^{-3}	2.1×10^{-3}	0.532	2.6×10^{-3}	8.1×10^{-3}
Magnetic Gradiometer (Confidence Level 1)	0.435	2.2×10^{-3}	1.8×10^{-3}	0.468	2.2×10^{-3}	6.8×10^{-3}
Magnetic Gradiometer (Confidence Level 0)	0.371	1.2×10^{-3}	1.0×10^{-3}	0.403	1.2×10^{-3}	3.7×10^{-3}
Electromagnetic Induction	0.758	9.8×10^{-3}	3.3×10^{-3}	0.823	9.5×10^{-3}	2.0×10^{-2}

[+] The declaration set generated using the *MTADS*-DAS is considered the full data set. Magnetic moment modeling and depth criteria were used to reduce the number of declarations. Confidence Level 2 refers to the set of declarations with a final IDA ranking of 2 or less. Confidence Level 1 refers to the set of declarations with a final IDA ranking of 1 or less. Confidence Level 0 refers to the set of declarations with a final IDA ranking of 0.

FAR, and P_{fa} for an R_{crit} of 0.5 m and 1.0 m.[3] Here, P_{fa}, the probability of false alarm, is represented by a surrogate, the fraction of the test site covered by false-alarm areas with R_{crit} radius.[4] In the past, IDA has used a number of methods to calculate surrogates for P_{fa} (Altshuler et al., 1995; Andrews et al., 1996). All these methods are based on the characteristic area of a detection (in this case related to R_{crit}). In this analysis, the *FAR* is small

---

3 In previous performance evaluations of other UXO detection systems including the Jefferson Proving Ground Phase I [Altshuler, et al. (1995)], a critical radius of 2 m was used. This large R_{crit} was required because of the navigation errors associated with the systems involved. The *MTADS* uses RTK-DGPS with accuracy of approximately 5 cm (McDonald et al., 1997). The result of this and the *MTADS*-DAS is that target location accuracy is substantially better than other systems. Therefore, a smaller R_{crit} is justified and appropriate.

4 In the strict sense, P_{fa} should be determined as the number of false alarms divided by the opportunities for a false alarm. We use a surrogate for P_{fa} because we were unable to accurately determine the opportunities for false alarms on the site. We emphasize that the number we use is a surrogate and should not be misinterpreted as the true P_{fa}.

relative to the size of the characteristic detection area. Thus, overlap of these areas associated with each false alarm does not result in a significant error. In the case of high *FAR*, it is critical to account for overlap to ensure that the surrogate P_{fa} is bounded by one.

We use the surrogate for P_{fa} to evaluate performance of the detector sys tem utilizing the Receiver Operating Characteristic (ROC) approach (Altshuler et al., 1995 and 1997). The *FAR* is calculated assuming an approximately 8-acre test site (30,686.6 m^2). No attempt has been made to account for areas not covered by *MTADS*. It should be noted that the *FAR* decreases as the critical radius increases because declarations originally outside R_{crit} are now counted as detections instead of false alarms. On the other hand, P_{fa} increases as R_{crit} is increased. This is a penalty resulting from requiring more area to be associated with each declaration. Since a doubling of R_{crit} results in a factor of approximately 4 increase in P_{fa} (with only a small increase in P_d), it is important to be careful when comparing P_{fa} at different R_{crit}s.

The ROC approach provides a mechanism to evaluate the relative performance of systems or algorithms for a given R_{crit}. Figures 3-2 and 3-3 show P_d versus P_{fa} for three sensors at R_{crit} of 0.5 m and 1.0 m, respectively. The solid lines are isoperformance curves calculated using a Gaussian model for the distribution functions of the target and clutter/noise signatures (Van Trees, 1968; Altshuler et al., 1997). The multiple points for the magnetometer presented for each R_{crit} are related to the false-alarm discrimination algorithm discussed in Section 3.1.3. Looking at an R_{crit} of 0.5 m, for the three points representing confidence levels 0, 1, and 2, which result from implementation of the discrimination algorithm, the performance does not improve significantly over the different confidence levels (the three points fall on a single isoperformance curve within statistical error). But there is improved performance using the discrimination algorithm over that of the full magnetometer data set. The same trend holds for R_{crit} of 1.0 m.

The performance of the magnetic gradiometer using the ROC approach for R_{crit} of 0.5 m and 1.0 m does not exhibit the improvement seen for the magnetometer. All points, except when the most stringent discrimination criterion is applied, fall on a single isoperformance curve within statistical error.

The EMI sensor has the best overall performance, exceeding even the magnetom-eter and magnetic gradiometer performance after implementation of the IDA discrimi-nation algorithm. The general performance trend for the magnetometer appears slightly

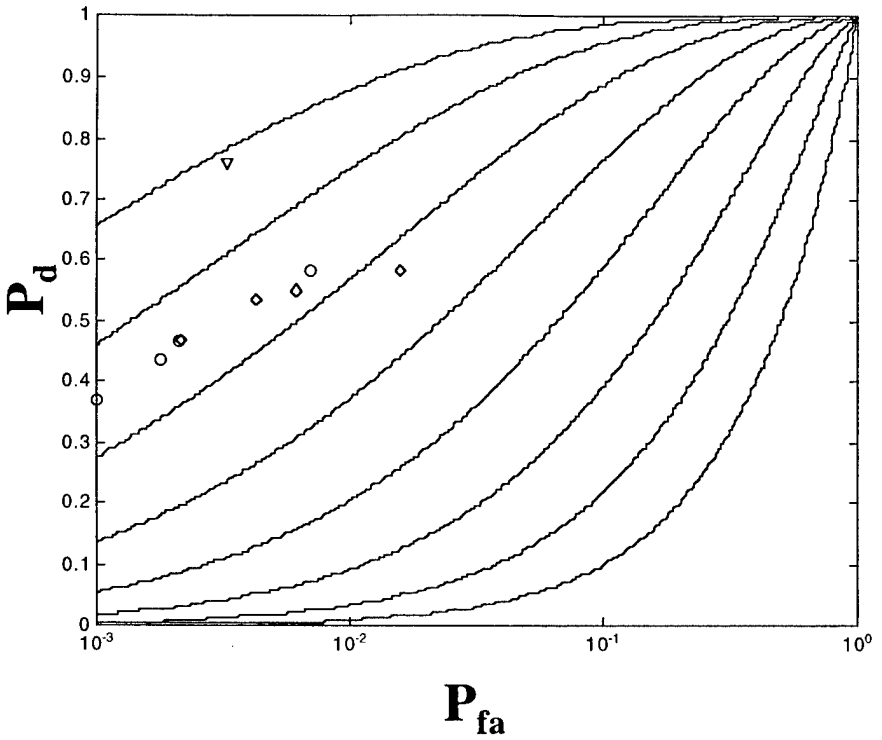

Figure 3-2. P_d versus P_{fa} for the Magnetometer (Diamonds), Magnetic Gradiometer (Circles), and EMI System (Triangle). R_{crit} is 0.5 m. For the magnetometer and magnetic gradiometer, confidence levels of 0, 1, and 2 and full data set are shown as diamonds and circles, respectively, moving from left to right.

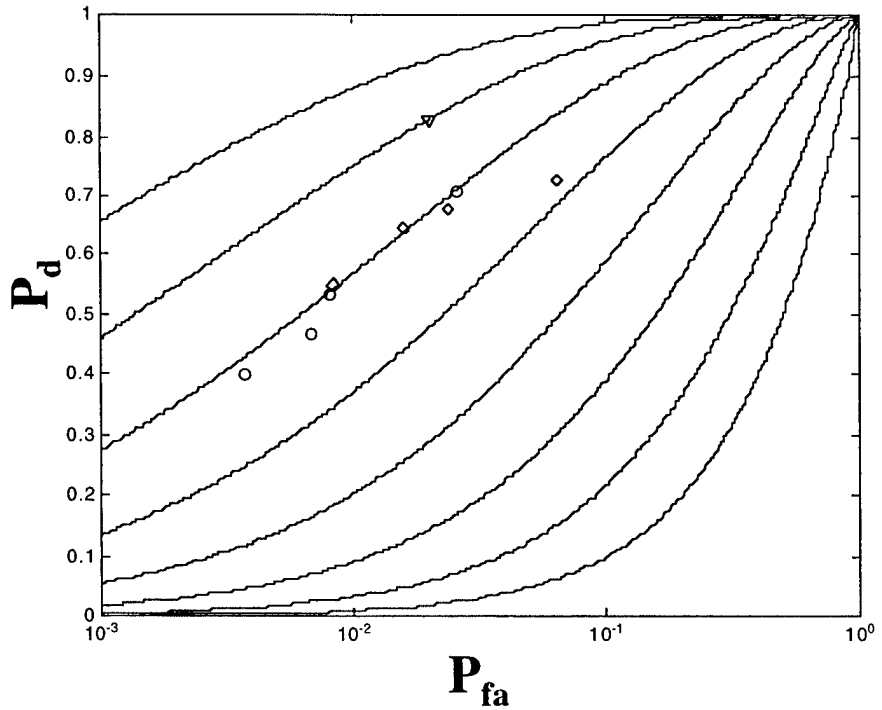

Figure 3-3. P_d versus P_{fa} for the Magnetometer (Diamonds), Magnetic Gradiometer (Circles), and EMI System (Triangle). R_{crit} is 1.0 m. For the magnetometer and magnetic gradiometer, confidence levels of 0, 1, and 2 and full data set are shown as diamonds and circles, respectively, moving from left to right.

better than that of the magnetic gradiometer (for data where false-alarm discrimination has been used). But the statistical significance of this trend is hard to determine because of the small sample size.

It is possible to evaluate the performance of the system by determining the isoperformance variable, d, for each point and including a measure of the confidence interval around d.[5] Figure 3-4 shows the isoperformance variable for each of the data point in Figure 3-3. The confidence intervals are determined assuming that the detection process follows a binomial distribution (Andrews et al., 1996; Simonson, 1998). From Figure 3-4 it is apparent that all three sensor types perform equally as well upon implementation of the IDA magnetic moment discrimination algorithm (sometimes referred to as a filter), if one accounts for statistical uncertainty. It should be noted that the uncertainty in the d for the EMI system appears to be barely overlapping the magnetometer and magnetic gradiometer. Given that the binomial estimation is a worst-case estimation (Simonson, 1998), and given the experience from other tests of EMI and magnetometers (Nelson et al., 1997), it is reasonable to assume that the EMI provides better detection capability than does the magnetometer for the generic shallow ferrous target.

3.1.2 Performance Dependence on Critical Radius

As discussed above, the probability of detection and false-alarm rate are dependent on the R_{crit} used to determine detections. Figures 3-5(a)–(c) show the probability of detection and number of detections as a function of R_{crit} for the magnetometer, magnetic gradiometer, and EMI systems, respectively. It is apparent that for the magnetic detection systems, the number of detections does not increase above an R_{crit} of approximately 0.75 m. The electromagnetic detection system exhibits even better P_d versus R_{crit} performance, with no significant increase in detection rates above approximately 0.5 m.

Table 3-3 gives the mean and standard deviation of the radial location accuracy and the depth accuracy[6] (both true and absolute) for all three sensor configurations for a 1-m critical radius. The EMI system exhibits the best location accuracy but also shows the largest depth error, with a trend of underestimating the depth of the ordnance item. In

---

5 d is a measure of the separation of two Gaussian distributions that characterize the ordnance signature and the clutter/noise. d is in units of standard deviation of the Gaussian distributions.

6 Both accuracy and error are used in this document to refer to the difference in the location and depth determined by the *MTADS*-DAS fitting algorithm and the baseline emplaced position of ordnance.

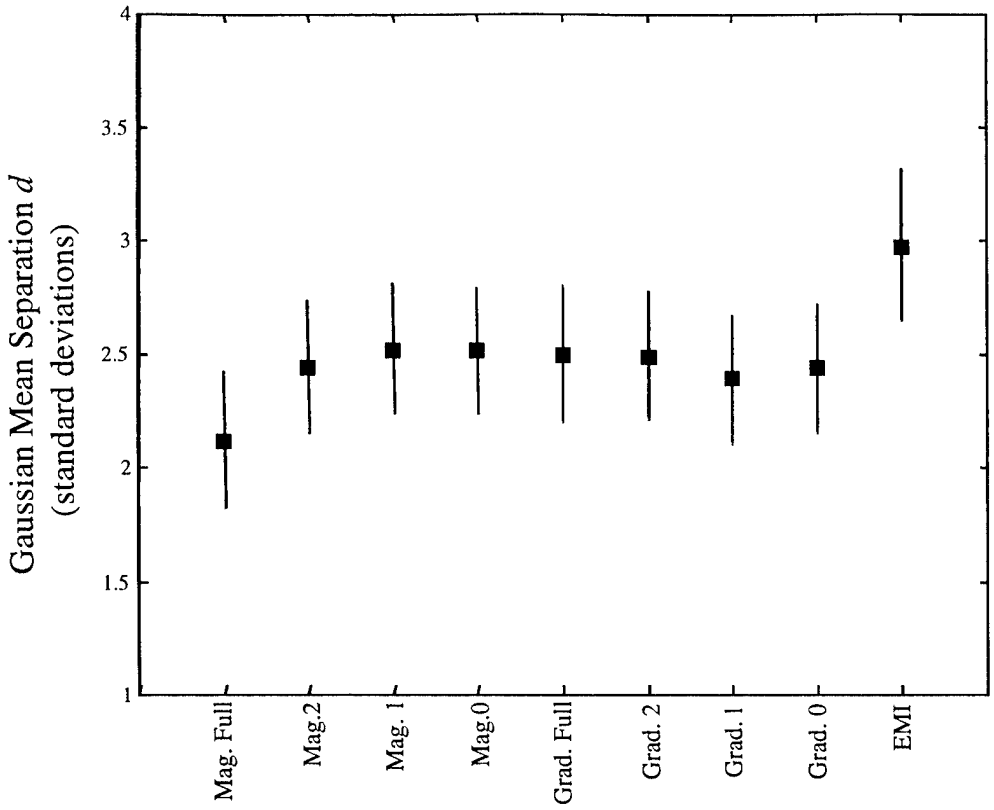

Figure 3-4. Relative Performance of Confidence Levels and Configurations at the MTR. The performance measure is in terms of *d*, the separation of the noise/clutter and full site distribution functions assuming a Gaussian behavior. The 90-percent confidence intervals are calculated using a binomial model for detection.

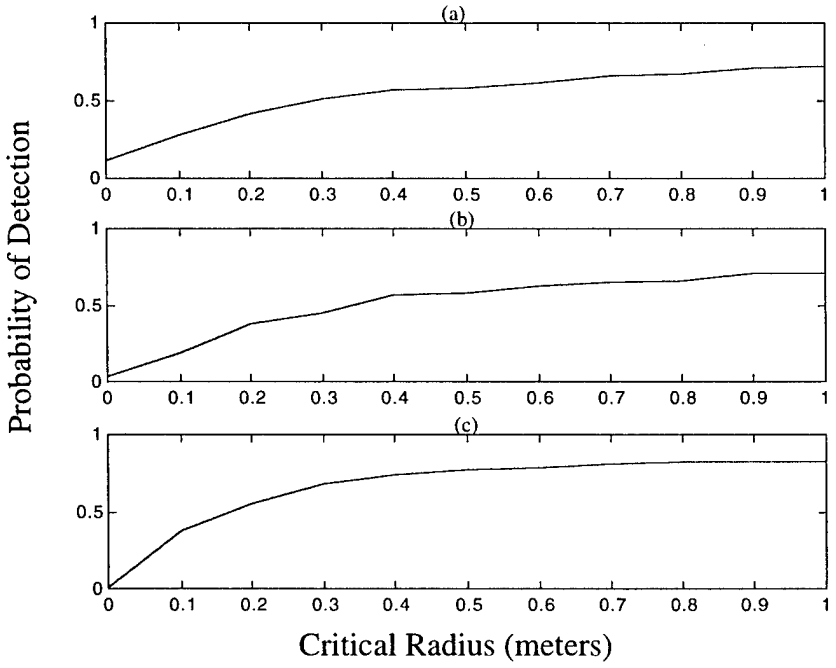

Figure 3-5. Detection Performance versus Critical Radius for the Emplaced Targets. (a) Magnetometer. (b) Magnetic Gradiometer. (c) EMI System.

Table 3-3. Detection Location Error and Depth Error for 1-m Critical Radius

Sensor	Radial Error (m)	Radial Standard Deviation (m)	Depth Error (m)	Depth Standard Deviation (m)	Magnitude Depth Error (m)	Magnitude Depth Standard Deviation (m)
Mag.	0.30	0.27	0.02	0.40	0.23	0.29
Grad.	0.32	0.24	0.04	0.45	0.24	0.37
EMI	0.22	0.16	–0.18	0.46	0.33	0.36

all cases the *MTADS* platform and *MTADS*-DAS perform quite well. The magnetometer has the best depth estimation capability, with a mean misestimation of approximately 20 cm.

3.1.3 False-Alarm Mitigation Techniques

A false-alarm mitigation technique developed by IDA is used to sort potential ordnance from nonordnance for both the magnetometer and magnetic gradiometer declaration set. The false-alarm mitigation uses a confidence-ranking scheme that gives a weight to each declaration based on the orientation of the magnetic moment, the size of the magnetic moment, and the GoF. In addition, declarations determined to be on the surface are ranked with the lowest confidence level because the test did not include surface ordnance,[7] but did include surface clutter. Therefore, even with some statistical uncertainty of the depth estimate, this technique should provide a reasonable method to mitigate the high false-alarm rate for surface clutter.

Table 3-4 shows the performance of the false-alarm mitigation techniques applied to the magnetometer data with R_{crit} of 1 m. The table gives performance at each stage of the algorithm: magnetic moment direction, GoF, and depth criterion. The confidence level represents the overall ranking, 0 being the highest, 6 being the lowest. Only the first three confidence levels are shown because after confidence level 2, no additional detections are recorded until the magnetic moment orientation filter is completely disengaged (which results in looking at the full data set). For the magnetometer data, all three confidence levels shown are substantially better than with no false-alarm mitigation. There appears to be no real improvement across these three confidence levels (see Figures 3-2 and 3-3). There is performance improvement when the first stage (moment

[7] There was a small set of surface ordnance emplaced along an edge of the MTR for this test. Since the ordnance was placed in a visible pattern, and IDA knew before evaluation where the surface ordnance was located, these surface items were excluded from the baseline and from the sensor data.

direction) is employed. After that there is no significant improvement. Given that the depth restriction used in this assessment (no surface ordnance) is site specific, the moment direction filter is the most robust false-alarm discriminator.

Table 3-4. Performance versus Stages of Algorithm Implementation for Magnetometer, R_{crit} = 1 m

Stage	Confidence Level 0		Confidence Level 1		Confidence Level 2	
	P_d	FAR (m^{-2})	P_d	FAR (m^{-2})	P_d	FAR (m^{-2})
Full Set+	0.726	2.0×10^{-2}	0.726	2.0×10^{-2}	0.726	2.0×10^{-2}
Moment	0.694	9.2×10^{-3}	0.710	9.9×10^{-3}	0.710	1.1×10^{-2}
Fit	0.581	3.1×10^{-3}	0.677	6.1×10^{-3}	0.710	8.7×10^{-3}
Depth	0.548	2.6×10^{-3}	0.645	5.2×10^{-3}	0.677	7.4×10^{-3}

+ The full set does not contain any mitigation. Thus, the values in the first row are identical for each algorithm confidence ranking.

Table 3-5 shows the performance of the false-alarm mitigation techniques applied to the magnetic gradiometer data. The approach is identical to that used for the magnetometer. For the magnetic gradiometer there appears to be no measurable improvement across these three confidence levels (see Figures 3-2 and 3-3). Here, there is statistically little improvement when applying the moment direction filter. The same is true for a GoF criterion.

Table 3-5. Performance versus Stages of Algorithm Implementation for Magnetic Gradiometer, R_{crit} = 1 m

Stage	Confidence Level 0		Confidence Level 1		Confidence Level 2	
	P_d	FAR (m^{-2})	P_d	FAR (m^{-2})	P_d	FAR (m^{-2})
Full Set+	0.710	8.3×10^{-3}	0.710	8.3×10^{-3}	0.710	8.3×10^{-3}
Moment	0.613	3.9×10^{-3}	0.613	4.2×10^{-3}	0.613	4.5×10^{-3}
Fit	0.403	1.4×10^{-3}	0.468	2.9×10^{-3}	0.532	3.3×10^{-3}
Depth	0.403	1.2×10^{-3}	0.468	2.2×10^{-3}	0.532	2.6×10^{-3}

+ The full set does not contain any mitigation. Thus, the values in the first row are identical for each algorithm confidence ranking.

The strength of the false-alarm mitigation technique is based on the restriction of the direction of the ordnance magnetic moment. The premise of this technique is that the net magnetization of ordnance is dominated by that magnetization induced by the geomagnetic field; i.e., the remanent magnetization is small (see Section 2.2). On the other hand, the source of a false alarm, clutter, is predicted to exhibit a more uniform angular

distribution of magnetic moments. Figures 3-6(a) and 3-7(a) show the distribution of magnetic moment direction for the detected ordnance for the magnetometer and magnetic gradiometer, respectively. The cutoff for the algorithm used to separate moments with a confidence level of 2 or less is approximately 30 deg.[8] The magnetometer data show only 1 out of 45 with a relative inclination of less than 30 deg. The magnetic gradiometer produces a larger number of ordnance having a relative inclination below 30 deg (6 out of 44).

Figures 3-6(b) and 3-7(b) show the distribution of the relative inclination of the false alarms. The magnetometer data exhibit a significant proportion of the magnetic moment angular distribution with a relative inclination below 30 deg for nonordnance. This is in contrast to the ordnance population. In addition, the distribution function for false alarms from the magnetic gradiometer also exhibits a significant population below a relative inclination of 30 deg.

3.1.4 Characterization of Missed Ordnance

Of the 62 unique targets emplaced at the Twentynine Palms MTR, the declaration set produced before implementation of the IDA false-alarm mitigation algorithm resulted in the detection of 45 and 44 targets using the magnetometer and magnetic gradiometer, respectively, at a critical radius of 1 m. An evaluation of the undetected targets was performed to identify any trends among them. Each target undetected by IDA was reexamined using the *MTADS*-DAS at the target location listed in the baseline. For each undetected target, a fit was performed around the baseline location, and the *MTADS*-DAS fitting parameters were recorded.[9] Based on this analysis, the undetected targets can be grouped into three categories: large location error, weak dipole fits, and small magnetic anomaly signatures.

1. **Large Location Error.** The magnetic dipole fits provided by the *MTADS*-DAS are highly dependent on the size of the declaration box (i.e., the area local to the anomaly used to determine the fit parameters). For the magnetometer and magnetic gradiometer, six targets and four targets, respectively, were not classified as detections because *MTADS*-DAS location errors were between

---

8 The angle used is measured with the geo-coordinate rotated so that the geomagnetic field is along the z-axis. This results in a geomagnetic field inclination of 90 deg. Thus, when this report refers to relative inclination, the reference is the rotated geo-coordinate system.

9 This could not be done for two ordnance items in the magnetic gradiometer set because neither item was surveyed by the *MTADS*.

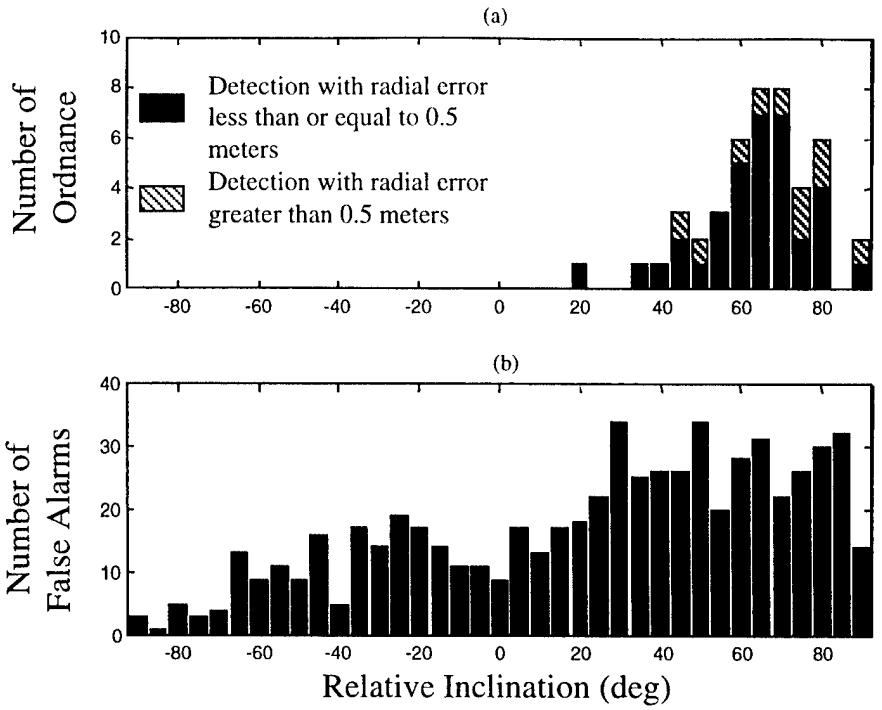

Figure 3-6. Distribution of Magnetic Moments Relative to the Geomagnetic Field as Measured by the Magnetometer. Relative inclination of 90 deg is aligned with the geomagnetic field. Relative inclination of 0 deg is orthogonal to geomagnetic field. (a) Ordnance. (b) False alarms.

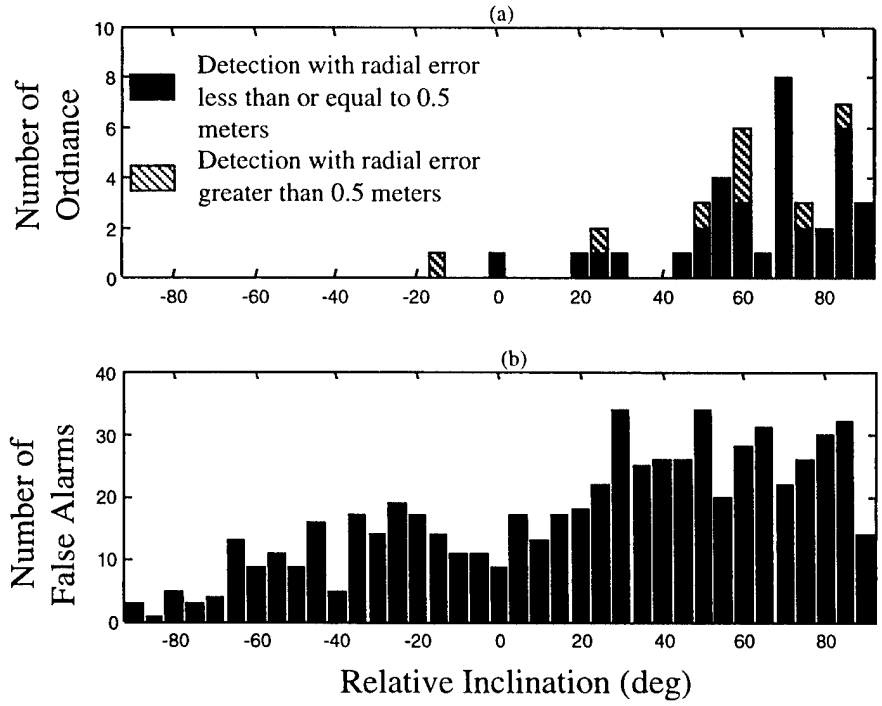

Figure 3-7. Distribution of Magnetic Moments Relative to the Geomagnetic Field as Measured by the Magnetic Gradiometer. Relative inclination of 90 deg is aligned with the geomagnetic field. Relative inclination of 0 deg is orthogonal to geomagnetic field. (a) Ordnance. (b) False alarms.

1 m and 2 m, which is outside the 1-m critical radius. The investigation of the largest target, a 2,000-lb bomb, provides good insight into the idiosyncrasies of the dipole-fitting algorithm. Examination of this target revealed that the IDA target declaration correctly identified the ordnance's *clearly* visible magnetic anomaly. But the location from the fit was incorrect. The anomaly for the 2,000-lb bomb was fitted using four different declaration boxes with slightly different orientations, centered on the baseline coordinate of the ordnance. Only one of these orientations provided a location within an R_{crit} of 1 m. The ordnance items discussed here were not classified as detections because the operator was unable to provide an optimal fit area for the dipole fitting algorithm.

2. **Weak Dipole Fits.** The small (e.g., 60-mm mortar) to large (e.g., 250-lb bomb) ordnance items were often obscured by the clutter background. In the presence of natural or anthropic clutter, the *MTADS*-DAS has difficulty fitting a given anomaly. Two targets for the magnetometer and seven for the magnetic gradiometer were not detected due to the faint dipole signatures. These correspond to small targets buried at depths greater than 1 m. To identify the signatures for these targets, it was necessary to lower the threshold chosen for the fit to $\pm 20\ \gamma$ for this investigation.

3. **Small Magnetic Anomaly Signatures.** Another nine (magnetometer) and seven (magnetic gradiometer) ordnance items were missed because the anomalies were not strong enough to fit. These were targets obscured by the cluttered background. Perhaps an automated procedure set at an appropriate threshold—for instance, using multiple-box orientations to optimize GoF—would fare better. Ultimately, the fitting algorithm is limited by the number of data points taken around the anomaly and the signal-to-noise ratio.

Figures 3-8 through 3-10 show the detected and undetected ordnance as a function of depth for the three sensors. The magnetometer and the magnetic gradiometer both struggle with detection of the deepest ordnance. This is, for the most part, a result of the small amplitude, spatially extended signature of the deep ordnance. Since the MTR at Twentynine Palms has a relatively high level of geological clutter, these broad signatures can be lost in the background. On the other hand, for smaller ordnance of all types, the misses tend to span the depths of emplacement.

The EMI system shows a more compelling trend. Only the deepest ordnance items are missed, and for the smaller, near-surface ordnance, there are no missed items. This suggests that the EMI system is very robust within the top 2 m, where no ordnance was missed.

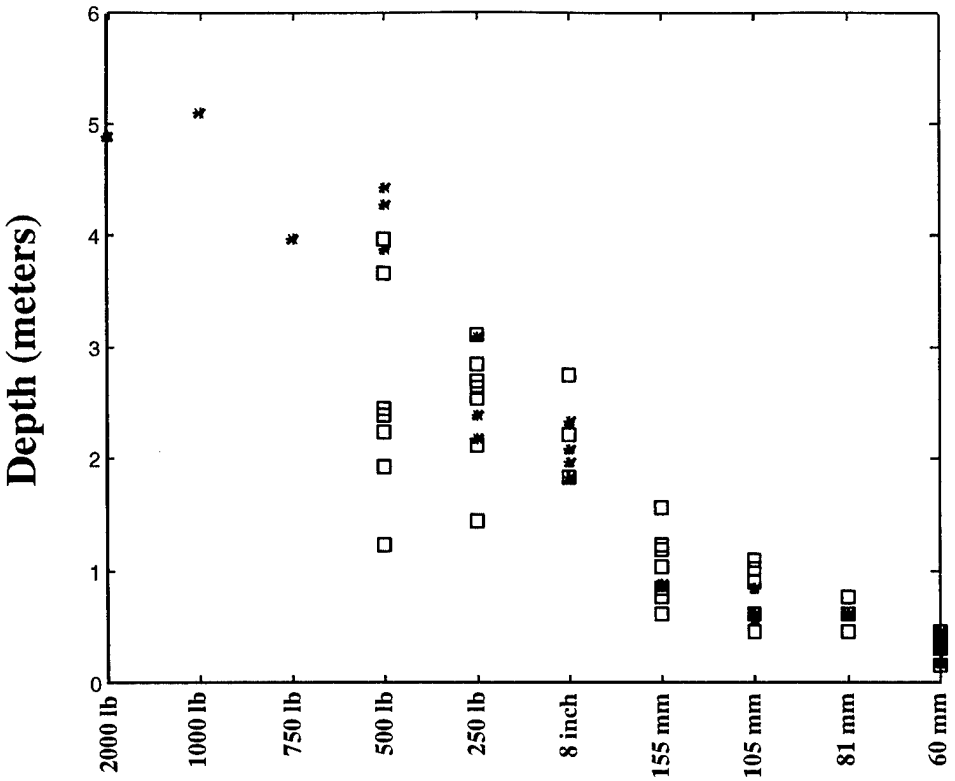

Figure 3-8. Type of Ordnance versus the Depth for Detected (Squares) and Nondetected (Stars) for the Magnetometer

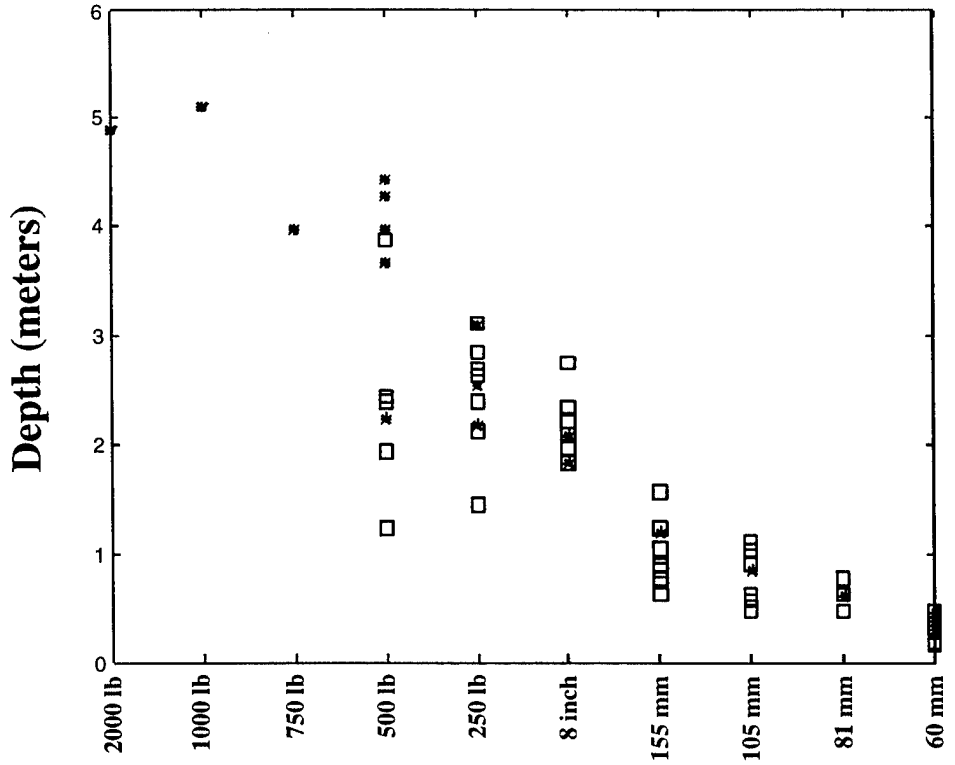

Figure 3-9. Type of Ordnance versus the Depth for Detected (Squares) and Nondetected (Stars) for the Magnetic Gradiometer

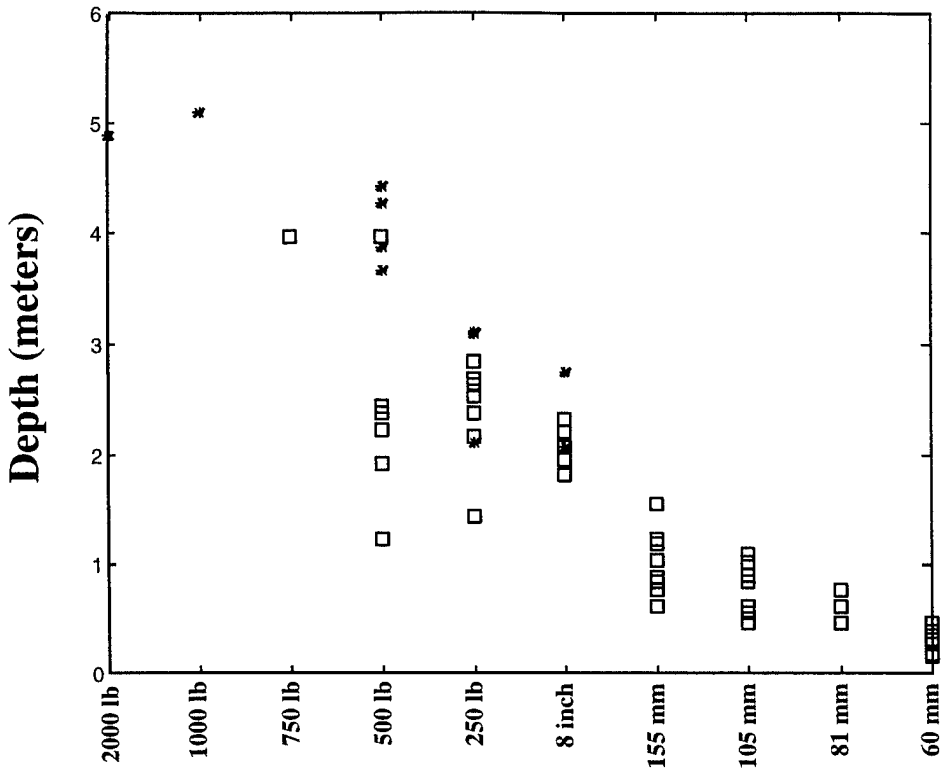

Figure 3-10. Type of Ordnance versus the Depth for Detected (Squares) and Nondetected (Stars) for the EMI System

3.1.5 False Alarms

There is a measured difference between the depth distribution for false alarms for the active EMI system and the passive magnetostatic detection techniques. Figure 3-11 shows the number of false alarms as a function of depth for each sensor. Although for all sensors there are a substantial number of false alarms in the first 0.1 m of the ground, the EMI does not produce many additional false alarms at greater depths (only 4 out of 197, or approximately 2 percent of the false alarms exist below 1 m). The magnetometer and magnetic gradiometer false-alarm depth distributions have approximately 4.3 and 10 percent of their respective false-alarm populations at depths below 1 m. Thus, the depth may provide some method for discrimination, but a number of issues must be addressed.

1. The EMI system shows poor depth accuracy (larger than the bins used to generate Figure 3-11). Thus, the clutter responsible for the EMI anomaly may have a different depth distribution function than shown in Figure 3-11.
2. The magnetometer tends to perform more poorly when detecting small objects near the surface (these can be UXO) than the EMI system.

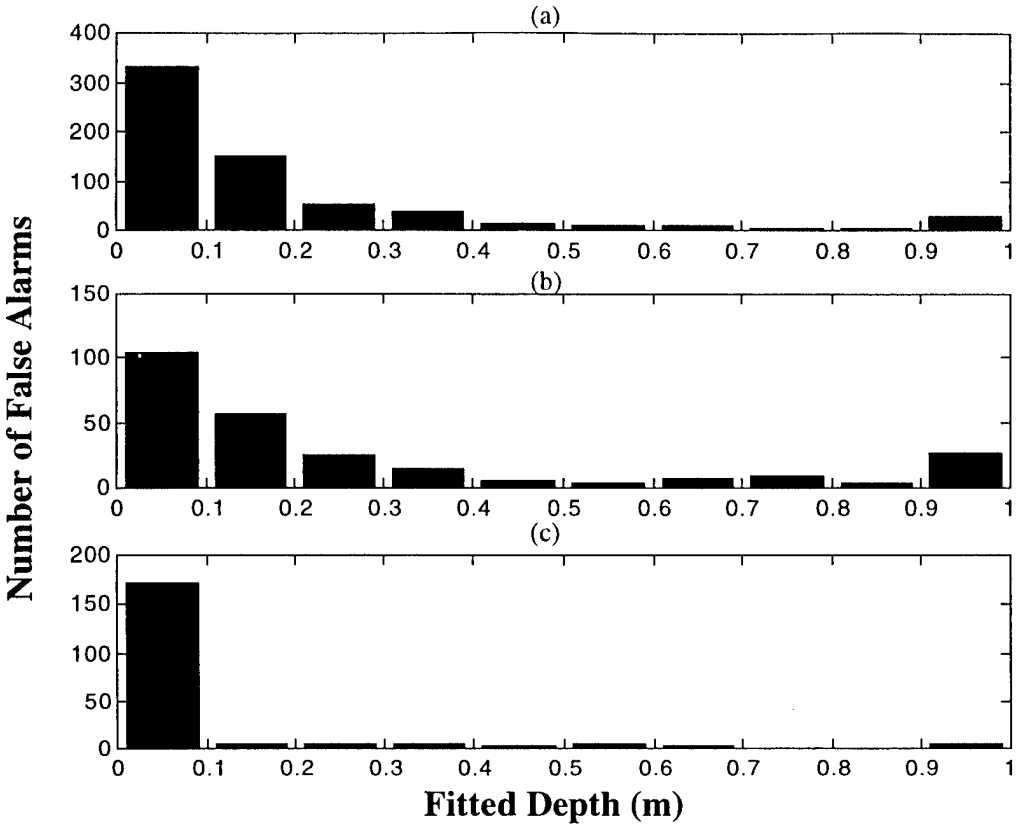

Figure 3-11. The Number of False Alarms as a Function of Fitted Depth. (a) Magnetometer. (b) Magnetic Gradiometer. (c) EMI System.

3.2 MODELED MAGNETIC MOMENTS AND MOMENT DIRECTION

The magnetic moment[10] for each ordnance item emplaced at the Twentynine Palms MTR has been modeled. Appendix A gives a table of the model moments for each ordnance item. The model assumes that the ordnance item can be approximated by a prolate spheroid of the same dimensions as the ordnance. For this single case, only induced magnetization is considered. For this data set, the calculation assumes that the geomagnetic field has an inclination of approximately 60 deg and a declination of approximately 14 deg, and that the magnitude of the geomagnetic field is 0.497 Oe. The relative magnetic permeability is assumed to be 100.

The modeled magnetic moment (also called the volume magnetization) for all ordnance items is then rotated into the geomagnetic coordinate system (see Figure 2-1) to permit comparison with the magnetic moment of all detected targets determined using the

---

[10] Here, the magnetic moment is in units of A-m^2. The difference between this and the magnetic moment often used is a factor of μ_0 ($4\pi \times 10^{-7}$ H/m).

MTADS-DAS. For this model the ordnance item is assumed to be a solid ferrous object. Real ordnance is hollow (with respect to the ferrous material) and contains breaks in the ferrous shell for the fuze, etc. In addition, although the false-alarm mitigation technique assumes that the remanent magnetization is small, it is not assumed to be zero. A small remanent magnetization (even only 20 percent of the maximum geomagnetically induced, which is the assumption for confidence level 2) can, in specific instances, measurably alter the magnitude and direction of the net magnetization. Therefore, the magnetic moment given in Appendix A provides only a starting point for estimating signatures.

3.2.1 Comparison with Fit Magnetic Moments from the Magnetometer Data

Figure 3-12(a) shows a comparison of the modeled magnetic moment and the fit magnetic moment for all individual ordnance items detected by the magnetometer. Although there appears to be correlation between the modeled and fit moments, the linear correlation coefficient is only 0.72. To understand the relative lack of strong correlation between the modeled magnetic moment and the fit magnetic moment, it is valuable to investigate how other parameters, such as GoF and ordnance type, influence the correlation.

Figure 3-12(a) includes detected ordnance with a poor GoF. For a dipole fit an acceptable GoF is a fit greater than 90 percent.[11] Figure 3-12(b) is the GoF as a function of the ratio of the fit magnetic moment (determined by the *MTADS*-DAS) to the modeled magnetic moment, referred to as the magnetic moment ratio. It shows that there are five ordnance items with magnetic moment ratios greater than 3.5; four of these are 60-mm mortars. Although these appear to be statistical outliers, they are more likely caused by the specific magnetic history, emplacement history, or size and orientation of these ordnance items. All these items have good dipole fits. Figure 3-12(c) shows the ratio of magnetic moments as a function of modeled magnetic moment. This figure shows that four (two points overlap) items with the smallest modeled magnetic moments (these are 60-mm mortars in the same physical orientation) also have largest magnetic moment ratio.

Figure 3-13(a) is a histogram of the distribution of the magnetic moment ratio. The mean magnetic moment ratio is 1.40 with a standard deviation of 1.17. This mean

---

[11] This level of fit was chosen on advice of one of the developers of the *MTADS*-DAS, Dr. Bruce Barrow, AETC, Inc. The GoF uses the Levenberg-Marquardt method. The scale for GoF runs from 0.0 to 1.0. The figures present the GoF using a scale from 0 to 100.

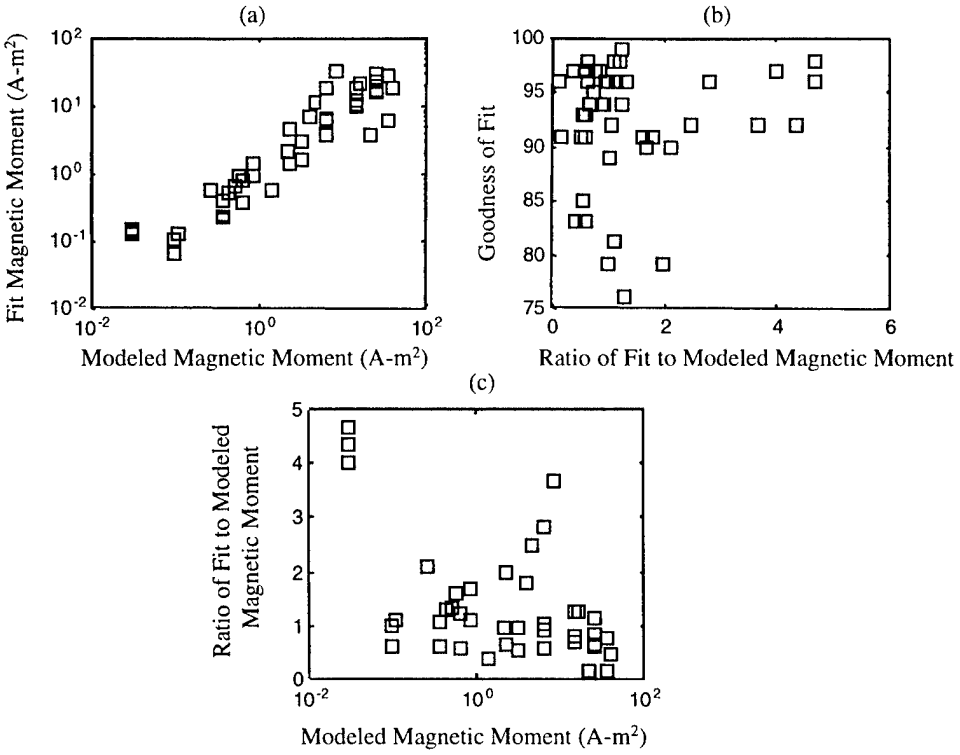

Figure 3-12. Scatter Plots of the Modeled Magnetic Moment and the Fitted Magnetic Moment (from the *MTADS*-DAS) for Magnetometer Data. (a) Modeled Magnetic Moment versus the Fitted Magnetic Moment. (b) Ratio of Magnetic Moment versus the GoF. (c) Ratio of Magnetic Moment versus the Modeled Magnetic Moment. Note that the largest magnetic moment ratio corresponds to the smallest moments (all 60-mm mortars). At the other extreme, the small magnetic moment ratio corresponds to the largest moment, 250-lb bombs.

magnetic ratio cannot be accounted for by assuming a hollow ordnance item because the effect of a hollow object would reduce only slightly the magnitude of the real moment relative to the modeled moment for a solid prolate spheroid (resulting in a mean magnetic moment ratio less than 1) (Altshuler, 1996; Nelson et al., 1998). On the other hand, a *small* remanent contribution to the net magnetization can cause this increase with the observed moment orientation distribution function.

There are also three ordnance items with a magnetic moment ratio of less than 1/3. Two of these are in the 0–0.25 bin; the third is in the 0.25–0.5 bin (see Figure 3-13). These are far from the modeled moments. These ordnance items are all 500-lb bombs.[12] This suggests that the size or another parameter used to model the magnetic moment of the 500-lb bomb is not accurate. Figure 3-13(b) shows the mean magnetic moment ratio

[12] In fact, seven of nine of the smallest magnetic moment ratios are 500-lb bombs.

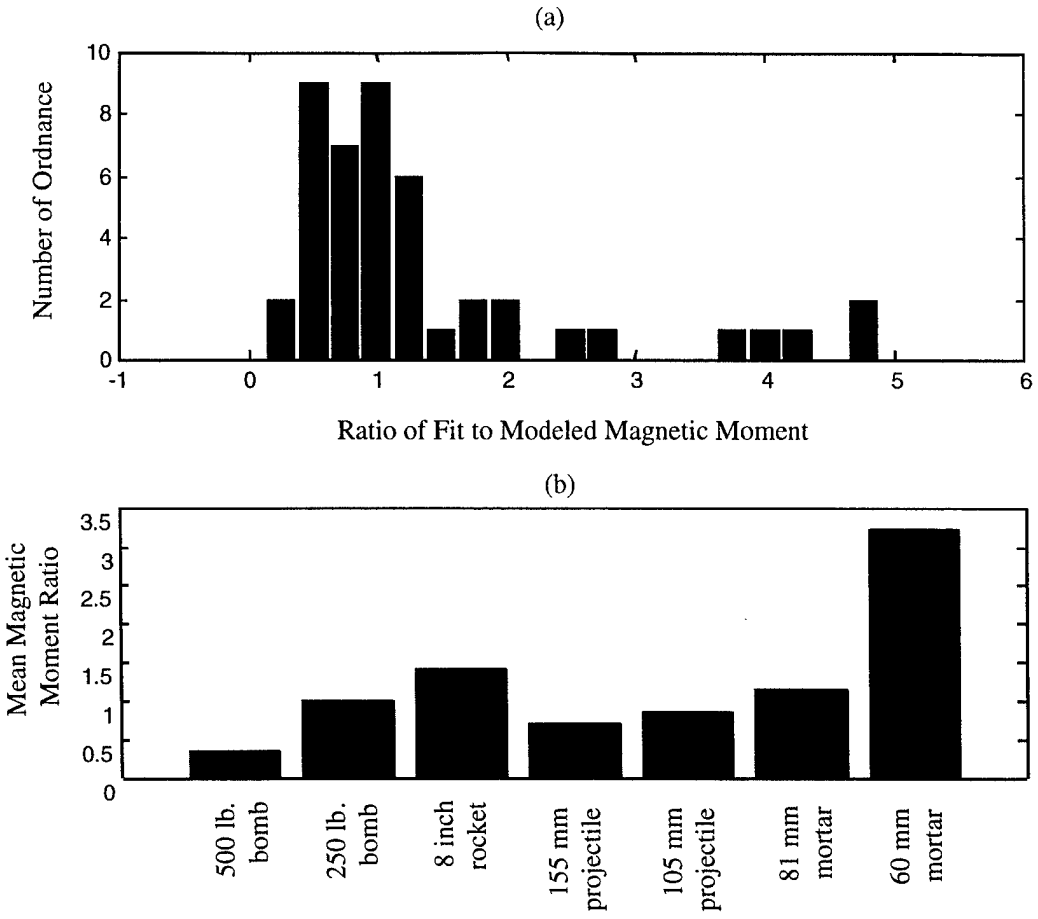

Figure 3-13. (a) Histogram of the Number of Ordnance Items as a Function of Ratio of Magnetic Moment. The bin size is 0.25. (b) Mean Magnetic Moment Ratio for the Seven Different Types of Ordnance Detected on the MTR. Both the 500-lb bombs and the 60-mm mortars are substantially different from the other ordnance items.

as a function of the type of ordnance. Having a magnetic moment ratio very different from 1, the 60-mm mortar and the 500-lb bomb show substantial differences from the model. Table 3-6 lists characteristics of the ordnance items that exhibit the largest discrepancy from a magnetic moment ratio of 1. Although one of the mortars has a large relative depth error, the emplacement depth is only 30 cm. Thus, the absolute error is less than 16 cm. On the other hand, there are large location and depths errors for two of the three 500-lb bombs. The two largest relative depth errors for these are a result of greater than 1.25-m depth errors. The remaining 500-lb bombs detected have a mean depth error of less than 25 cm. The last 500-lb bomb has a relatively poor GoF, 83 percent, the poorest for all 500-lb bombs. For the 500-lb bombs, it appears that these three poor detections are anomalies.

Table 3-6. Fit Properties of Ordnance Not Consistent with Magnetic Moment Model for Magnetometer

Ordnance Type[+]	Modeled Moment ($A\text{-}m^2$)	Fit Moment ($A\text{-}m^2$)	Moment Ratio	Relative Depth Error[++]	Radial Error (m)	GoF (percent)
60-mm mortar	*0.03*	*0.14*	*4.67*	*0.53*	*0.02*	*98*
60-mm mortar	*0.03*	*0.14*	*4.67*	*0.17*	*0.09*	*96*
60-mm mortar	0.03	0.13	4.33	0.03	0.02	92
60-mm mortar	*0.03*	*0.12*	*4.00*	*0.10*	*0.08*	*97*
500-lb bomb	*65.7*	*6.0*	*0.09*	*0.42*	*0.90*	*96*
500-lb bomb	35.2	3.8	0.11	0.35	0.72	91
500-lb bomb	68.6	18.53	0.27	0.06	0.70	83

[+] Ordnance listed in italics are also detected by the magnetic gradiometer with poor correspondence with the modeled signature.

[++] The relative depth error is the ratio of the magnitude of the difference between the emplaced depth and the fit depth to the emplaced depth.

3.2.2 Comparison with Fit Magnetic Moment Direction from Magnetometer Data

We compare the fit magnetic moment direction (inclination and declination) to the modeled magnetic moment direction. To simplify the comparison, inclination and declination are converted to the relative inclination discussed in Sections 2.2 and 3.1.3. Figure 3-14 shows the comparison of the relative inclinations. The relative inclination for the fitted and modeled moments shows virtually no correlation, which suggests that a small remanent magnetization should be added to the net magnetization of the ordnance. Doing so will alter the direction of the magnetic moment, at times significantly. In addition, there is potential that the *MTADS*-DAS does not robustly fit the direction of the magnetic moment in a noisy environment. Still, the general conclusion from the model—that the majority of ordnance should have magnetic moment orientations that are preferentially directed along the geomagnetic field—appears to be supported by the distribution of ordnance as a function of relative inclination (see Figure 3-6).

3.2.3 Comparison with Fit Magnetic Moments from Magnetic Gradiometer Data

Figure 3-15(a) shows a comparison of the modeled magnetic moment and the fit magnetic moment for all individual ordnance items detected by the magnetic

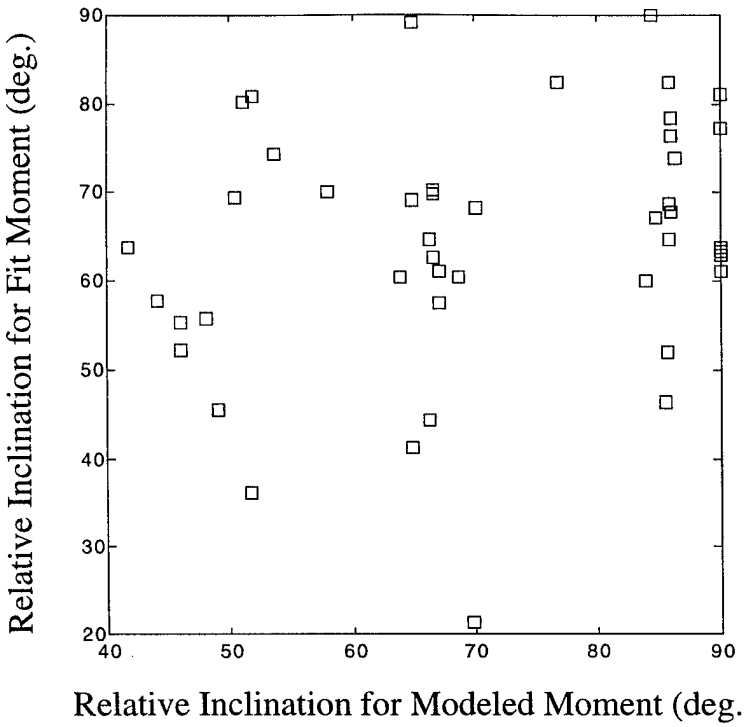

Figure 3-14. Scatter Plot of the Relative Inclination for the Modeled Magnetic Moment versus that of the Fitted Magnetic Moment. There is minimal correlation between the model and the fitted data.

gradiometer. There appears to be less correlation between the modeled and fit moments than in the case of the magnetometer. For the magnetic gradiometer data the linear correlation coefficient is 0.54. One reason for this might be the decrease in spatial sampling for the magnetic gradiometer system, which is approximately 6 cm along track but only 0.5 m cross track, compared to 0.25 m cross track for the magnetometer configuration. Figure 3-15(b) shows the GoF as a function of the ratio of the fit magnetic moment to the modeled magnetic moment. Because the GoF for the magnetic gradiometer data is poorer than that of the magnetometer data, it is difficult to draw strong conclusions. But for this data, some of the poorest fits appear to have either high ratios (greater than 3) or low ratios (less than 1/3). Figure 3-15(c) shows the ratio of magnetic moments as a function of modeled magnetic moment. As with the magnetometers, the 60-mm mortars and 500-lb bombs have the largest and smallest magnetic moment ratios, respectively. Still, there are a number of poorly modeled moments. For example, there is an 8-in. rocket[13] with a magnetic moment ratio of 6.64. But this rocket has a GoF of only 66 percent and has substantial location errors (a 2.23-m depth error and a 0.88-m location error) and thus appears to be an outlier relative to the other 8-in. rockets.

---

[13] This rocket was not detected in the magnetometer data analysis.

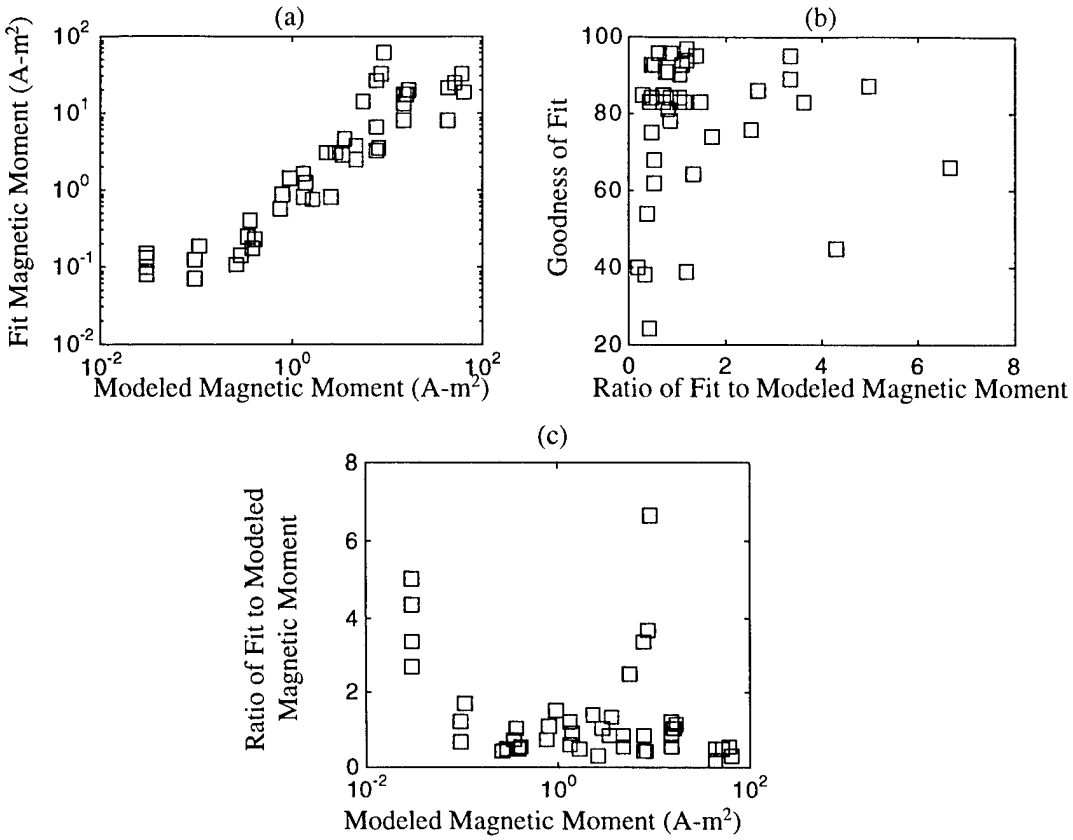

Figure 3-15. Scatter Plots of the Modeled Magnetic Moment and the Fitted Magnetic Moment (from the *MTADS*-DAS) for Magnetometer Data. (a) Modeled Magnetic Moment versus the Fitted Magnetic Moment. (b) Ratio of Magnetic Moment versus the GoF. (c) Ratio of Magnetic Moment versus the Modeled Magnetic Moment. Note that in general the largest magnetic moment ratios correspond to the smallest moments (all 60-mm mortars). At the other extreme, the small magnetic moment ratios correspond to the largest moment, 250-lb bombs.

Figure 3-16(a) is a histogram of the distribution of the magnetic moment ratio. The mean magnetic moment ratio is 1.37, with a standard deviation of 1.39. Figure 3-16(b) shows the mean magnetic moment ratio for each type of ordnance. It is apparent from this figure that, as with the magnetometer data, the magnetic gradiometer fit moment deviates from the model most extensively for the 60-mm mortars and 500-lb bombs. In addition, the 8-in. rocket also deviates from a mean ratio of 1. But if the outlier discussed above is not counted, the mean magnetic moment ratio for 8-in. rockets drops to 1.41.

Table 3-7 lists ordnance with magnetic moment ratios that are either greater than three or less than 1/3. The entries in italics are also included in Table 3-6 (for the magnetometer). Of the three 60-mm mortars in common with the magnetometer set,

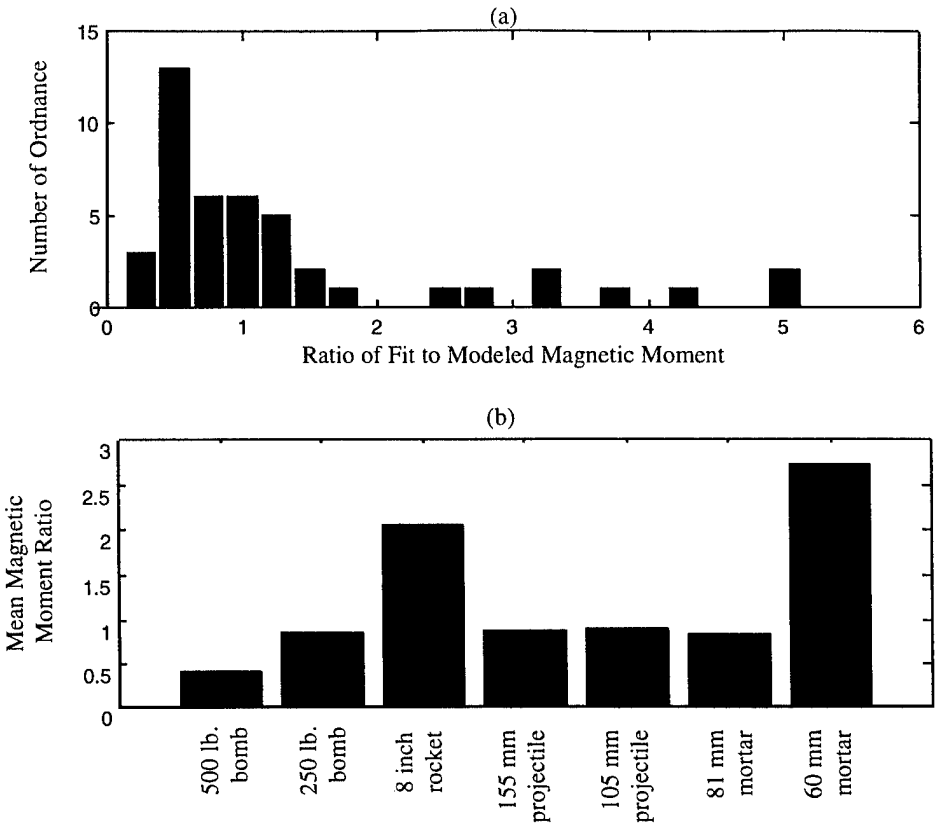

Figure 3-16. (a) Histogram of the Number of Ordnance as a Function of Ratio of Magnetic Moment. The bin size is 0.25. (b) Mean Magnetic Moment Ratio for the Seven Different Types of Ordnance Detected on the MTR. The 500-lb bombs, 8-in. rockets, and 60-mm mortars are substantially different from the other ordnance items.

Table 3-7. Fit Properties of Ordnance Not Consistent with Magnetic Moment Model for Magnetic Gradiometer

Ordnance Type[+]	Modeled Moment ($A\text{-}m^2$)	Fit Moment ($A\text{-}m^2$)	Moment Ratio	Relative Depth Error[++]	Radial Error (m)	GoF (percent)
60-mm mortar	*0.03*	*0.15*	*4.71*	*0.13*	*0.11*	*87*
60-mm mortar	*0.03*	*0.13*	*4.08*	*0.07*	*0.11*	*45*
60-mm mortar	*0.03*	*0.13*	*3.14*	*0.03*	*0.13*	*89*
155-mm proj.	2.6	0.8	0.31	0.02	0.08	97
8-in. rocket	9.1	60.2	6.64	0.96	0.88	66
8-in. rocket	7.98	26.7	3.35	0.23	0.16	89
500-lb bomb	43.8	8.2	0.19	0.37	0.93	40
500-lb bomb	*65.7*	*18.15*	*0.28*	*0.19*	*0.48*	*85*

[+] Ordnance listed in italic are also detected by the magnetometer with poor correspondence with the modeled signature.

[++] The relative depth error is the ratio of the magnitude of the difference between the emplaced depth and the fit depth to the emplaced depth.

two have relatively good fits, while one has a very poor fit. The trend for the 500-lb bombs is slightly different. The nonitalicized entry was not detected from the magnetometer data and has a very poor GoF. On the other hand, the target that is common to both the magnetometer and magnetic gradiometer set has very different characteristics. The fitted magnetic moment for this bomb using the magnetic gradiometer data is three times that fitted from the magnetometer data.

3.2.4 Comparison with Fit Magnetic Moment Direction from Magnetic Gradiometer Data

A comparison of the relative inclinations for the modeled magnetic moment and the fit magnetic moment for the magnetic gradiometer shows a trend similar to the magnetometer. Again, the relative inclination for the fitted and modeled moments shows virtually no correlation. The general conclusion from the model—that the majority of ordnance should have magnetic moment orientations that are preferentially directed along the geomagnetic field—appears to be supported by the distribution of ordnance as a function of relative inclination [see Figure 3-7(a)] but not as strongly. This is most likely caused by the poorer fit quality of the magnetic gradiometer data.

3.2.5 Comparison of Fit Magnetic Moments Magnitude and Direction Between the Magnetometer and Magnetic Gradiometer

To understand the robustness of the algorithm used to do false-alarm mitigation, it is important to know the accuracy of the fit algorithms used by the *MTADS*-DAS. One way to test the accuracy is to compare the fit algorithm for the magnetometer data with that for the magnetic gradiometer data. Figure 3-17(a) shows the magnetic moment ratios for ordnance common to both the magnetometer and magnetic gradiometer. The data exhibit a trend, but with some scatter, which results in a linear correlation coefficient of approximately 0.58. There are a couple of common ordnance items which show large magnetic moment ratios (and a couple that show small ratios) for both sensors. Table 3-8 lists characteristics of the ordnance. The data show that moments anomalously different from the modeled moment (i.e., greater or less than the modeled moment by a factor of 2 or 1/2, respectively) are fairly similar for both sensors.

On the other hand, the primary parameter used for discrimination is the relative inclination. Figure 3-17(b) shows the relative inclination for ordnance common to both the magnetometer and magnetic gradiometer. With a linear correlation coefficient of

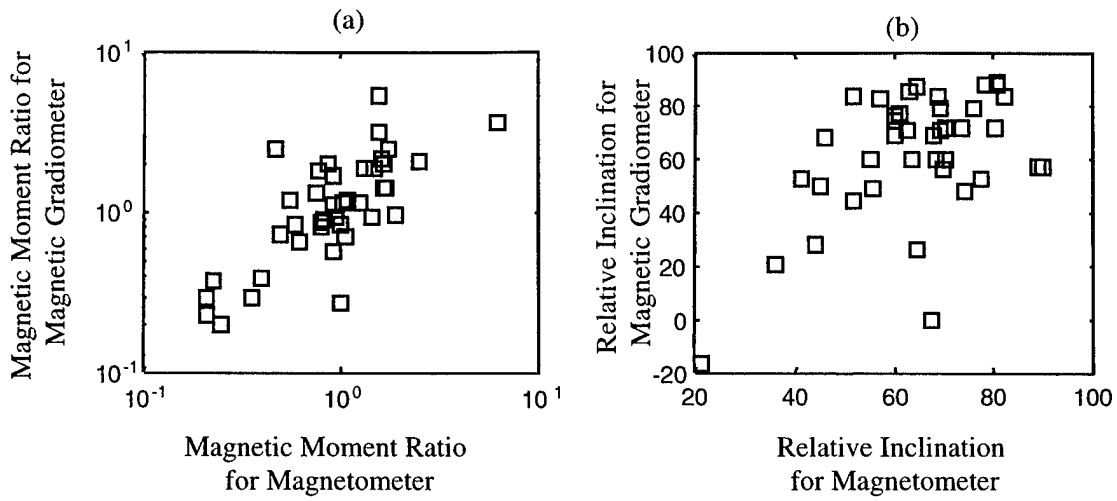

Figure 3-17. (a) Scatter Plot of the Magnetic Moment Ratio for Common Targets Between the Magnetometer and Magnetic Gradiometer Data Sets. (b) Scatter Plot of the Relative Inclination for Common Targets Between the Magnetometer and Magnetic Gradiometer Data Sets.

Table 3-8. Fit Properties Not Consistent with Magnetic Moment Model for Either Magnetometer or Magnetic Gradiometer Data Common to Both Data Sets

Ordnance Type	Moment Ratio Mag.	Moment Ratio Grad.	Depth Error (m) Mag.	Depth Error (m) Grad.	Radial Error (m) Mag.	Radial Error (m) Grad.
60-mm mortar	4.0	4.71	0.03	0.04	0.09	0.11
60-mm mortar	4.67	4.08	0.16	0.09	0.02	0.11
60-mm mortar	4.67	3.14	0.03	0.13	0.08	0.0
60-mm mortar	4.33	2.51	0.01	0.12	0.02	0.13
155-mm proj.	0.56	0.31	0.0	0.01	0.16	0.4
8-in. rocket	2.32	3.35	0.4	0.5	0.36	0.16
500-lb bomb	0.09	0.28	1.64	0.74	0.90	0.48

0.51, these data do not show a strong trend. Table 3-9 lists the ordnance items that have relative inclination less than the approximate 30-deg cutoff used to sort the data. Five of the seven ordnance items are detected by both sensors. Although none of these items exhibit anomalously variant magnetic moment ratios, the differences in relative inclination can be substantial. Only target ID number 1025 (an 8-in. rocket) is labeled with a low confidence level in both data sets because of the relative inclination.

Table 3-9. Ordnance with Small Relative Inclination for Either the Magnetometer or Magnetic Gradiometer

	Magnetometer		Magnetic Gradiometer		Modeled Moment	
Target ID	Magnetic Moment ($A\text{-}m^2$)	Relative Inclination (deg)	Magnetic Moment ($A\text{-}m^2$)	Relative Inclination (deg)	Magnetic Moment ($A\text{-}m^2$)	Relative Inclination (deg)
1025	4.7	21.4	4.8	−16.8	3.5	57.1
1060	0.12	67.22	0.19	0.34	0.11	84.43
1044	0.95	36.2	1.43	21.3	0.95	48.78
1015	—	—	3.33	25.6	7.74	47.86
1032	18.52	64.7	26.71	26.2	7.98	65.5
1031	6.00	44.4	6.67	27.61	7.98	65.5
1011	25.85	36.44	—	—	50.24	75.89

3.3 SENSOR PERFORMANCE

This section characterizes the system location performance for detected ordnance by evaluating the *MTADS*-DAS parameters and determining trends. For each sensor type, the entire declaration set (the full set) is matched to emplaced ordnance. A critical radius of 1 m is used to determine the set of declarations that match emplaced ordnance in the target baseline. The magnetometer declarations match to 45 emplaced ordnance items, the magnetic gradiometer declarations match to 44 emplaced ordnance items, and the EMI sensor declarations match to 51 emplaced ordnance items within the 1-m critical radius.

3.3.1 Sensor Performance: Radial Location Accuracy

For each sensor declaration which matches an emplaced ordnance item within the 1-m critical radius, the coordinates of the fitted anomaly and radial location accuracy or radial location error are recorded (radial location accuracy = fitted anomaly location – actual location of detected ordnance item). The results of the analysis follow below.

3.3.1.1 Magnetometer

The magnetometer data set results in the detection of 35 ordnance items within a 0.5-meter R_{crit}, and 45 targets within a 1-m R_{crit}. The mean radial location accuracy is 0.30 m with a standard deviation of 0.27 m (see Table 3-3). Figures 3-18(a)–(d) show a series of scatter plots for different fit and modeled parameters for the magnetometer data.

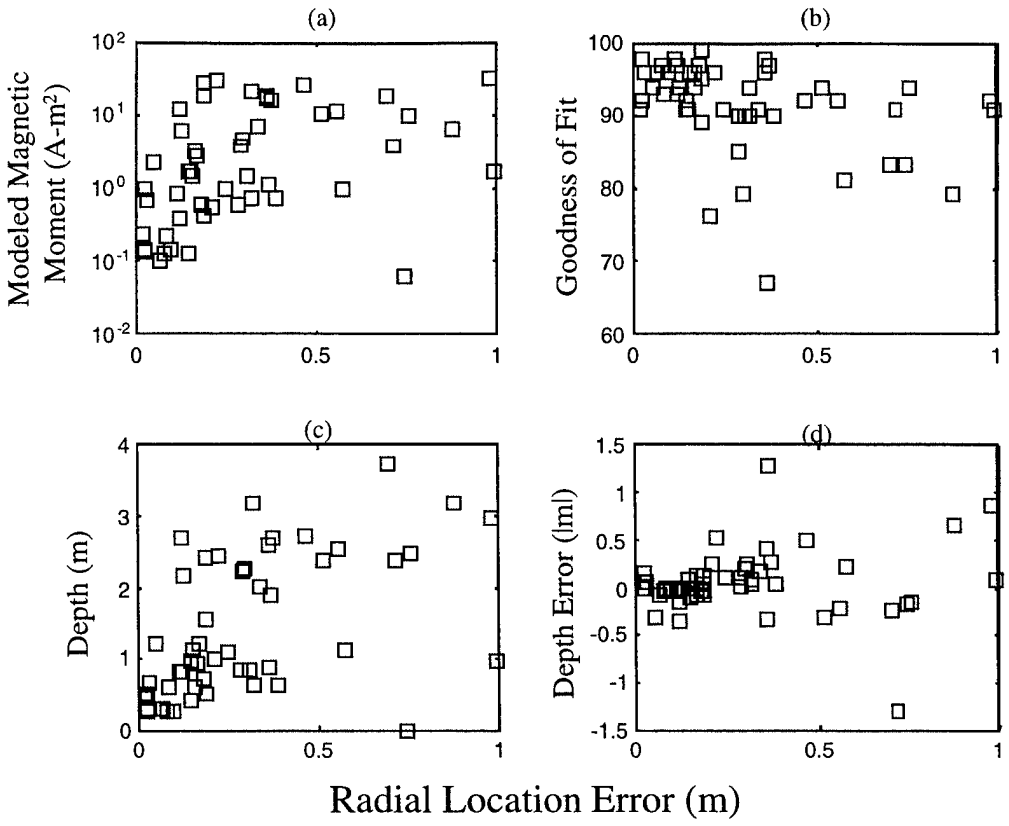

Figure 3-18. Radial Location Error for the Magnetometer. (a) Versus Modeled Magnetic Moment. (b) Versus GoF. (c) Versus Depth. (d) Versus Depth Error.

There is minimal correlation between magnetic moment and radial location error: the position accuracy for the various size objects is roughly equivalent. There is some correlation between radial location accuracy and GoF: of the 10 targets with radial location error greater than 0.5 m, 4 anomalies have fits less than 85 percent, but the 6 additional anomalies with large location errors have fits greater than 90 percent. Therefore, we cannot say definitively that those targets with poor fits are responsible for decreasing the overall location accuracy.

A weak trend exists for increased radial error to be associated with increased depth. Finally, larger radial errors for targets appear to correlate with large depth errors, but the correlation is not strong. Note that there is no correlation between the sign of the depth error and the radial location accuracy.

3.3.1.2 Magnetic Gradiometer

The magnetic gradiometer detects 36 targets within a 0.5-m R_{crit} and 44 targets within a 1-m R_{crit}. The mean radial location accuracy is 0.32 m with a standard deviation

of 0.24 m (see Table 3-3). Figures 3-19(a)–(d) show a series of scatter plots for different fit and modeled parameters for the magnetic gradiometer data. As with the magnetometer, the magnetic gradiometer location accuracy is weakly correlated at best to the fit magnetic moment. On the other hand, the GoF is slightly more correlated to the location accuracy: the poorer location accuracies correlate with the poorer fits. For GoF greater than 90 percent, radial errors are generally less than 0.4 m. There is a trend for higher radial error to be associated with anomalies that have a GoF less than 90 percent. The sensor's location accuracy shows weak correlation with object depth. There is also weak correlation between radial location accuracy and depth error. Again, there appears to be no correlation with the sign of the depth error. For radial error less than 0.5 m, the normalized depth error is generally less than 50 percent.

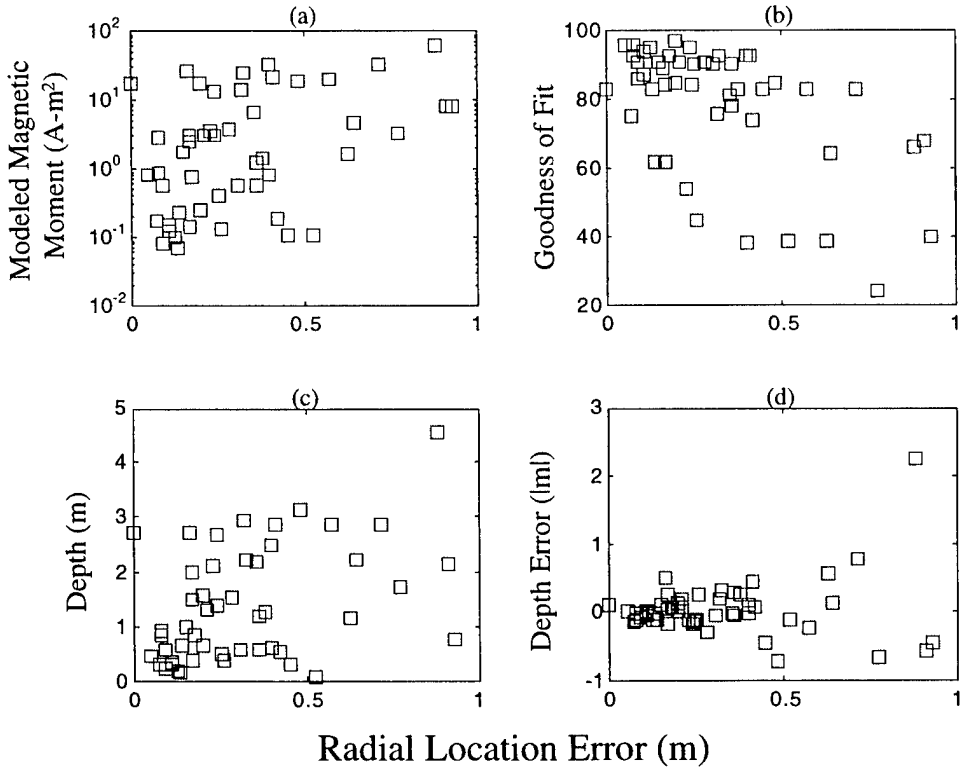

Figure 3-19. Radial Location Error for the Magnetic Gradiometer. (a) Versus Modeled Magnetic Moment. (b) Versus GoF. (c) Versus Depth. (d) Versus Depth Error.

3.3.1.3 EMI Sensor

The EMI sensor exhibits very good success detecting the emplaced ordnance. Forty-seven targets are detected within the 0.5-m R_{crit}. The mean radial location accuracy is 0.22 m with a standard deviation of 0.16 m (see Table 3-3). Figure 3-20 shows a series of scatter plots for different fit parameters for the EMI data. The EMI system has better

location accuracy than either the magnetometer or the magnetic gradiometer. There is no noticeable trend between location accuracy and size (either ferrous or nonferrous). Most targets which have a GoF greater than 80 percent have a location error less than 0.2 m. Again, as with both the magnetometer and the magnetic gradiometer, only the depth error (magnitude) appears to be correlated with the radial accuracy, and this weakly.

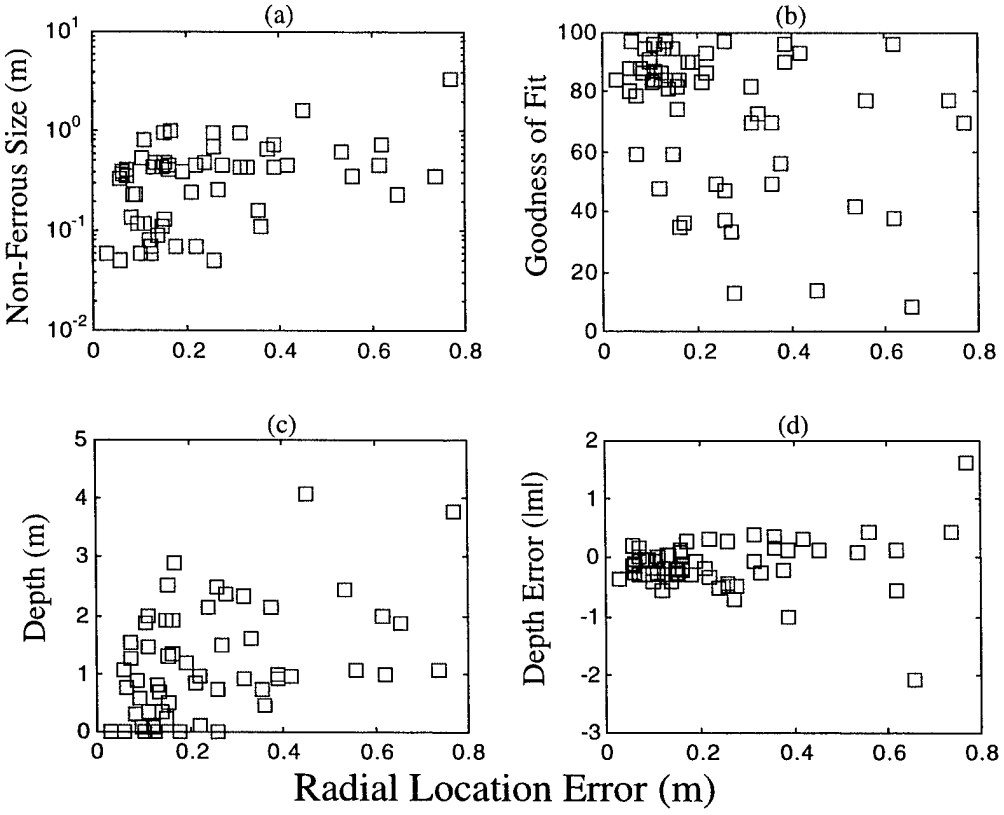

Figure 3-20. Radial Location Error for the EMI System. (a) Versus Modeled Magnetic Moment. (b) Versus GoF. (c) Versus Depth. (d) Versus Depth Error.

The overall location accuracy for all sensors is quite good, and the EMI sensor data show especially good location accuracy. Ultimately, though, there is no compelling trending of location data with the other *MTADS*-DAS fit parameters.

3.3.2 Sensor Performance: Depth, Depth Accuracy

For each sensor declaration which matched an emplaced target within the 1-m critical radius, the fitted depth and depth error (depth error = fitted depth – actual depth of the emplaced target) is recorded. The results of our analysis are discussed below.

Since the baseline items are emplaced at realistic depths—large objects are typically emplaced at depths deeper than the smaller ordnance items—an analysis of the

trends for each sensor provides physical insight into the sensor's ability to detect ordnance of various sizes and at various depths. For all three sensor types, the fitted depth of the ordnance is fairly well correlated to the fitted moment; for the EMI system, the fitted depth is also correlated to nonferrous size. This is consistent with the emplacement protocol.

3.3.2.1 Magnetometer

The average magnetometer depth accuracy[14] for the entire set of targets is approximately 0.23 m, with a standard deviation of 0.32 m. Of the 45 declarations that matched baseline ordnance, the magnetometer detected 33 targets with a depth accuracy of less than 0.25 m, 40 targets with a depth accuracy of less than 0.5 m, and all but two targets within 1.0 m. These final two are more than three standard deviations away from the mean. Removing the outliers results in a mean depth error of 0.17 m, with a standard deviation of 0.18 m. As shown in Figure 3-21(a), the depth error is not correlated with the fit magnetic moment of the object. In fact, Figures 3-21(b)–(d) show that the depth accuracy is independent of depth and is only weakly correlated to the GoF parameters. Of the 45 targets, 9 targets have a GoF less than 90 percent; it is important to note, nevertheless, that poor fits do not correlate with poor depth accuracy for this sensor.

3.3.2.2 Magnetic Gradiometer

Given the poor fit of the model used in the *MTADS*-DAS, the magnetic gradiometer has surprisingly similar depth accuracy to that of the magnetometer [see Figures 3-22(a)–(d)]. The average depth accuracy for the entire set of targets is approximately 0.26 m, with a standard deviation of 0.37 m. There are 29 targets located within 0.25 m, 37 targets within 0.5 m, 43 targets within 1 m, and 1 outlier at 2 m. This last ordnance item, a 250-lb bomb with a depth error of 2.23 m, is actually close to another bomb, which causes the error in estimation of the depth. By removing this ordnance item from the baseline, the mean depth accuracy improves to 0.22 m, with a standard deviation of 0.21 m. In general, depth accuracy for the magnetic gradiometer is poorly correlated to the magnitude of the magnetic moment [see Figure 3-22(a)]. There is also poor correlation between the fitted depth and the depth accuracy.

---

[14] We refer to the depth accuracy as the magnitude of difference between the emplaced depth and fitted depth. The depth error is the true difference.

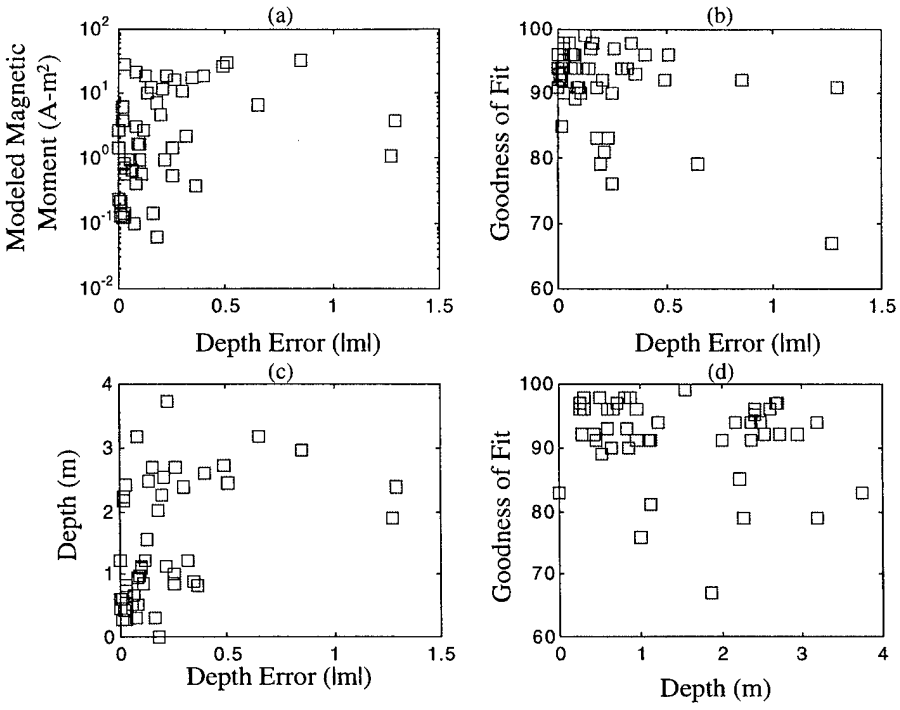

Figure 3-21. Depth and Depth Error for the Magnetometer. (a) Depth Error versus Modeled Magnetic Moment. (b) Depth Error versus GoF. (c) Depth Error versus Depth. (d) Depth versus GoF.

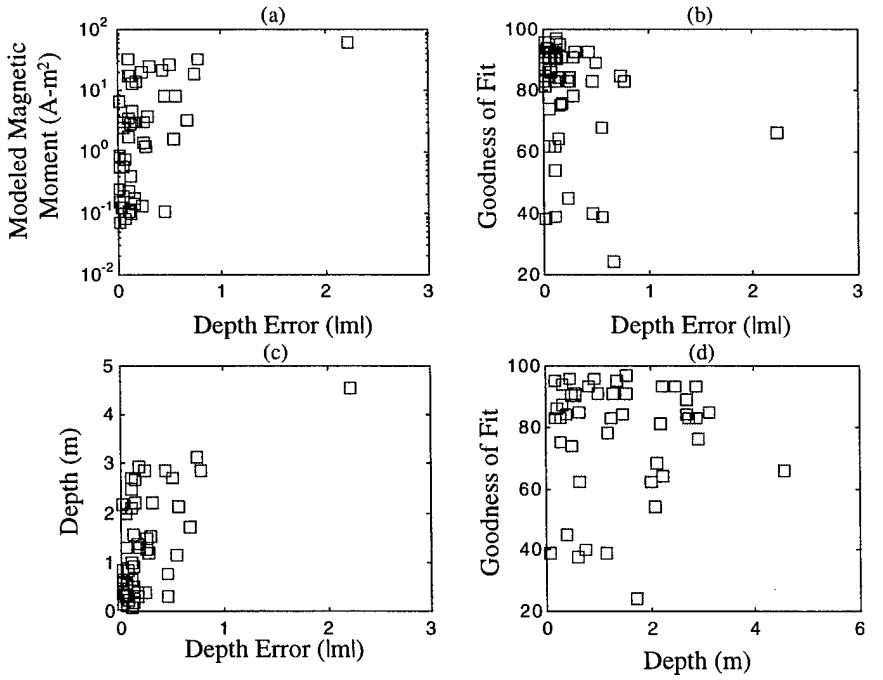

Figure 3-22. Depth and Depth Error for the Magnetic Gradiometer. (a) Depth Error versus Modeled Magnetic Moment. (b) Depth Error versus GoF. (c) Depth Error versus Depth. (d) Depth versus GoF.

3.3.2.3 EMI Sensor

The EMI system exhibits trends similar to the other two sensors. In general, the depth and depth accuracy are poorly correlated to the other fit parameters [see Figures 3-23(a)–(d)]. The GoF for most ordnance is the lowest of all the sensors. The EMI system shows a systematic misestimation of depth (a mean undererestimation of 0.18 m). The average depth error is the largest for all three sensors: approximately 0.33 m with a standard deviation of 0.36 m. The EMI located 44 targets within a depth of 0.5 m, with 7 additional ordnance items at depths greater than 0.5 m. As with the two other sensors, there are a number of detections that are more than three standard deviations from the mean magnitude of the depth error. Removing these and recalculating the mean magnitude of the depth error yields 0.27 m, with a standard deviation of 0.19 m.

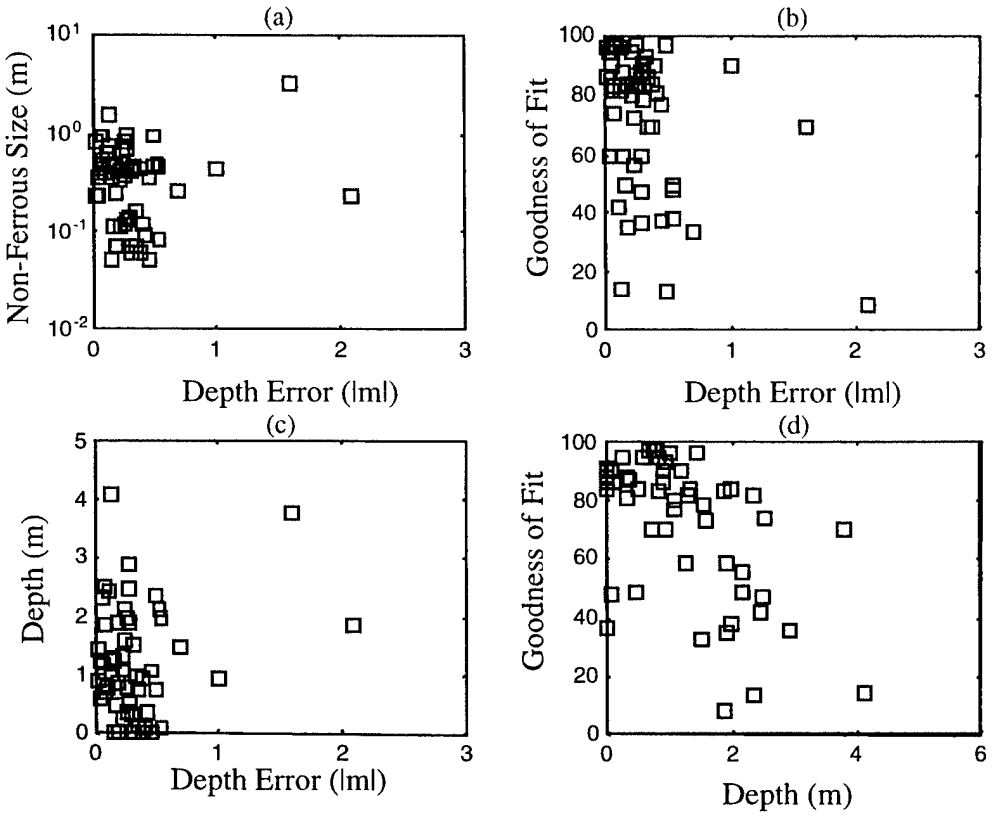

Figure 3-23. Depth and Depth Error for the EMI. (a) Depth Error versus Nonferrous Size. (b) Depth Error versus GoF. (c) Depth Error versus Depth. (d) Depth versus GoF.

3.4 DETECTIONS AND FALSE ALARMS COMMON TO MAGNETOMETER AND EMI

An analysis of the declarations common to the magnetometer and the EMI systems was performed to understand the general trends associated with detection by multiple systems. This section contains a comparison of the *MTADS*-DAS fit parameters

for this sensor pair. A common detection is declared for all ordnance matched to a declaration of both sensors in the pair. A common false alarm is declared for any false alarms within 1.0 m of each other. The magnetometer and EMI pair of sensors is referred to as ME.

3.4.1 Common Detections

All declarations within a 1.0-m R_{crit} of a baseline ordnance item are considered to determine the common detections for the ME pair. Thus, the distance between declarations can be as great as 2.0 m. The different fit parameters are considered to establish trends that might be exploitable for combining or fusing the two data sets.

3.4.1.1 Detection Location Offset

The location offset is the difference between the fitted location of each detected baseline item (on the *x-y* plane) for the EMI system and the magnetometer. To determine any positional trends in the actual fitted location from the two sensors, the relative east and north position of fitted location for the sensor pair is also examined.

Forty baseline items are common detections for the ME sensor pair. The mean radial distance between detections is 0.27 m, with a standard deviation of 0.22 m. Twenty-four common declarations have a location offset of less than 0.25 m [see Figure 3-24(a)], and only 6 common detections are separated by greater than 0.5 m. None of the common detections are separated by more than 0.88 m. Figure 3-24(c) shows the location error for the magnetometer versus that of the EMI system. It is evident from the figure that the location errors are highly clustered within an area of radius 0.5 m surrounding the baseline item. There is also a suggestion that large location errors for the EMI system tend to be correlated with large location errors for the magnetometer. But the corollary is not true. There are no statistically significant easting or northing location offsets ([Figure 3-24(b)]. Both the mean and the median are within the 0.05-m location error estimate for the RTK-DGPS.

The overall performance suggests that the location errors exhibited by the sensors are small and tend to be similar, although outliers were not correlated. The location error appears to be caused by survey-to-survey location inaccuracies and noise and not by a statistically significant intrinsic property of the ordnance, the *MTADS* system, or the MTR.

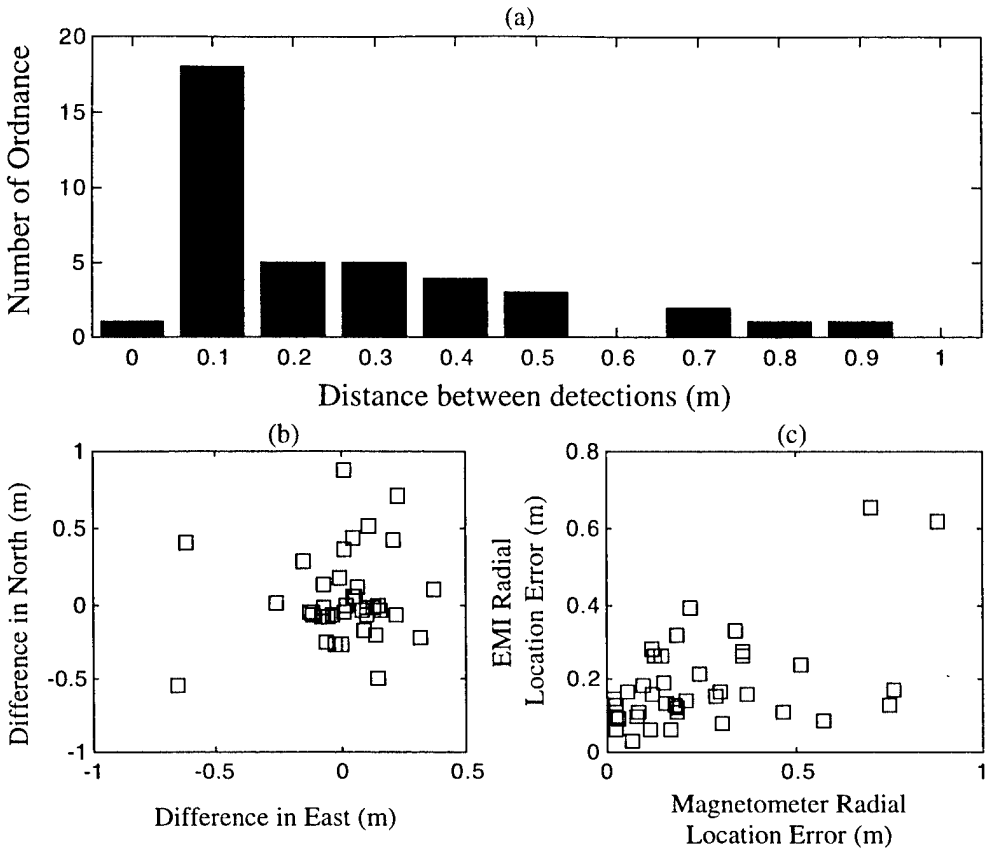

Figure 3-24. Fitted Location Comparison for EMI and Magnetometer. (a) Distribution of Distance Between EMI and Magnetometer Location. (b) Difference in East versus North. (c) Radial Location Error for Magnetometer versus EMI.

3.4.1.2 Detection Depth Offset

The depth offset is the difference between the fitted depth of each detected baseline item (on the *x*-*y* plane) for the two sensors, that is, the target depth estimated from the EMI data subtracted from that estimated from the magnetometer data. The depth offset can be positive or negative. The trend of the sign indicates whether one sensor consistently estimates the depth of the baseline item to be greater than the fitted depth from the other sensor.

In the ME sensor set, 33 of 40 baseline items have a depth offset within ±0.5 m of one another, and 16 of these are within ±0.25 m. There were four detections with depth offsets between –1.0 and –2.0 m [see Figure 3-25(a)]; these are due to the relatively poor depth predictions from the EMI sensor data (and considering the excellent location accuracy, probably due to an ineffective model for calculating depth). The general trend is that the EMI analysis produces a depth that is shallower than that estimated from the

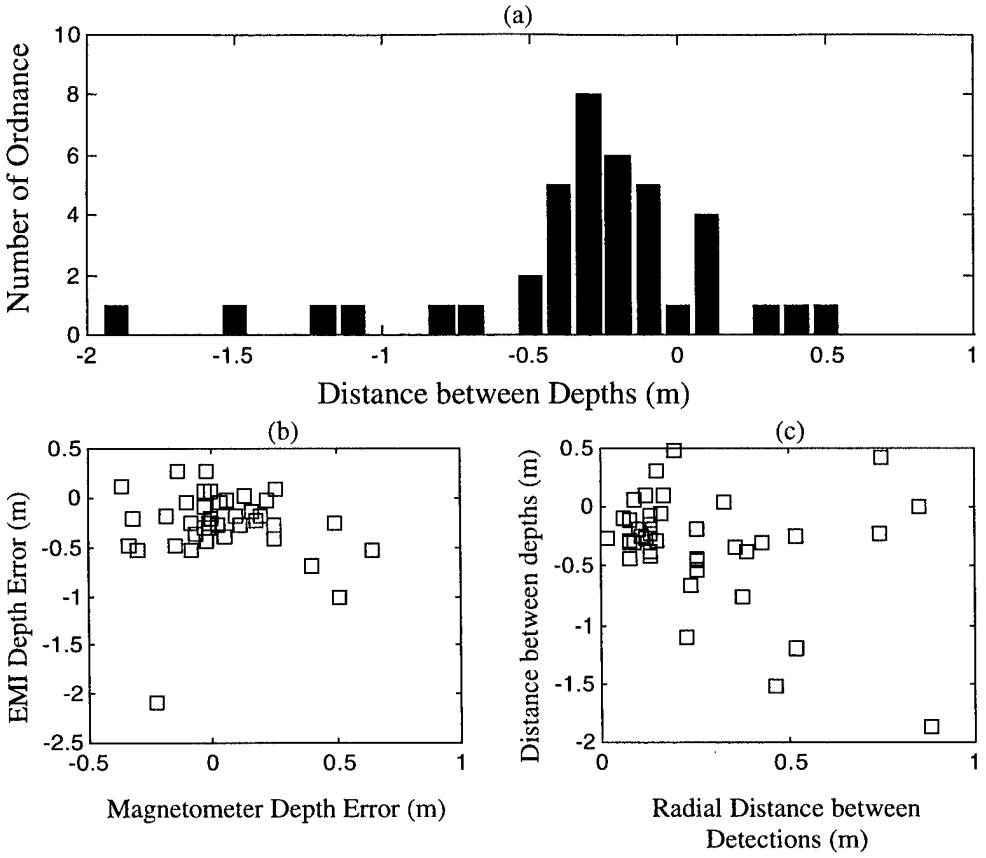

Figure 3-25. Fitted Depth Comparison for EMI and Magnetometer. (a) Distribution of Depth for EMI and Magnetometer. (b) Depth for Magnetometer versus EMI. (c) Radial Distance versus Depth Distance.

magnetometer data. The mean depth offset for the pair is –0.33 m (the negative value results from larger depth for the estimates using the magnetometer data) with a standard deviation of 0.46 m. Thirty-three out of forty depth estimations for the EMI are less than those of the magnetometer.

Figure 3-25(b) shows the depth error for the EMI sensor data relative to magnetometer sensor data. The EMI mean depth error for commonly detected targets is –0.28 m with a standard deviation of 0.39 cm, while the magnetometer has a mean depth error of 0.04 m with a standard deviation of 0.23 m. There is no apparent trend between large depth error in one sensor and large depth error in the other.

Figure 3-25(c) shows the radial distance between the two detections and the depth distance between detections. There is no apparent correlation between large differences in depth and larger radial differences.

3.4.1.3 Detection GoF Comparison

Each time the *MTADS*-DAS attempts to fit a designated anomaly with the appropriate model, a measure of the relative fit of the model to the actual data is established. Because the fit methodology requires the use of data where any field anomaly caused by the presence of a magnetic, conducting, or magnetic and conducting buried anomaly is less than the background level, the dynamic range of the GoF parameter is small. Thus, a fit of less than 0.90 is quite poor. These poor fits are generally associated with very noisy background or atypical compact objects in the ground. Because of the lack of robustness of this metric, the general statistical trends resulting from a comparison using the ME pair may yield very little insight to the system performance.

Common detections for both the magnetometer and EMI system exhibit weakly correlated GoFs [see Figure 3-26(a)]. Only 13 common detections have both fits ≥ 90 percent (this is the entire set of EMI fits at that level), while 32 common detections have at least one GoF parameter ≥ 90 percent. The conclusion from the general trends is that the sources of poor GoFs are dependent on the type of sensor. There appears to be little additional information available to strengthen the detection/discrimination process by comparison of GoFs.

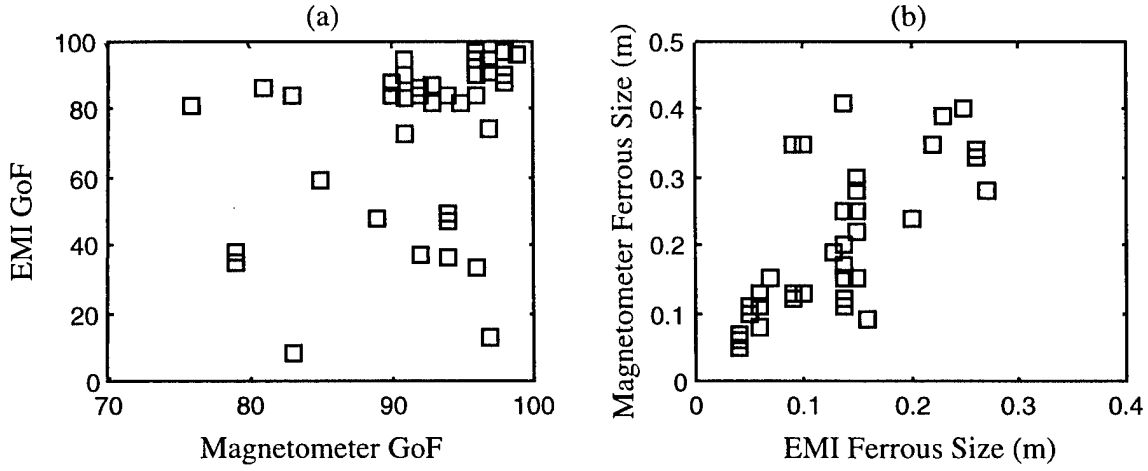

Figure 3-26. Comparison of Fitted Parameters for Magnetometer and EMI. (a) Magnetometer GoF versus EMI GoF. (b) Ferrous Size for Magnetometer versus EMI Ferrous Size.

3.4.1.4 Detection Size Comparison

The *MTADS*-DAS produces several other fit parameters. The set related to size and magnetic moment is not independent. The size of each object is defined as the effecctive radius of a sphere with a designated permeability that can exhibit a geomagnetically

induced magnetic moment consistent with the fitted moment. For the EMI system, which can detect both ferrous and nonferrous materials, an equivalent radius is calculated for each material type. Here, the only difference between the calculations is magnetic permeability and electrical conductivity. Thus, the ferrous and nonferrous sizes are related by a simple scaling constant (dependent on the material characteristics chosen).

The ferrous sizes of the magnetometer and EMI combination are correlated (correlation coefficient = 0.76) [see Figure 3-26(b)]. The fitted ferrous size of all but three magnetometer detections was larger than the corresponding fitted ferrous size for the EMI sensor.

3.4.2 False Alarms Common to the ME Pair

To determine whether there are trends in false-alarm space, we analyzed the false alarms common to the ME sensor pair. In this case, determining common false alarms is nontrivial because contrary to the common detection sets, the source and location of the false alarm is unknown. Thus, we used the following process to establish the common false alarms. The full declaration set for each sensor was parsed into two subsets: declarations that match baseline items and declarations that are false alarms. The two false-alarm sets were then compared by location only (in the x-y plane). A false alarm from one set within 1.0 m (the critical false-alarm radius) of a false alarm from another set was classified as a common false alarm for that sensor pair. It is possible to have more than one false alarm from one sensor set within the designated critical false-alarm radius of the second set, but only the nearest neighbor pair was considered in this analysis. We chose the 1.0-m critical false-alarm radius because of the overwhelming trend to common detection of the baseline items of less than 0.5-m location offset; 1.0 m is approximately three standard deviations from the mean separation for a detection pair.

Using this set of common false alarms, we examined the sensor pair for trends in location offset, depth offset, GoF, and size. The trends in the data show some degree of correlation between the fitted parameters, which confirms our hypothesis that the vast majority of false alarms are the result of compact, near-surface anomalies that act as clutter for the sensor.

3.4.2.1 False-Alarms Location Offset

From the full set of 197 EMI and 608 magnetometer false alarms, there are 67, 86, 92, and 113 common false alarms for critical false-alarm radii of 0.5, 0.75, 1.0, and 2.0 m, respectively. Figure 3-27(a) shows the distribution of distance between the false

alarm locations for the two sensors. The distribution has a median at about 0.38 m. The long tail is probably the result of labeling two discrete false alarms a common false alarm caused by a single clutter item. There is the potential that false alarms that are not really common could be identified by other fit parameters, such as depth. Unluckily, since most clutter is within the first half meter of the ground (see Figure 3-11), false alarms from two different sources are likely to have similar depths.

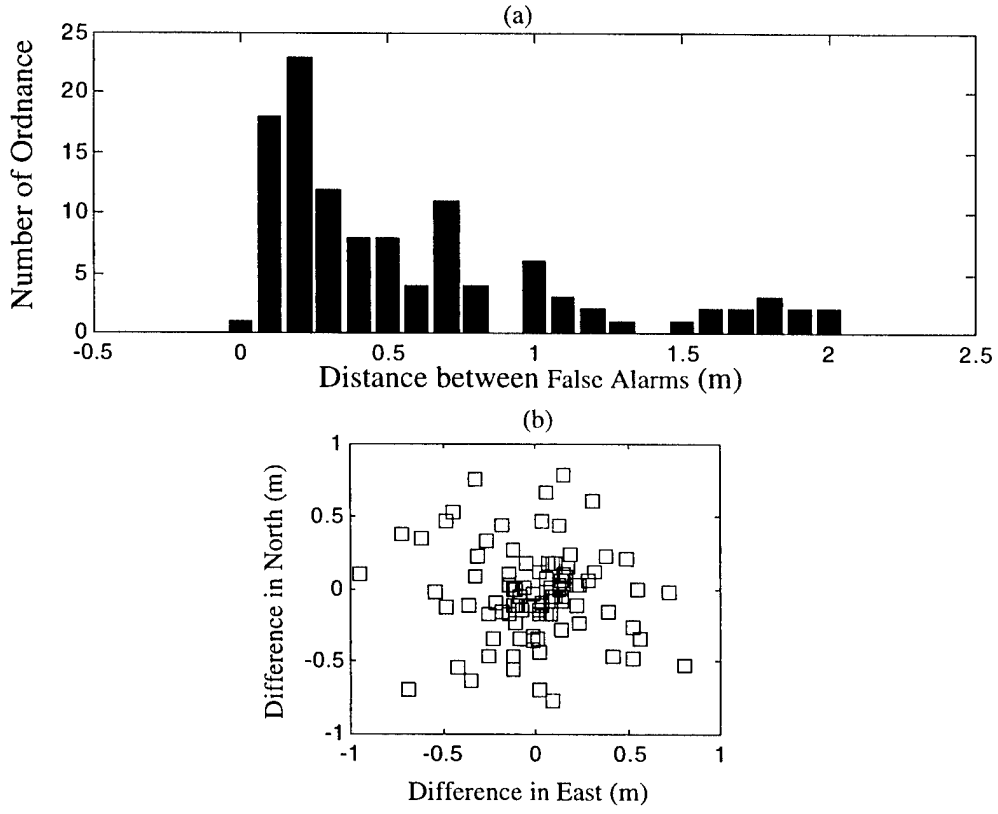

Figure 3-27. Fitted Location Comparison for EMI and Magnetometer Common False Alarms. (a) Distribution of Distance Between EMI and Magnetometer Location. (b) Difference in East versus North.

For this analysis, common false alarms are considered to be only those that have a radial location offset of less than 1.0 m; this subset of false alarms comprises roughly 81 percent of the common false alarms at a critical radius of 2.0 m. The 1.0-m false-alarm critical radius is based on the three-standard-deviation point for common detections for the magnetometer and EMI system.

Figure 3-27(b) shows the location offset for the sensor pair in the east versus north directions. As with the ordnance, the mean and median offsets in each direction are less than the 5-cm location error expected from the RTK-DGPS. In addition, both standard deviations are approximately 30 cm.

3.4.2.2 False-Alarm Depth Offset

For the ME sensor combination, the distribution of depth offsets reveals that 71 of the 92 common false alarms have a depth offset between ±0.25 m. Figure 3-28(a) shows the distribution of the depth offset. Only two outliers exist in this plot: one where the magnetometer fits the anomaly 2.6 m deeper than the EMI system (this is probably not a common detection) and one where the EMI system fits the depth approximately 1 m deeper than the magnetometer. The EMI sensor appears to consistently underestimate the depth of the target; 72 out of 92 (78 percent) common false alarms have the EMI detection depth less than the magnetic detection depth. This is almost identical to the relative depth for the commonly detected ordnance (83 percent). Thus, there is no apparent difference between the depth offset for ordnance and clutter.

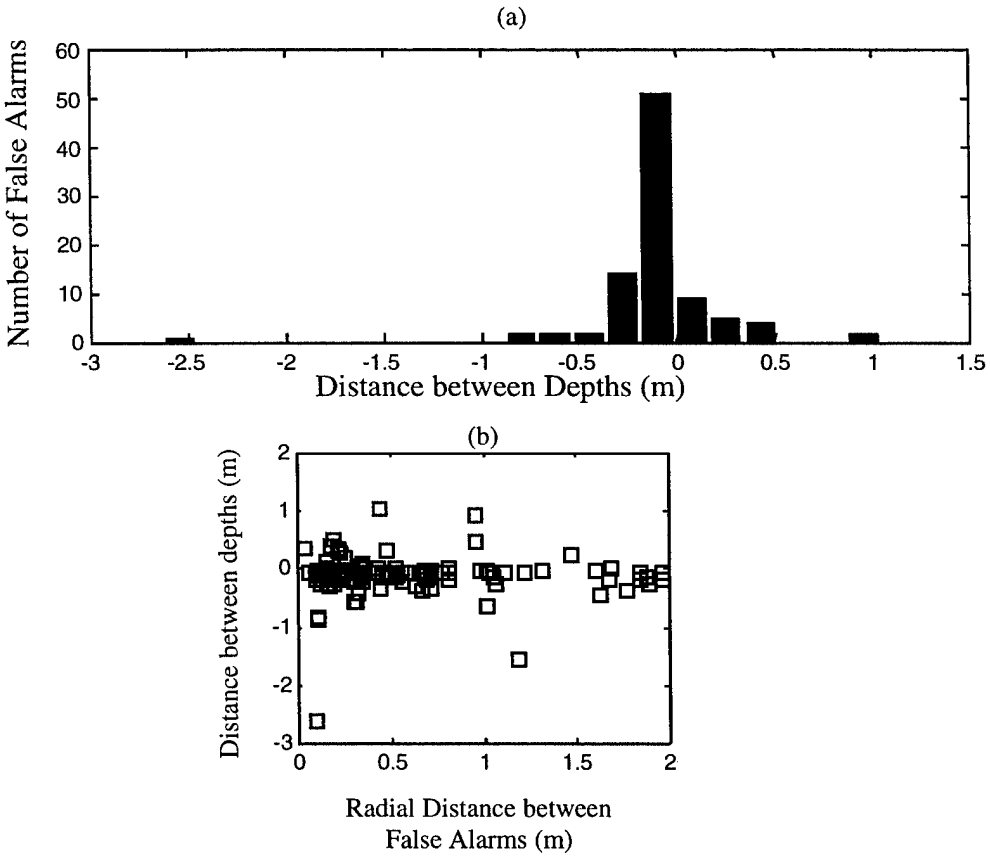

Figure 3-28. Fitted Depth Comparison for EMI and Magnetometer Common False Alarms. (a) Distribution of Depth for EMI and Magnetometer. (b) Radial Distance versus Depth Distance.

Figure 3-28(b) shows a scatter plot of the radial location offset versus the depth offset for common detections. The radial offset and depth offset appear to be uncorrelated.

3.4.2.3 False-Alarm GoF Comparison

The correlation between GoFs of the ME pairs is very low [see Figure 3-29(a)], perhaps due to poor fits from the EMI data. As the figure shows, many declarations with a GoF over 0.9 for the magnetometer have corresponding EMI GoF of less than 0.50 (22 out of 45). This contrasts with the results for the common ordnance detected. There, of the 30 ordnance items with GoF > 0.9 for the magnetometer, only six (20 percent) have an EMI GoF less than 0.5. This suggests that the EMI fitting algorithm has a harder time fitting clutter objects, which are likely to be asymmetric. At the same time, most objects exhibit a strong magnetic dipole moment that fits well to the simple model for magnetic signatures. Thus, a difference in GoFs for the two systems might provide potential for discrimination using the "fused" data set. It should be noted that the reciprocal pattern is not true. Good GoF for the EMI always corresponds to good GoF for the magnetometer.

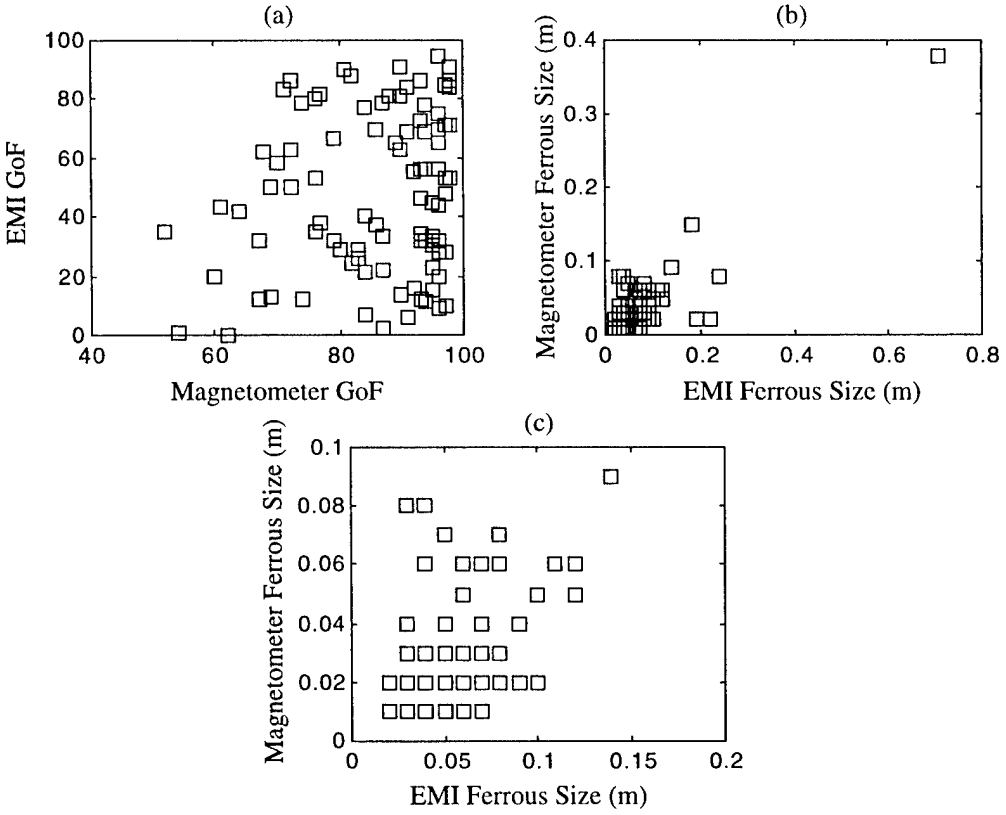

Figure 3-29. Comparison of Fitted Parameters for Magnetometer and EMI for Common False Alarms. (a) Magnetometer GoF versus EMI GoF. (b) Ferrous Size for EMI versus Magnetometer Ferrous Size. (c) Ferrous Size for EMI versus Magnetometer Ferrous Size for Small Sizes.

3.4.2.4 False-Alarm Size Comparison

The ferrous sizes of the magnetometer and EMI combination are well correlated (correlation coefficient = 0.84). The fitted ferrous size of all but seven of the magnetometer false alarms was greater than or equal to the corresponding fitted ferrous size for the EMI sensor. Figure 3-29(b) shows a scatter plot of fitted ferrous size for the magnetometer and EMI. Figure 3-29(c) is a scatter plot of the smallest sized objects.

4.0 NRL DECLARATION ANALYSIS

This chapter contains an analysis of target declarations selected by NRL using the *MTADS*-DAS for the three surveys[1] at the MTR at Twentynine Palms. NRL did all analysis and provided IDA three spread sheets (one each for magnetometer, magnetic gradiometer, and EMI) containing the analysis results. As with the analysis of the IDA declaration presented in Chapter 3, NRL examined detection and false-alarm performance and analyzed sensor-specific declaration parameters provided by the *MTADS*-DAS. The data from the *MTADS*-DAS include several parameters used to characterize sensor performance. For the magnetometer and magnetic gradiometer, these parameters include magnitude of the fit magnetic moment, inclination and declination of the fit magnetic moment (and also ferrous size), depth, northing coordinate, easting coordinate, and GoF. For the EMI sensor the parameters include depth, northing coordinate, easting coordinate, ferrous and nonferrous size, and GoF. Along with detection performance (this includes both detection rates and false-alarm rates), the fitted parameters for each detection are analyzed. In addition, trends and common features for both detections and false alarms are presented for the ME sensor pair.

The chapter is broken down into six sections. The first section presents the detection and false-alarm rates and a discussion of false-alarm mitigation applied to the NRL magnetometer and magnetic gradiometer data. The second section is an analysis of the location and depth accuracy relative to fitted parameters available from the *MTADS*-DAS. The third section gives an evaluation of the trends in both detection and false-alarm space for the ME sensor pair. The fourth section is a comparison of the results obtained by IDA (presented in Chapter 3) and those obtained by NRL during its sensor data analysis. The final two sections present information on unique false alarms and data fusion using logical operations.

---

1 These three survey runs are the same runs analyzed by IDA in Chapter 3. For that reason it is possible to do a one-to-one comparison between the IDA results and the NRL results.

4.1 GENERAL PERFORMANCE RESULTS

We compare each declaration data set generated by NRL using the *MTADS*-DAS to the emplaced target baseline, using only the nongrouped ordnance (see Section 3.1.1). To match target declarations to the baseline, we determine if the relative northing/easting position of the declaration is within the critical radius, R_{crit}, of the center of the emplaced ordnance item. If the declaration falls outside R_{crit}, the declaration is classified as a false alarm. Because of NRL's substantial field experience with the MTR at Twentynine Palms, their performance may be enhanced by man-in-the-loop discrimination.

4.1.1 Detection and False-Alarm Rates

A modified declaration set is produced for each sensor type. For the magnetometer and magnetic gradiometer, only a relative inclination test is used to discriminate between potential targets and potential false alarms. This abbreviated discrimination algorithm is used because the relative inclination discriminator is more robust than the other contributions used on the IDA declaration set, and the experienced operator visually preprocessed the data to eliminate targets that were too small or on the surface. Thus, only relative inclination is needed to perform a second round of discrimination. The conditions used are the following:

- Confidence level 0—The relative inclination is greater than 40 deg.
- Confidence level 1—The relative inclination is between 35 deg and 40 deg and all of confidence level 0.
- Confidence level 2—The relative inclination is between 30 deg and 35 deg and all of confidence level 1.

Detection probabilities and false-alarm rates can be determined for the three sets of data. Table 4-1 lists P_d, *FAR*, and P_{fa} for an R_{crit} of 0.5 m and 1.0 m. Here, as in Chapter 3, after use of the discrimination algorithm, P_{fa} is represented by a surrogate: the fraction of the test site covered by false-alarm areas with R_{crit} radius. The *FAR* is calculated assuming an approximately 8-acre test site (30,686.6 m^2). No attempt has been made to account for areas not covered by *MTADS*.

The ROC approach provides a mechanism to evaluate the relative performance of systems or algorithms for a given R_{crit}. Figures 4-1 and 4-2 show the probability of detection versus probability of false alarm for all sensors at R_{crit} of 0.5 m and 1.0 m, respectively. The solid lines are isoperformance curves (discussed in Chapter 3) calculated by

Table 4-1. Detection and False-Alarm Performance of *MTADS* from NRL Analysis

Sensor+	R_{crit} 0.5 m			R_{crit} 1.0 m		
	P_d	*FAR* (m^{-2})	P_{fa}	P_d	*FAR* (m^{-2})	P_{fa}
Magnetometer (Full Data Set)	0.694	7.7×10^{-3}	6.1×10^{-3}	0.823	7.4×10^{-3}	2.4×10^{-2}
Magnetometer (Confidence Level 2)	0.677	5.1×10^{-3}	4.1×10^{-3}	0.790	4.9×10^{-3}	1.5×10^{-2}
Magnetometer (Confidence Level 1)	0.661	4.9×10^{-3}	3.9×10^{-3}	0.774	4.7×10^{-3}	1.5×10^{-2}
Magnetometer (Confidence Level 0)	0.645	4.6×10^{-3}	3.6×10^{-3}	0.742	4.4×10^{-3}	1.4×10^{-2}
Magnetic Gradiometer (Full Data Set)	0.548	8.2×10^{-3}	6.5×10^{-3}	0.774	7.7×10^{-3}	2.4×10^{-2}
Magnetic Gradiometer (Confidence Level 2)	0.516	5.4×10^{-3}	4.2×10^{-3}	0.726	4.9×10^{-3}	1.6×10^{-2}
Magnetic Gradiometer (Confidence Level 1)	0.516	4.9×10^{-3}	3.9×10^{-3}	0.726	4.4×10^{-3}	1.4×10^{-2}
Magnetic Gradiometer (Confidence Level 0)	0.500	4.6×10^{-3}	3.6×10^{-3}	0.710	4.1×10^{-3}	1.3×10^{-2}
Electromagnetic Induction	0.790	4.9×10^{-3}	3.8×10^{-3}	0.839	4.8×10^{-3}	1.5×10^{-2}

+ The declaration set determined by using the *MTADS*-DAS is considered the full data set. For this set only magnetic moment modeling was used to reduce the number of declarations. Confidence Level 2 refers to the set of declarations with a final IDA ranking of 2 or less (relative inclination greater than 30 deg). Confidence Level 1 refers to the set of declarations with a final IDA ranking of 1 or less (relative inclination greater than 35 deg). Confidence Level 0 refers to the set of declarations with a final IDA ranking of 0 (relative inclination greater than 40 deg).

using a Gaussian model for the distribution functions of the target and clutter/noise signatures.[2] The multiple points presented for each sensor are related to the false-alarm discrimination algorithm using the relative inclination. Looking at an R_{crit} of 0.5 m (Figure 4-1) for the four points (representing confidence levels 0, 1, 2, and the full set) that result from implementation of the discrimination algorithm, the magnetometer performance does not improve over the three different confidence levels (the three points fall on a single isoperformance curve within statistical error). There is, however, a slight performance improvement using the discrimination algorithm over that of the full magnetometer data set. The trend for an R_{crit} of 1.0 m is a little different. There is virtually no performance improvement from the full magnetometer set to the confidence levels 1 and 2 sets, and a decrease in performance at confidence level 0. Note that the statistical significance of this is limited because of the small number of targets.

2 The Gaussian model used here assumes the same variance for the noise/clutter and the ordnance.

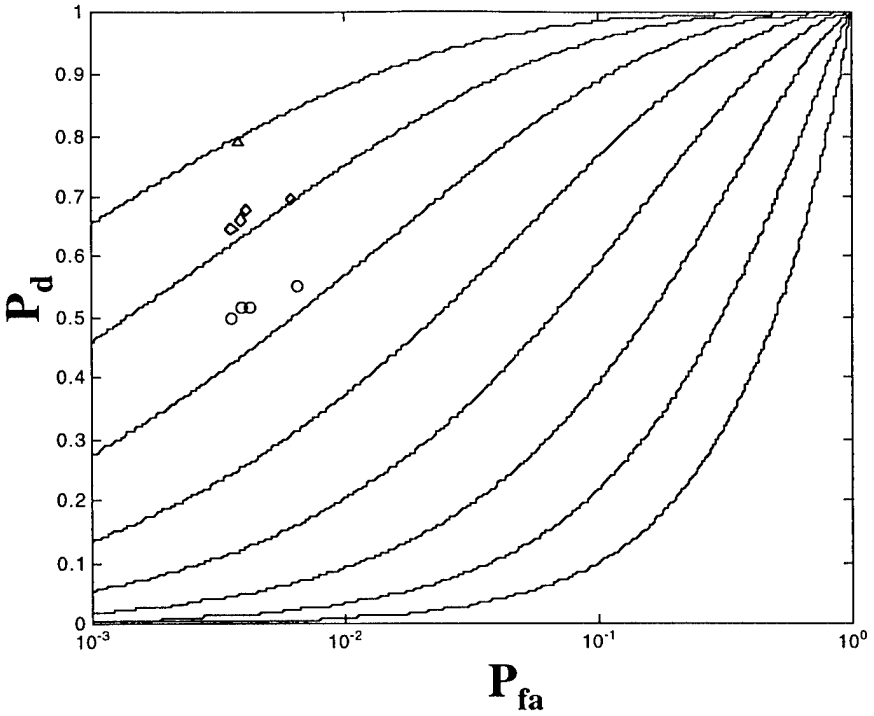

Figure 4-1. Probability of Detection versus Probability of False Alarm for the Magnetometer (Diamonds), Magnetic Gradiometer (Circles), and EMI System (Triangle). R_{crit} is 0.5 m. For the magnetometer and magnetic gradiometer, confidence levels of 0, 1, and 2 (using only relative inclination) and full data set are circles from left to right, respectively.

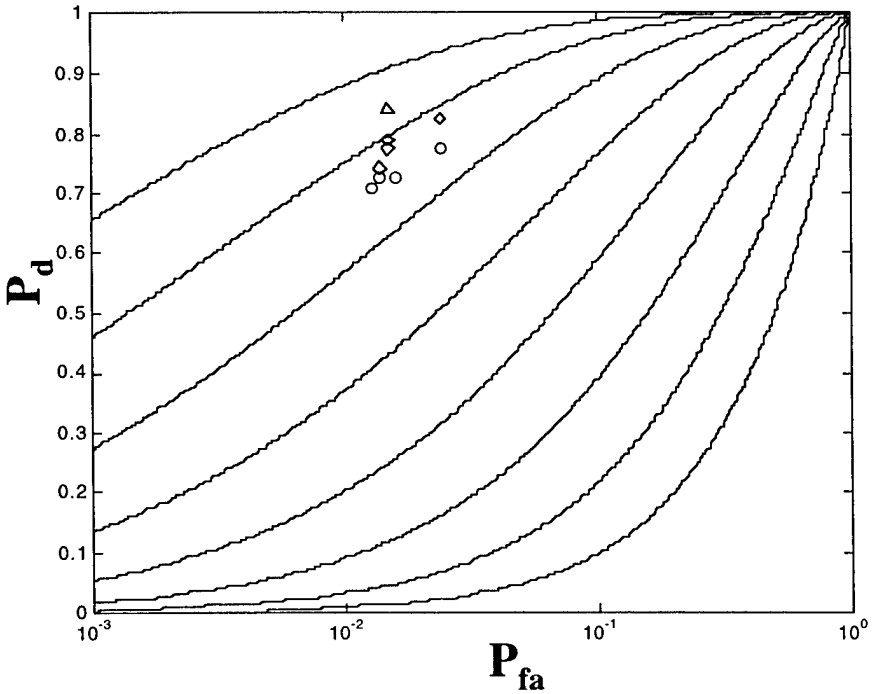

Figure 4-2. Probability of Detection versus Probability of False Alarm for the Magnetometer (Diamonds), Magnetic Gradiometer (Circles), and EMI System (Triangle). R_{crit} is 1.0 m. For the magnetometer and magnetic gradiometer, confidence levels of 0, 1, and 2 (using only relative inclination) and full data set are circles from left to right, respectively.

Figures 4-1 and 4-2 also show performance of the magnetic gradiometer using the ROC approach for R_{crit} of 0.5 m and 1.0 m, respectively. For the magnetic gradiometer, the slightly improved performance seen for the magnetometer is again seen for the 0.5-m R_{crit}. The performance remains the same with implementation of the discrimination algorithm for R_{crit} of 1.0 m.

After implementation of the relative inclination discrimination algorithm, the EMI sensor has the best overall performance, exceeding even the magnetometer and magnetic gradiometer performance. The performance of the magnetometer is better than that of the magnetic gradiometer, even for the full data set.

4.1.2 Performance Dependence on Critical Radius

As discussed above, the probability of detection and false-alarm rate are dependent on the R_{crit} used to determine detections. Figures 4-3(a)–(c) show the probability of detection and number of detections as a function of R_{crit} for the magnetometer, magnetic gradiometer, and EMI system, respectively. For the magnetic detection systems, the number of detections increases slowly above an R_{crit} of approximately 1 m. This gradual increase in the number of ordnance items detected above an R_{crit} of 1.0 m may be caused by detections that are "lucky" matches (Altshuler et al., 1996) or by potentially true detections with very poor location accuracy (more than three standard deviations above the mean). The EMI detection system exhibits even better P_d versus R_{crit} performance, with no significant increase in detection rates above approximately 0.6 m. Table 4-2 contains the mean and standard deviation of the radial location accuracy and the depth accuracy[3] (both true and absolute) for all three sensor configurations for a 1-m critical radius. The EMI system exhibits the best location accuracy, but also shows the largest depth error, with a trend of underestimating the depth of the ordnance item. In all cases, for both location and depth accuracy, the *MTADS* platform and *MTADS*-DAS performed quite well.

4.1.3 False-Alarm Mitigation Technique

A relative inclination-based false-alarm mitigation technique is used to sort potential ordnance from nonordnance for both the magnetometer and magnetic gradiometer

---

[3] Both accuracy and error are used in this document to refer to the difference in the location and depth determined by the *MTADS*-DAS fitting algorithm and the baseline emplaced position of ordnance.

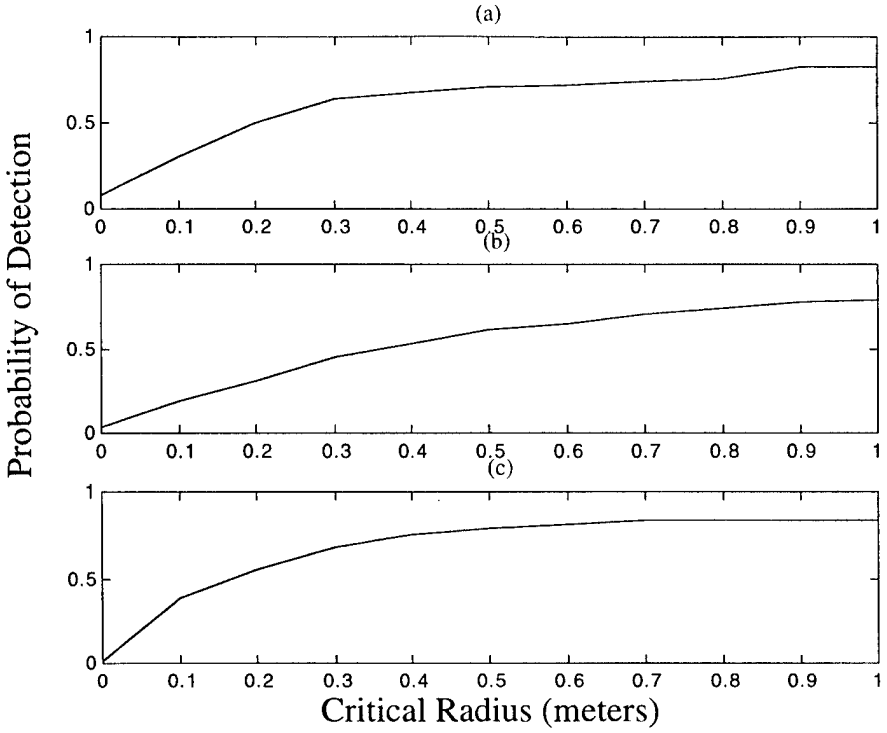

Figure 4-3. Detection Performance versus Critical Radius for the Emplaced Targets. (a) Magnetometer. (b) Magnetic Gradiometer. (c) EMI System.

Table 4-2. Detection Location Error and Depth Error for 1-m Critical Radius

Sensor	Radial		Depth		Magnitude Depth	
	Mean Error (m)	Standard Deviation (m)	Mean Error (m)	Standard Deviation (m)	Mean Error (m)	Standard Deviation (m)
Magnetometer	0.28	0.24	0.10	0.39	0.26	0.31
Magnetic Gradiometer	0.37	0.26	0.09	0.66	0.28	0.61
EMI	0.27	0.16	–0.19	0.52	0.37	0.41

declaration set. The false-alarm mitigation is performed using a confidence rankings scheme that weights each declaration based on the orientation of the magnetic moment relative to the geomagnetic field. The false-alarm mitigation technique relies on a preferential direction of the ordnance magnetic moment. This technique assumes ordnance magnetization is dominated by that magnetization induced by the geomagnetic field; i.e., the remanent magnetization is small. On the other hand, the source of false alarms, clutter, is predicted to exhibit a more uniform angular distribution of magnetic

moments. Figures 4-4(a) and 4-5(a) show the distribution of magnetic moment direction for the detected ordnance for the magnetometer and magnetic gradiometer, respectively. The cut-off for the algorithm used for the NRL data to separate moments with a confidence level of 2 or less is approximately 30 deg.[4] The magnetometer data show only 2 out of 51 ordnance items with a relative inclination of less than 30 deg. In this figure the data is binned in 5-deg groups centered at 5-deg intervals, i.e., 25, 30, 35, etc. The magnetic gradiometer produces similar number of ordnance items that possess a relative inclination below 30 deg (3 out of 48).

Figures 4-4(b) and 4-5(b) show the distribution of the relative inclination of the false alarms. For the magnetometer there is a significant population of the angular distribution for nonordnance with a relative inclination below 30 deg, in contrast to the ordnance population. In addition, the distribution function for false alarms from the magnetic gradiometer also exhibits a significant population below a relative inclination 30 deg.

4.1.4 False Alarms

The depth distribution for false alarms exhibits an interesting difference between the active EMI system and the passive magnetostatic detection techniques. Figure 4-6 shows the number of false alarms as a function of depth for each sensor. Although for all sensors there are a substantial number of false alarms in the first 0.1 m of the ground, the EMI does not produce many additional false alarms at greater depths (only 3 out 146 false alarms exist below 1 m). On the other hand, for the magnetometer and magnetic gradiometer, the distribution has approximately 10 percent of the false alarm population at depths below 1 m.[5] This feature may provide some method for discrimination, but a number of issues must be addressed.

- The EMI system shows poor depth accuracy (larger than the bins used to generate Figure 4-6). Thus, the clutter responsible for the EMI anomaly may have a different depth distribution function than shown in Figure 4-6.
- The magnetometer and magnetic gradiometer tend to perform more poorly detecting small objects near the surface (these can be UXO) than the EMI system.

---

4 The angle used is measured with the geo-coordinate rotated so that the geomagnetic field is along the z-axis. This results in a geomagnetic field inclination of 90 deg. Thus, when this report refers to relative inclination, the reference is the rotated geo-coordinate system.

5 In this analysis the data show a greater percentage of false alarms at greater depths compared to the targets picked by IDA discussed in Section 3.1.4. This difference is the result of the depth discrimination done by the analyst at NRL responsible for picking targets.

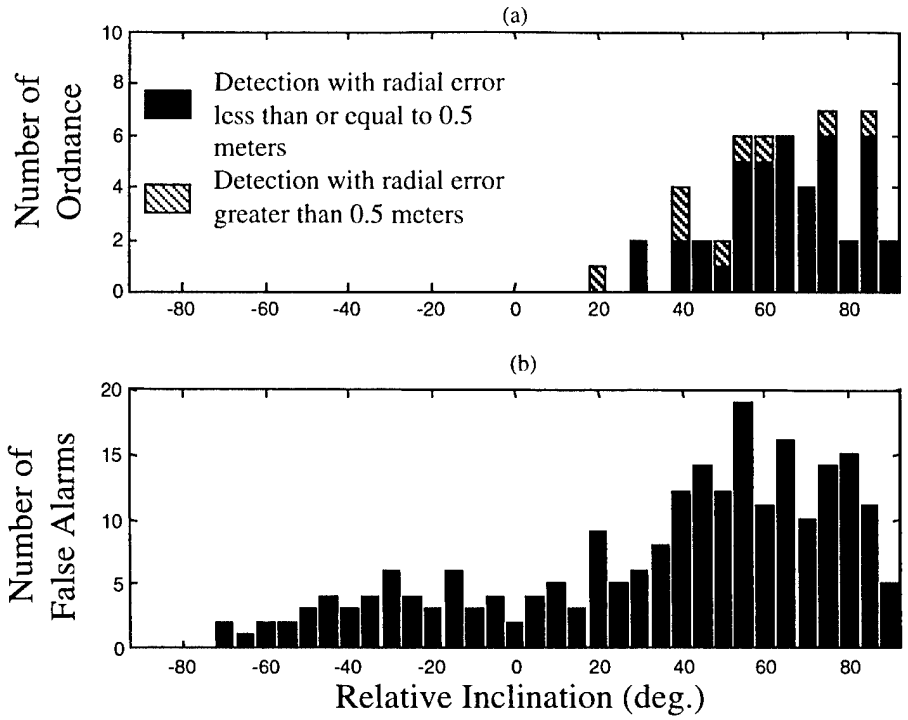

Figure 4-4. Distribution of Magnetic Moments Relative to the Geomagnetic Field as Measured by the Magnetometer. Relative Inclination of 90 deg is Aligned with the Geomagnetic Field. Relative Inclination of 0 deg is Orthogonal to Geomagnetic Field. (a) Ordnance. (b) False Alarms.

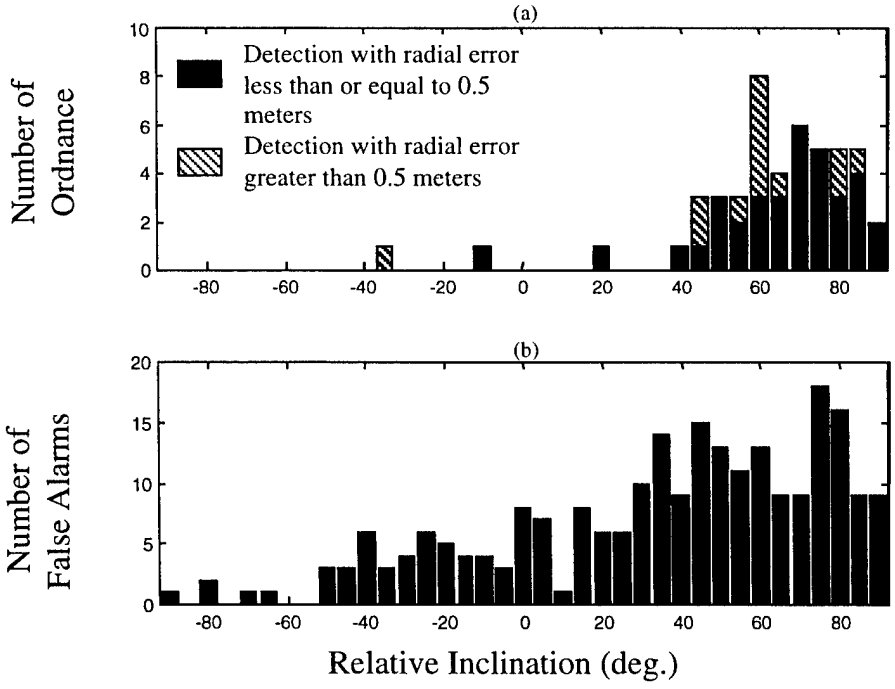

Figure 4-5. Distribution of Magnetic Moments Relative to the Geomagnetic Field as Measured by the Magnetic Gradiometer. Relative Inclination of 90 deg is Aligned with the Geomagnetic Field. Relative Inclination of 0 deg is Orthogonal to Geomagnetic Field. (a) Ordnance. (b) False Alarms.

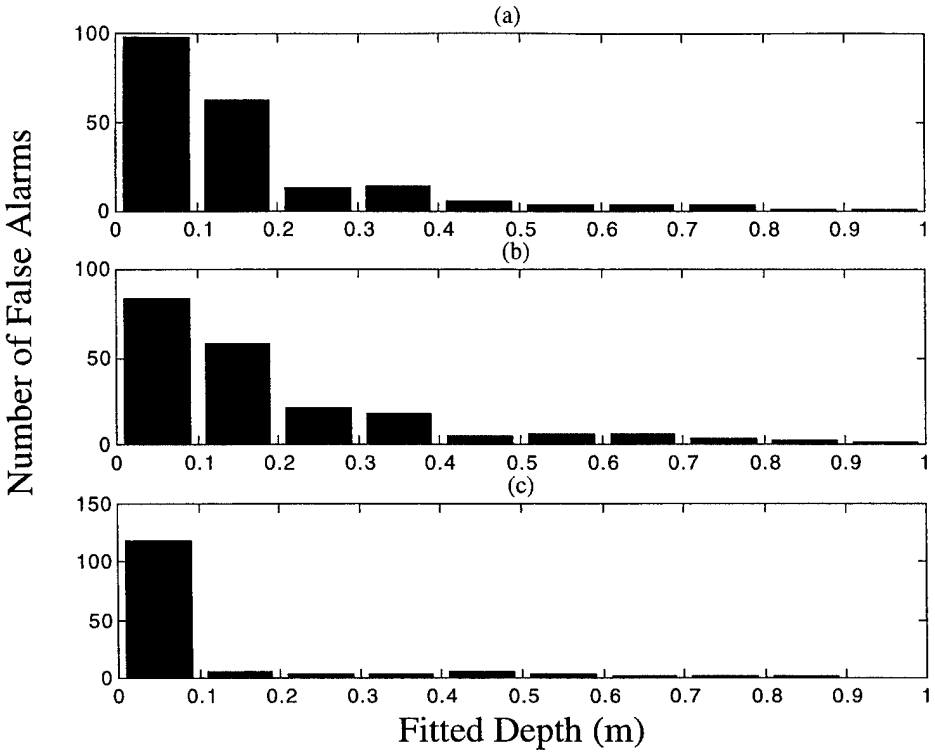

Figure 4-6. Number of False Alarms as a Function of Fitted Depth. (a) Magnetometer. (b) Magnetic Gradiometer. (c) EMI System.

4.2 SENSOR PERFORMANCE

This section characterizes the system location performance for detected ordnance by evaluating the *MTADS*-DAS parameters and determining trends. For this set of calculations, the grouping of targets is not used. For each sensor type, the entire declaration set is matched to ungrouped sets of emplaced ordnance. A critical radius of 1 m is used to determine the set of declarations that match emplaced ordnance from the target baseline. Within a 1-m critical radius, analysis of the NRL declaration set resulted in the following detection statistics:

- 51 out of 62 (82.3 percent) ungrouped baseline items with the magnetometer,
- 48 out of 62 (77.4 percent) baseline items with the magnetic gradiometer, and
- 52 out of 62 (83.9 percent) baseline items with the EMI sensor.

Below we discuss physical trends for each group of baseline items detected by a sensor.

4.2.1 Sensor Performance: Radial Location Accuracy

For each sensor declaration which matches an emplaced ordnance item within the 1-m critical radius, the coordinates of the fitted anomaly and radial location accuracy or radial location error are recorded (radial location accuracy = fitted anomaly location – actual location of detected ordnance item). The results of the analysis follow.

4.2.1.1 Magnetometer

The mean radial location accuracy for the targets detected by the *MTADS* platform is 0.28 m, with a standard deviation of 0.24 m. Since the fitted dipole moment is weakly correlated to the location accuracy, the magnitude of the radial location error does not appear to affect the magnitude of the fit magnetic moment of the selected anomaly [see Figure 4-7(a)].

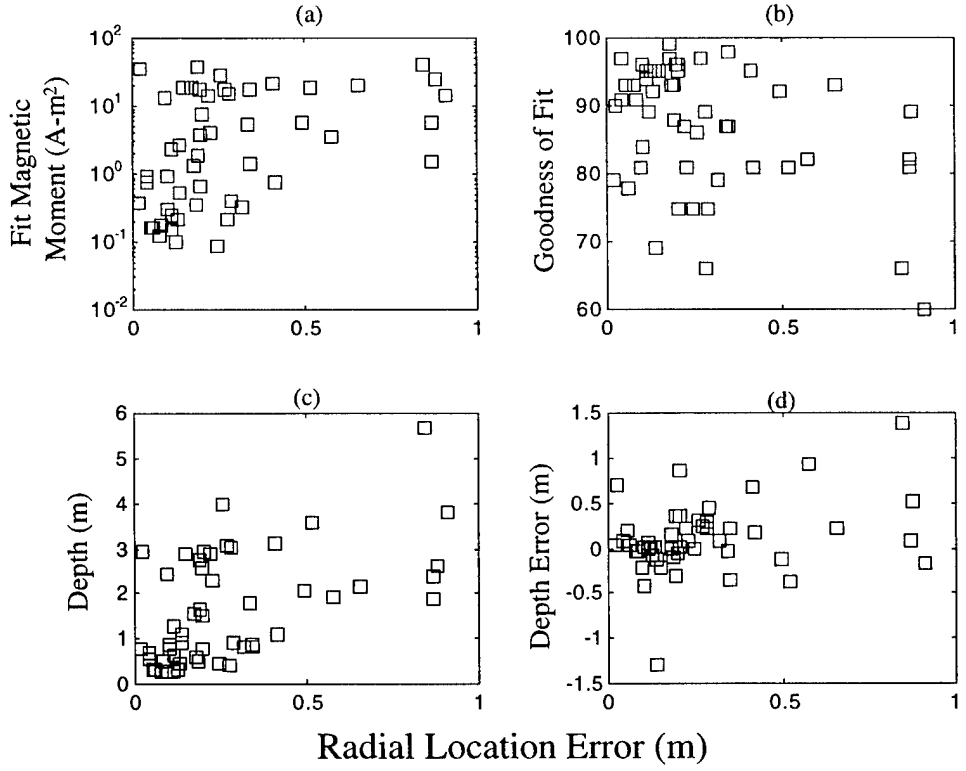

Figure 4-7. Radial Location Error for the Magnetometer. (a) Versus Fit Magnetic Moment. (b) Versus GoF. (c) Versus Depth. (d) Versus Depth Error.

The GoF parameter is found not to be an accurate metric for the radial location accuracy [see Figure 4-7(b)]. There is a general trend that location accuracy decreases with decreasing GoF. A GoF greater than 0.85 is a strong indication of a low radial error: only 2 of the 33 detected baseline items with a GoF greater than 0.85 have a radial error larger than 0.5 m. But a low fit parameter does not correlate with the radial error.

Eighteen detected ordnance items have a GoF of 0.85 or below. Of those, twelve have a radial error less than 0.5 m. In addition, four detected ordnance items, ranging from a 60-mm mortar to 750-lb bomb, have GoF less than 0.75 (see Table 4-3). The radial error for these four ordnance items ranges between 0.14 m and 0.91 m.

Table 4-3. Radial and Depth Errors for Poorly Fit Ordnance Detected by Magnetometer

Description	GoF	Radial Error (m)	Relative Depth Error
60 mm	0.66	0.28	0.55
250 lb	0.69	0.14	– 1.18
500 lb	0.66	0.84	0.25
750 lb	0.60	0.91	– 0.05

There is minimal correlation between depth or depth error and location accuracy [see Figure 4-7(c) and (d)]. Again, the best locator accuracy is often associated with good depth accuracy, but the trend is not compelling.

4.2.1.2 Magnetic Gradiometer

The mean radial location accuracy for the targets detected by the *MTADS* platform is 0.37 m with a standard deviation of 0.24 m. A plot of the magnitude of the fit magnetic moment versus radial location error reveals a low correlation between these fit parameters [see Figure 4-8(a)].

GoF for the magnetic gradiometer is not as good a measure as it is for the magnetometer [see Figure 4-8(b)]. There are 11 detected targets with GoF less than 0.5 (23 percent), 2 of which had radial errors less than 0.5 m. Almost 43 percent have a GoF of 0.75 or less compared to less than 10 percent for the magnetometer, and 11 (23 percent) have a GoF less than 0.5 (see Table 4-4). Deeper objects show more scatter in location accuracy than do shallow objects [see Figures 4-8(c) and (d)]. As expected, the fitted target depth did not correlate with the location accuracy, although the largest depth errors had large radial location errors.

4.2.1.3 EMI

The mean radial location accuracy for the detected baseline items is 0.22 m with a standard deviation of 0.16 m. Comparing target selection of the individual sensors, the EMI system has the best location accuracy. The size of the object does not seem to be well correlated with the location accuracy [Figure 4-9(a)].

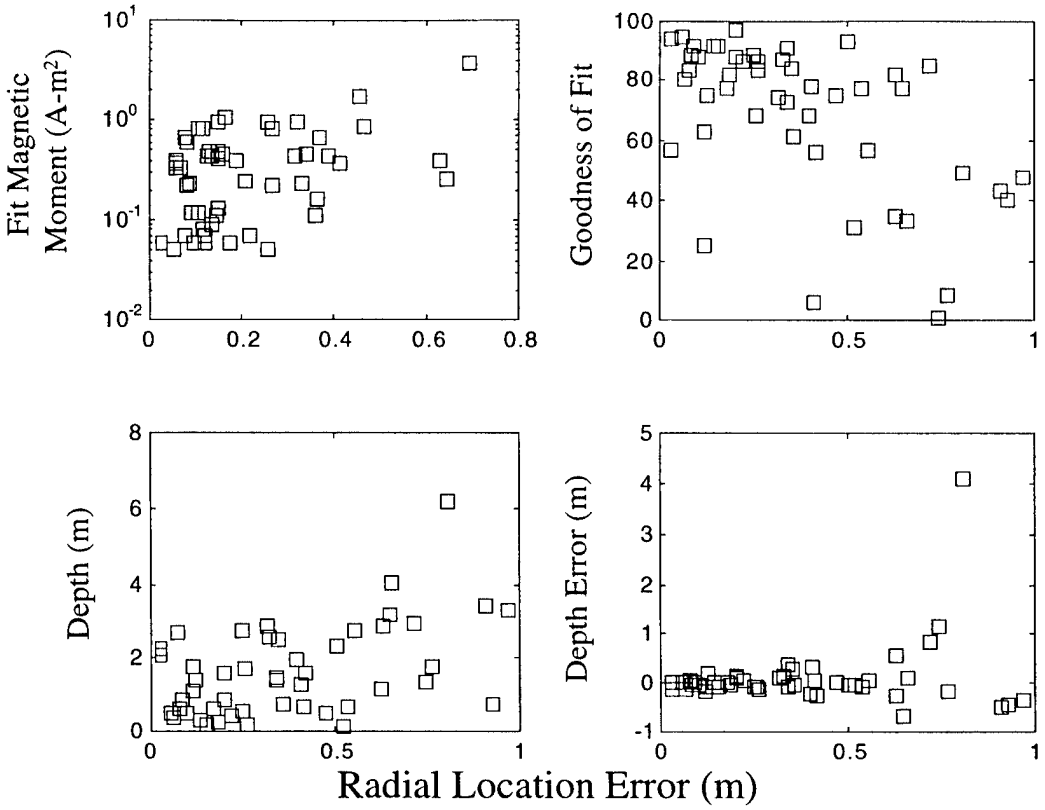

Figure 4-8. Radial Location Error for the Magnetic Gradiometer. (a) Versus Fit Magnetic Moment. (b) Versus GoF. (c) Versus Depth. (d) Versus Depth Error.

Table 4-4. Radial and Depth Errors for Poorly Fit Ordnance Detected by Magnetic Gradiometer

Baseline Item	GoF	Radial Error (m)	Relative Depth Error
8 in.	0.01	0.74	0.88
60 mm	0.06	0.41	0.06
155 mm	0.08	0.76	–0.10
81 mm	0.25	0.12	–0.09
105 mm	0.31	0.52	–0.38
250 lb	0.33	0.66	0.02
105 mm	0.35	0.63	0.47
105 mm	0.40	0.93	–0.61
60 mm	0.43	0.91	–0.15
60 mm	0.48	0.97	–0.12
250 lb	0.49	0.81	0.66

There were 11 targets with a GoF less than 0.40; the radial location accuracy of this subgroup of targets was less than 0.7 m [see Figure 4-9(b)]. The GoF parameter is not a good metric for location accuracy: poor correlation is exhibited. In addition, the

fitted depth of the object was not found to have a strong relation with the location error. Figures 4-9(c) and (d) show that there is more scatter in depth error for large errors.

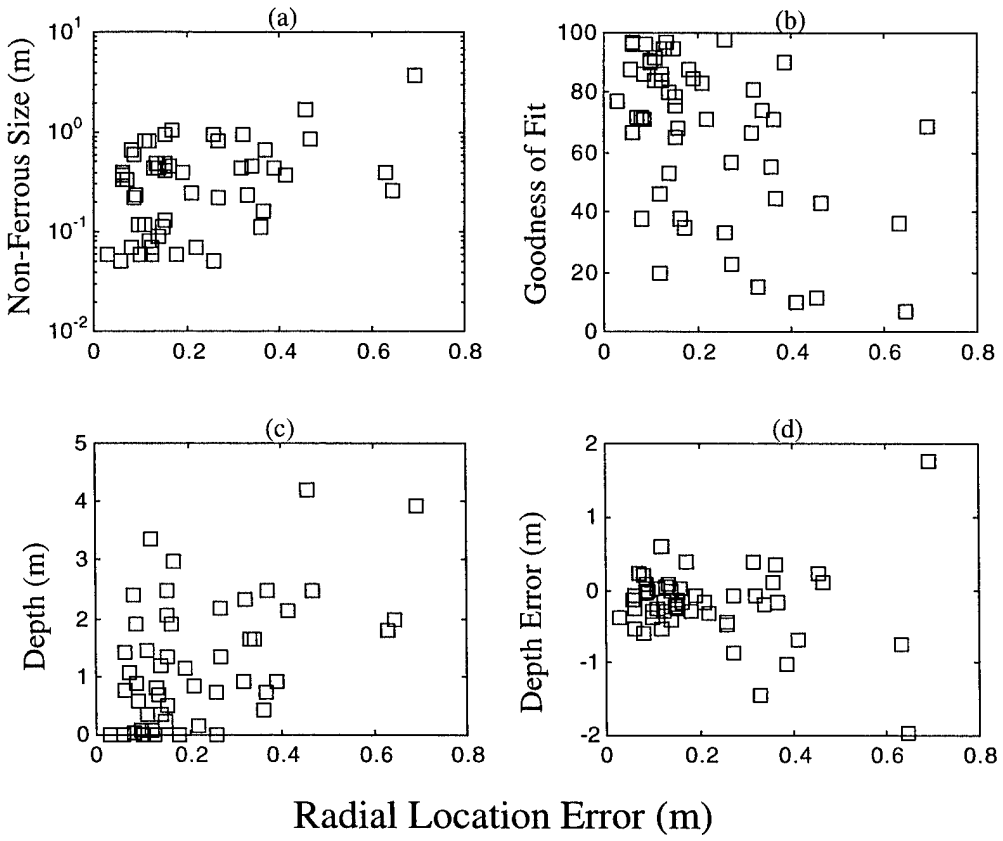

Figure 4-9. Radial Location Error for the EMI System. (a) Versus Nonferrous Size. (b) Versus GoF. (c) Versus Depth. (d) Versus Depth Error.

4.2.2 Sensor Performance: NRL Depth Accuracy

In this section, we analyze the NRL depth accuracy for the targets which matched baseline items within a 1-m halo.

4.2.2.1 Magnetometer

The average depth offset[6] for the detected baseline items is 0.26 m, with a standard deviation of 0.31 m. The mean relative depth offset[7] was 0.173, with a standard deviation of 0.200. Table 4-5 lists the targets having relative depth errors greater than ±0.25.

---

6 Depth offset is the positive difference between the fit depth and the actual depth of a baseline item.

7 Relative depth offset is the depth offset normalized to the fit depth of the baseline item. Relative depth error maintains the sign.

Table 4-5. Ordnance with Large Relative Depth Error

Description	Rel. Depth Error	Actual Depth (m)	Radial Error (m)	Fit
250 lb	–1.18	2.38	0.14	0.69
81 mm	0.64	0.61	0.61	0.62
155 mm	–0.57	1.19	0.10	0.84
60 mm	0.56	0.15	0.05	0.93
60 mm	0.55	0.18	0.28	0.66
60 mm	0.49	0.46	0.29	0.75
105 mm	0.48	1.01	0.58	0.82
500 lb	–0.40	1.22	0.34	0.98
8 in.	0.30	2.07	0.20	0.75

The objects with large relative depth errors tend to be objects with small magnetic signatures buried within 1 m of the surface. The clutter may have contributed to the poor GoF.

There is a weak relation between the fit depth and the relative depth error (the linear correlation coefficient is –0.72): the near-surface objects tend to have higher relative depth errors, as would be expected.

There is poor correlation between the magnetic moment and depth error [see Figure 4-10(a)]. There also is no general trend between magnetometer moment and relative depth error.

GoF is a weak metric for depth accuracy: the correlation coefficient between depth and GoF is close to zero [see Figure 4-10(d)]. The correlation between GoF and relative depth error is also very nearly zero, which suggests that the relative depth errors can not be attributed to poor fits. Very deep objects (>3 m) had radial errors between 0.6 and 1.0 m. Six out of ten targets with fit depth greater than 3 m were detected. Among these targets were a 500-lb bomb, a 750-lb bomb, and an 8-in. shell.

4.2.2.2 Magnetic Gradiometer

The average depth offset for the baseline items detected by the magnetic gradiometer is 0.28 m, with a standard deviation of 0.61 m. Excluding one 8-in. shell with an anomalous depth error of 4 m,[8] the average depth offset is 0.19 m, with a standard

[8] IDA also found this 8-in. shell with a depth error of 0.14 m and a radial error of 0.64 m.

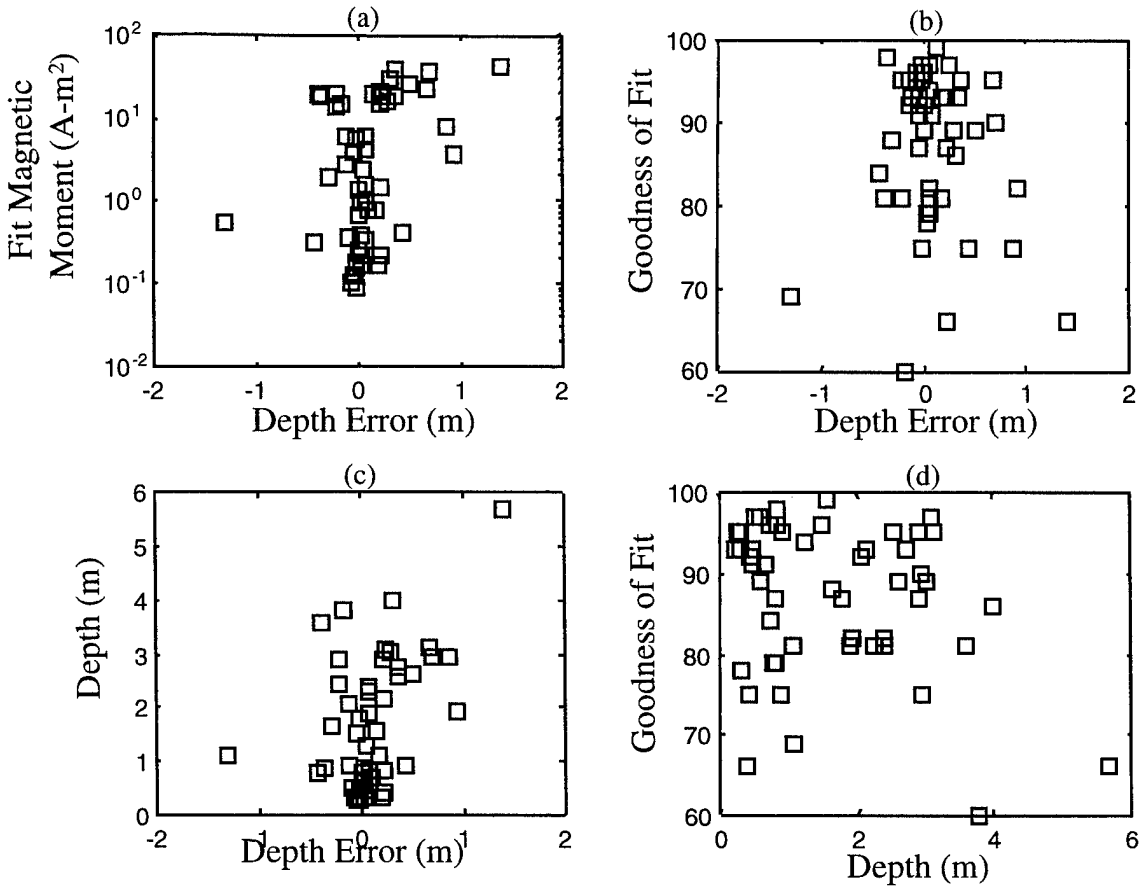

Figure 4-10. Depth and Depth Error for the Magnetometer. (a) Depth Error versus Fit Magnetic Moment. (b) Depth Error versus GoF. (c) Depth Error versus Depth. (d) Depth versus GoF.

deviation of 0.22 m. The average relative depth error is 0.20 m, with a standard deviation of 0.18 m. There were 11 targets with relative depth errors greater than 0.25: one 500-lb bomb, two 250-lb bombs, one 155-mm shell, three 105-mm shells, two 60-mm mortars, and two 8-in. shells.

The magnitude of the magnetic moment shows some correlation with the depth error [Figure 4-11(a)]: we found the correlation coefficient to be 0.76. The 8-in. shell that is responsible for the 4-m depth error also has the largest fitted dipole moment. The magnitude of the magnetic moment was not correlated with the relative depth error.

There is no correlation between fit depth and the GoF. There is also virtually no correlation between relative depth error and GoF; of the 11 targets with relative depth error greater than 0.25, five targets had a GoF greater than 80 percent. There was no strong trend between fit depth and relative depth error; therefore, we cannot say deeper objects had larger depth errors.

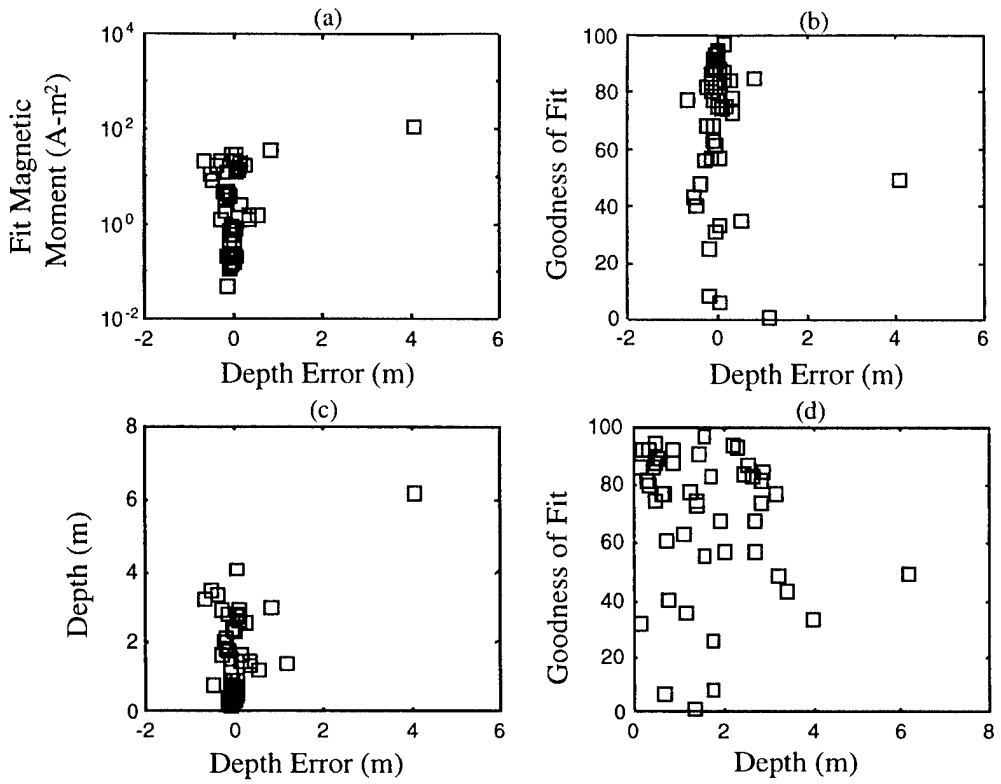

Figure 4-11. Depth and Depth Error for the Magnetic Gradiometer. (a) Depth Error versus Fit Magnetic Moment. (b) Depth Error versus GoF. (c) Depth Error versus Depth. (d) Depth versus GoF.

4.2.2.3 EMI

The average fit depth error is –0.19 (an underestimation of depth) with a standard deviation of 0.52 m. Table 4-6 lists the eight baseline items having relative depth errors 1.00 or larger.

Table 4-6. Ordnance with Relative Depth Error Greater than 1.00

Description	Rel. Depth Error	Actual Depth (m)	Radial Error (m)	GoF
60 mm	–45.00	0.46	0.26	0.33
105 mm	–29.5	0.61	0.08	0.72
81 mm	–7.71	0.61	0.12	0.46
105 mm	–5.57	0.46	0.10	0.90
60 mm	–2.07	0.46	0.22	0.71
81 mm	–1.24	0.76	0.14	0.53
500 lb	–1.11	1.92	0.39	0.90
50 lb	–1.00	3.96	0.65	0.07

The fit depth of all the baseline items in the above table is less than the actual target depth. In addition, six of the eight targets were emplaced between 0.46 m and 0.61 m.

The correlation between EMI nonferrous size and depth error is low (correlation coefficient = 0.57) [see Figure 4-12(a)], suggesting that size appears to have a weak effect on the depth error.

With a linear correlation coefficient of –0.56, the correlation of GoF with depth is also quite weak [see Figure 4-12(b)]. Of the 52 baseline items detected by the EMI sensor, 13 targets have a GoF less than 50 percent, and 6 have a GoF less than 30 percent. It is therefore not reasonable to employ GoF as the sole selection parameter.

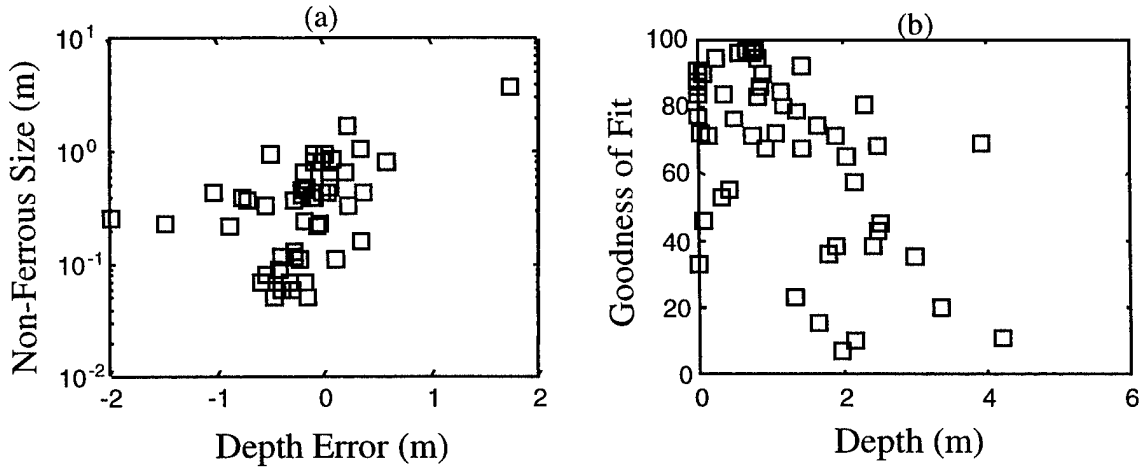

Figure 4-12. Depth and Depth Error for the EMI. (a) Depth Error versus Nonferrous Size. (b) Depth versus GoF.

4.3 DETECTIONS AND FALSE ALARMS COMMON TO MAGNETOMETER AND EMI

We analyze the declarations common to the magnetometer and the EMI systems to understand the general trends associated with detection by multiple systems. A common detection is declared for all ordnance matched to a declaration of both sensors in the pair. A common false alarm is declared for any false alarms within 1.0 m of each other.

4.3.1 Common Detections

All declarations within a 1.0-m R_{crit} of a baseline ordnance item are considered to determine the common detections for the ME pair. Thus, the distance between

declarations can be as great as 2.0 m. The different fit parameters are considered to establish trends that might be exploitable for combining or fusing the two data sets.

4.3.1.1 Detection Location Offset

Forty-seven baseline items are common detections for the ME sensor pair. The mean radial distance between detections is 0.29 m, with a standard deviation of 0.21 m. Twenty-four common declarations had a location offset of less than 0.25 m [see Figure 4-13(a)], and only 7 common detections were separated by greater than 0.5 m. None of the common detection were separated by more than 1.05 m. Figure 4-13(c) shows the location error for the magnetometer versus that of the EMI system. It is evident from the figure that the location errors are highly clustered within an area of radius 0.5 m surrounding the baseline item. There is also a suggestion that large location errors for the EMI system tend to be correlated with large location errors for the magnetometer. But the corollary is not true. There are no statistically significant easting or northing location offsets [see Figure 4-13(b)]. Both the mean and the median are within the 0.05-m location error estimate for the RTK-DGPS.

The overall performance suggests that the location errors exhibited by the sensors are small and tend to be similar. The location error appears to be caused by survey-to-survey location inaccuracies and noise and not by a statistically significant intrinsic property of the ordnance, the *MTADS* system, or the MTR.

4.3.1.2 Detection Depth Offset

The depth offset is the difference between the fitted depth of each detected baseline item (on the x-y plane) for the two sensors, that is, the target depth estimated from the EMI data subtracted from that estimated from the magnetometer data. The depth offset can be positive or negative. The trend of the sign indicates whether one sensor consistently estimates the depth of the baseline item to be greater than the fitted depth from the other sensor.

In the ME sensor set, 34 of 48 baseline items have a depth offset within 0.5 m of one another, and 15 of these are within 0.25 m. There are seven detections with depth offsets between 1.0 and 2.0 m [see Figure 4-14(a)]; this is due to the relatively poor depth predictions from the EMI sensor data (and considering the excellent location accuracy, probably due to an ineffective model for calculating depth). The general trend is that the EMI analysis produces a depth that is less than that estimated from the magnetometer

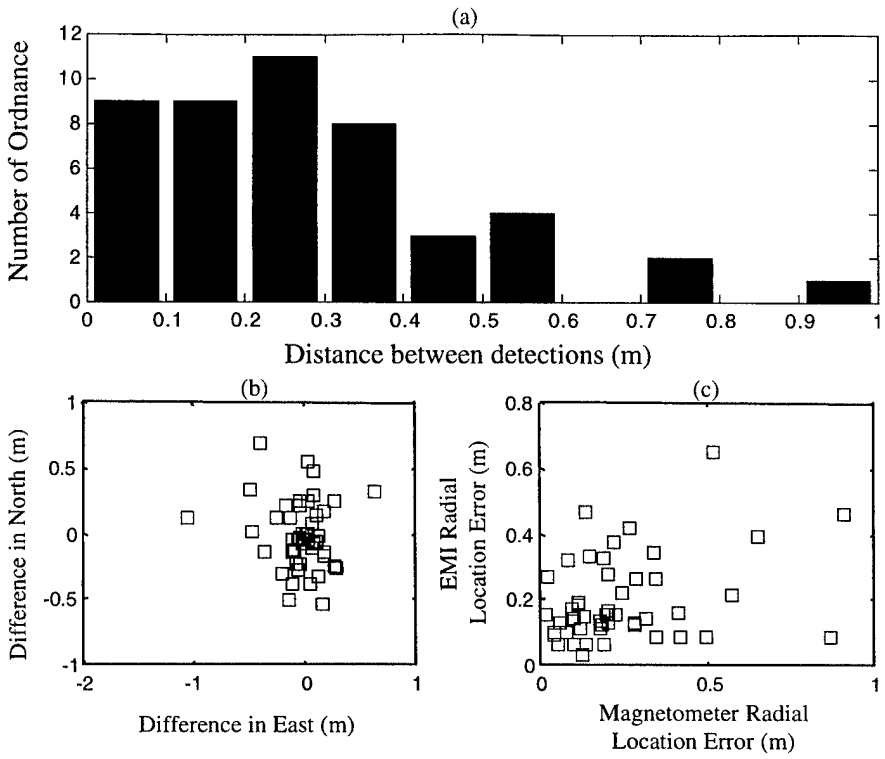

Figure 4-13. Fitted Location Comparison for EMI and Magnetometer. (a) Distribution of Distance Between EMI and Magnetometer Location. (b) Difference in East versus North. (c) Radial Location Error for Magnetometer versus EMI.

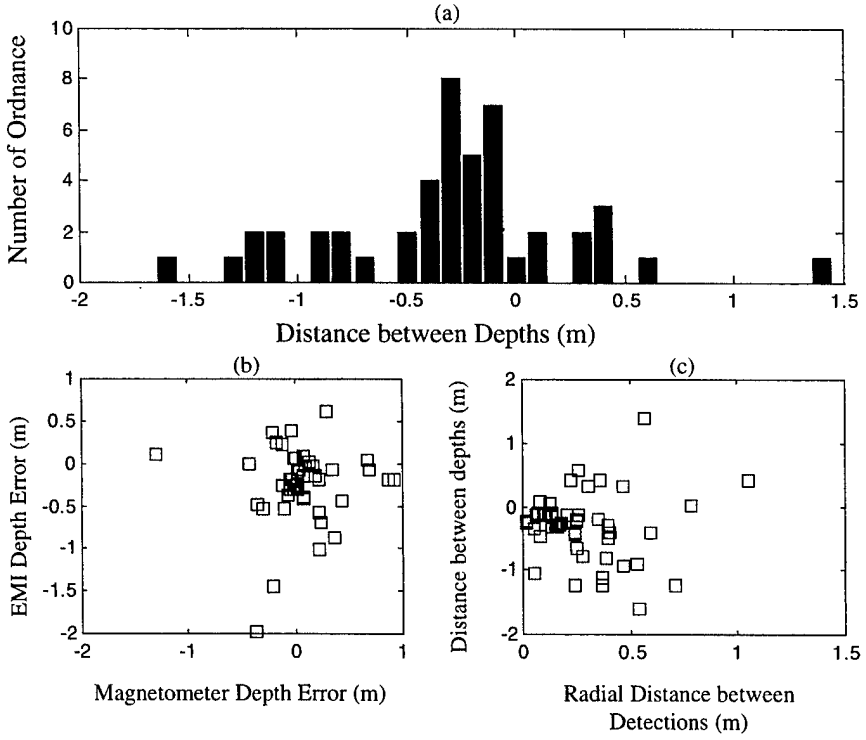

Figure 4-14. Fitted Depth Comparison for EMI and Magnetometer. (a) Distribution of Depth for EMI and Magnetometer. (b) Depth Error for Magnetometer versus EMI. (c) Radial Distance versus Depth Distance.

data. For the 10 ordnance items where the magnetometer depth estimation is less than that of the EMI, only 3 common detections are within 25 cm. The mean depth offset for the pair is –0.31 m (the negative value results from larger depth for the estimates using the magnetometer data) with a standard deviation of 0.46 m.

Figure 4-14(b) shows the depth error for the EMI sensor data relative to magnetometer sensor data. The EMI mean depth error for commonly detected targets is –0.25 m with a standard deviation of 0.44 cm, while the magnetometer has a mean depth error of 0.06 m with a standard deviation of 0.35 m. There is no apparent trend between large depth error in one sensor and large depth error in the other.

Figure 4-14(c) shows the radial distance between the two detections and the depth distance between detections. There is no apparent correlation between large differences in depth and larger radial differences.

4.3.1.3 Detection GoF Comparison

Common detections for both the magnetometer and EMI exhibit weakly correlated GoFs [see Figure 4-15(a)]. Only 11 common detections have both fits ≥ 90 percent (this is the entire set of EMI fits at that level), while 25 common detections have at least one GoF parameter ≥ 90 percent. The conclusion from the general trends is that the sources of poor GoFs are dependent on the type of sensor. There appears to be little additional information available to strengthen the detection/discrimination process by comparison of GoFs.

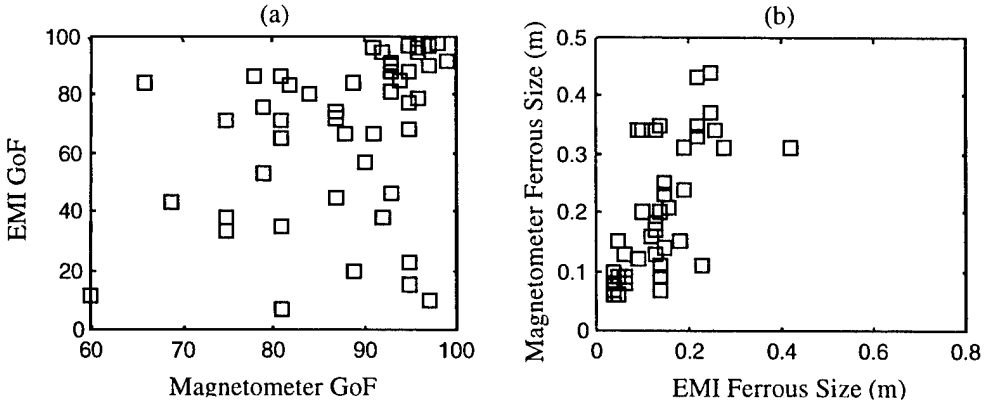

Figure 4-15. Comparison of Fitted Parameters for Magnetometer and EMI. (a) Magnetometer GoF versus EMI GoF. (b) Ferrous Size for EMI versus Magnetometer Ferrous Size.

4.3.1.4 Detection Size Comparison

The ferrous sizes of the magnetometer and EMI combination are correlated (correlation coefficient = 0.67) [see Figure 4-15(b)]. The fitted ferrous size of all but seven magnetometer detections is larger than the corresponding fitted ferrous size for the EMI sensor.

4.3.1.5 Targets Detected by Either Magnetometer or EMI

Table 4-7 describes ordnance items detected by one sensor only. The magnetometer tends to miss shallow emplaced targets (typically small) or deeper targets at or near maximum penetration, while the EMI tended to miss ordnance emplaced at greater depths (these can be large).

Table 4-7. Targets Detected by Only One Sensor

Ordnance	Depth (m)	Missed By
8 in.	2.32	EMI
60 mm	0.38	MAG
60 mm	0.85	MAG
105 mm	0.30	MAG
250 lb	2.10	EMI
250 lb	2.16	MAG
250 lb	2.53	MAG
500 lb	3.66	EMI
500 lb	4.27	EMI

4.3.2 False Alarms Common to the ME Pair

To determine whether there are trends in false-alarm space, we analyze the false alarms common to the ME sensor pair. In this case, determining common false alarms is nontrivial because contrary to the common detection sets, the source and location of the false alarm is unknown. Thus, we use the following process to establish the common false alarms. The full declaration set for each sensor is parsed into two subsets: declarations that match baseline items and declarations that are false alarms. The two false-alarm sets are then compared by location only (in the x-y plane). A false alarm from one set within 1.0 m (the critical false-alarm radius) of a false alarm from another set is classified as a common false alarm for that sensor pair. It is possible to have more than one false alarm from one sensor set within the designated critical false-alarm radius of the second set, but only the nearest neighbor pair is considered in this analysis. We choose the 1.0-m

critical false-alarm radius because of the overwhelming trend to common detection of the baseline items of less than 0.5-m location offset; 1.0 m is more than three standard deviations from the mean separation for a detection pair.

Using this set of common false alarms, we examine the sensor pair for trends in location offset, depth offset, GoF, and size. The trends in the data show some degree of correlation between the fitted parameters, which confirms our hypothesis that the vast majority of false alarms are the result of compact, near-surface anomalies that act as clutter for the sensor.

4.3.2.1 False-Alarms Location Offset

From the full set of 146 EMI and 228 magnetometer false alarms, there are 47, 57, and 59 common false alarms for critical false-alarm radii of 0.5, 0.75, 1.0 m, respectively. Figure 4-16(a) shows the distribution of distance between the false alarm locations for the two sensors. The distribution has a median at about 0.34 m. There is the potential that false alarms that are not really common could be identified by other fit parameters, such as depth. Unluckily, since most clutter is within the first half meter of the ground (see Figure 4-6), false alarms from two different sources are likely to have similar depths.

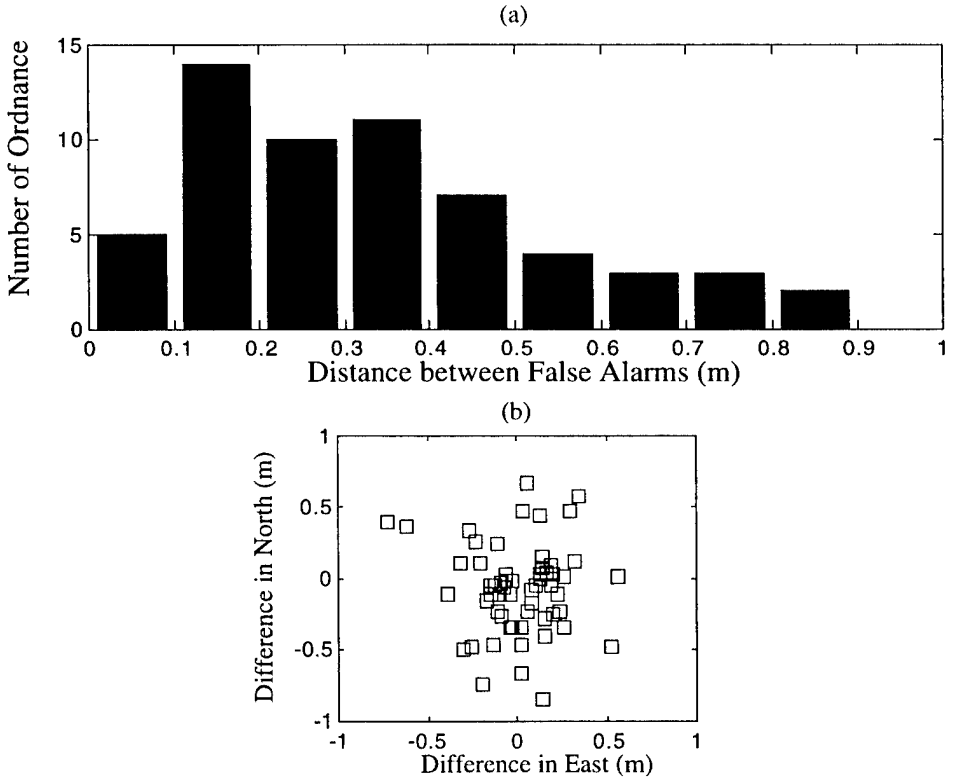

Figure 4-16. Fitted Location Comparison for EMI and Magnetometer Common False Alarms. (a) Distribution of Distance Between EMI and Magnetometer Location. (b) Difference in East versus North.

Figure 4-16(b) shows the location offset for the sensor pair in the east versus north directions. As with the ordnance, the mean and median offsets in each direction are approximately equal to the 5-cm location error expected from the RTK-DGPS. In addition, both standard deviations are approximately 30 cm.

4.3.2.2 False-Alarm Depth Offset

For the ME sensor combination, the distribution of depth offsets reveals that 47 of the 59 common false alarms have a depth offset between ±0.25 m. Figure 4-17 shows the distribution of the depth offset. The EMI sensor appears to consistently underestimate the depth of the target; 47 out of 59 (80 percent) common false alarms have the EMI detection depth less than the magnetic detection depth. This is almost identical to the relative depth for the commonly detected ordnance (79 percent). Thus, there is no apparent difference between the depth offset for ordnance and clutter.

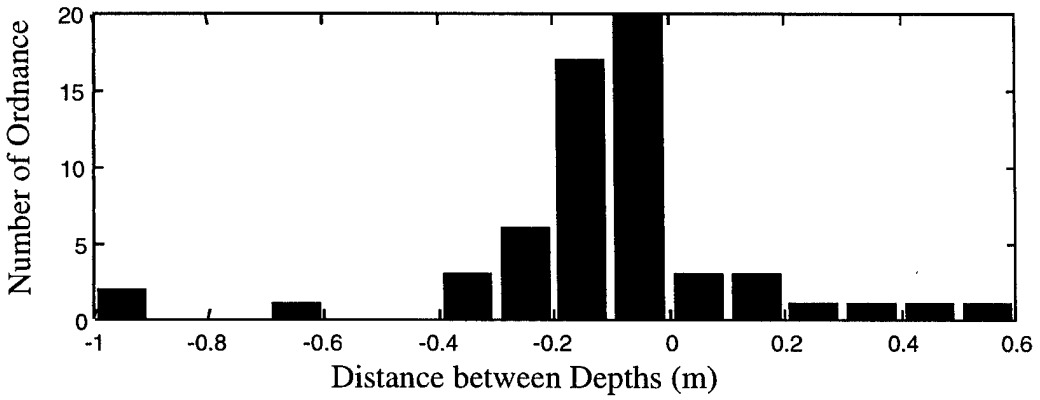

Figure 4-17. Distribution of Depth Offset for EMI and Magnetometer Common False Alarms

Table 4-8 lists the 12 ME pairs having a depth offset greater than ±0.25 m. Except for four items, the fit depths of each sensor are within 0.5 m of the surface. Though seven of the fit parameters for the magnetometer false alarms are greater than 90, the respective fit parameters for the EMI are low. The last common false alarm listed in Table 4-8 with a –3.17 m depth offset is probably not a common false alarm but rather the detection of two closely spaced items with very different depths.

4.3.2.3 False-Alarm GoF Comparison

The correlation between GoFs of the ME pairs is very low, perhaps due to poor fits from the EMI data. Only two common false alarms had a GoF greater than 90 percent for the EMI, and both of these had GoFs greater than 90 percent for the magnetometer.

Table 4-8. GoF for Large Depth Offset

Mag. Fit Depth (m)	Mag. GoF	EMI Fit Depth (m)	EMI GoF	Depth Offset (m)
0.10	96	0.62	51	0.52
0.19	93	0.65	53	0.46
0.11	98	0.45	72	0.34
1.34	89	1.07	83	–0.20
0.44	61	0.16	76	–0.27
0.42	81	0.14	43	–0.28
0.37	93	0.00	43	–0.37
0.37	93	0.00	55	–0.37
0.37	97	0.00	16	–0.37
4.12	96	3.52	16	–0.60
0.96	87	0.06	72	–0.90
3.17	79	0.00	69	–3.17

In contrast to the results for the common ordnance detected, many declarations with a GoF over 0.9 for the magnetometer have corresponding EMI GoF of less than 0.50 (17 out of 43). These results suggest that the EMI fitting algorithm has a harder time fitting clutter objects, which are likely to be asymmetric. At the same time, most objects exhibit a strong magnetic dipole moment that fits well to the simple model for magnetic signatures. Thus, a difference in GoFs for the two systems might provide potential for discrimination using the "fused" data set. It should be noted that the reciprocal pattern is not true. Good GoF for the EMI always corresponds to good GoF for the magnetometer.

4.3.2.4 NRL Ferrous Size Comparison

The average fit ferrous size for the magnetometer is 8.7 cm, compared to 3.8 cm for the EMI. Figure 4-18 shows a scatter plot of EMI ferrous size versus magnetometer ferrous size. At 0.80, the correlation is quite high, but the EMI consistently underestimates size relative to the magnetometer. For 56 out of the 59 common false alarms, the ferrous sizes determined from the magnetometer data were greater than those determined from the EMI.

4.4 COMPARISON OF DETECTION PERFORMANCE FOR NRL AND IDA DATA

In this section we present a detection performance comparison for the analysis product generated by IDA and NRL using the same raw sensor data. This comparison

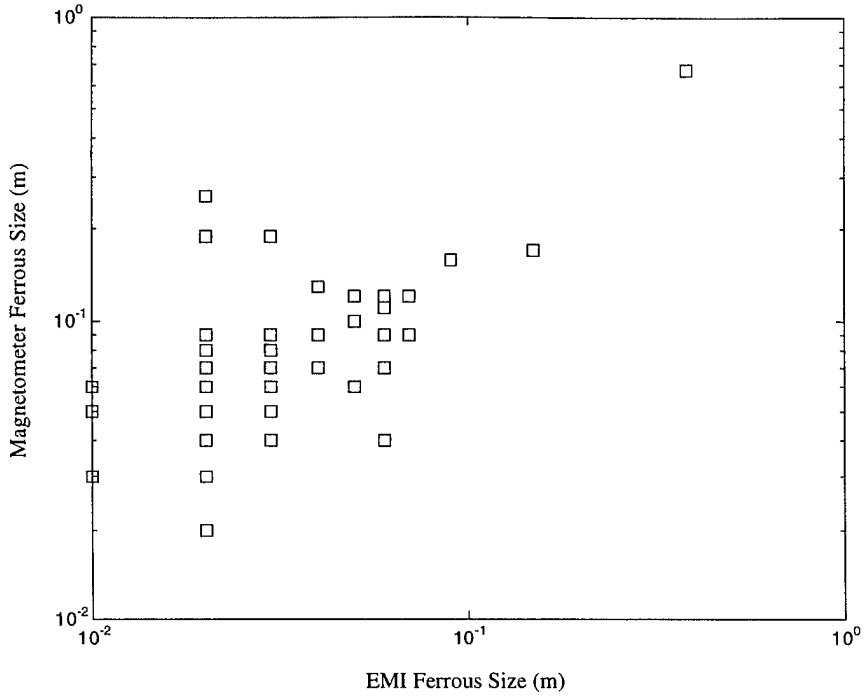

Figure 4-18. Comparison of Fitted Ferrous Size for Magnetometer versus EMI Ferrous Size

demonstrates the variability between users of the same analysis software package (the *MTADS*-DAS). Although both analysts have a strong background in the phenomenology of UXO detection, the NRL analyst has significantly more experience over many test sites, in particular, the Twentynine Palms MTR. The result is a slightly better, though not statistically significant, overall performance of NRL with the magnetometer and EMI data and much better performance with the magnetic gradiometer data.

4.4.1 Detection and False-Alarm Performance

Figures 4-19(a)–(c) show the relative performance of the IDA and NRL target picking using the ROC formalism. Table 4-9 presents the results for both IDA and NRL for an R_{crit} of 1 m.

NRL consistently outperforms IDA in the identification of ordnance. The largest difference is the magnetometer. Here, even with the implementation of the magnetic moment direction discrimination, the NRL detection rate is superior. On the other hand, for both the magnetic gradiometer and EMI system, the difference in performance is not as great. If fact, given the statistical nature of the detection process, the differences are not significant.

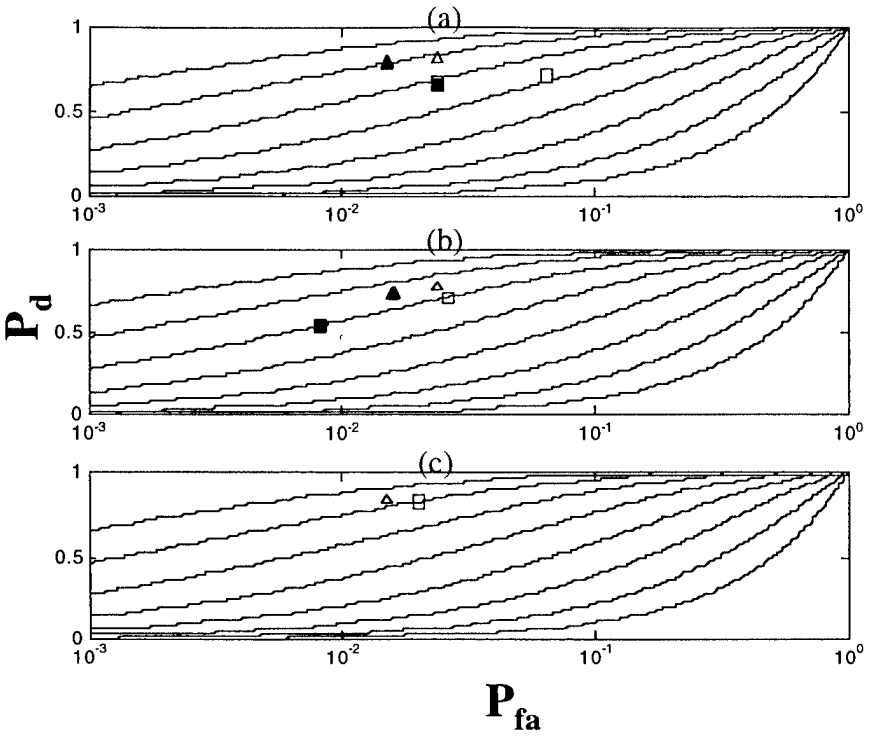

Figure 4-19. P_d versus P_{fa} for NRL Processing (Triangles) and IDA Processing (Squares). The open marks are for the full declaration set. The solid symbols result from implementing the appropriate discrimination algorithms for each data set (as described in this chapter and Chapter 3) to a confidence level of 2. (a) Magnetometer. (b) Magnetic Gradiometer. (c) EMI.

Table 4-9. Detection and False-Alarm Performance of *MTADS* from IDA and NRL Analysis with a 1-m R_{crit}

	IDA			NRL		
Sensor	P_d	*FAR* (m^{-2})	P_{fa}	P_d	*FAR* (m^{-2})	P_{fa}
Magnetometer (Full Data Set)	0.726	2.0×10^{-2}	6.5×10^{-2}	0.823	7.4×10^{-3}	2.4×10^{-2}
Magnetometer (Confidence Level 2)	0.677	7.4×10^{-3}	2.4×10^{-2}	0.790	4.9×10^{-3}	1.5×10^{-2}
Magnetic Gradiometer (Full Data Set)	0.710	8.3×10^{-3}	2.6×10^{-2}	0.774	7.7×10^{-3}	2.4×10^{-2}
Magnetic Gradiometer (Confidence Level 2)	0.532	2.6×10^{-3}	8.1×10^{-3}	0.726	4.9×10^{-3}	1.6×10^{-2}
EMI	0.823	9.5×10^{-3}	2.0×10^{-2}	0.839	4.8×10^{-3}	1.5×10^{-2}

4.4.2 Comparison of Missed Targets

Ordnance items detected by IDA but not by NRL (and vice versa) are refit using the *MTADS*-DAS software to determine their general characteristics. The results follow.

4.4.2.1 Magnetometer

A total of 44 ordnance items were detected by both IDA and NRL. Table 4-10 lists targets missed by one of the groups using the magnetometer data. IDA missed those ordnance items with a small dipole signature or in a cluttered environment. In addition, two large ordnance items, a 500-lb bomb and a 750-lb bomb, were not detected.

Table 4-10. Ordnance Found by Only One Group Using the Magnetometer Data

Ordnance	Depth (m)	Missed By	Refit Comment
8 in.	2.32	IDA	Weak Anomaly
8 in.	1.83	IDA	Weak Anomaly
8 in.	1.95	IDA	Weak Anomaly
60 mm	0.46	IDA	Fit outside 1-m R_{crit}
105 mm	0.55	IDA	Not surveyed completely
250 lb	2.53	NRL	Weak Anomaly
500 lb	4.27	IDA	Fit outside 1-m R_{crit}
750 lb	3.96	IDA	Weak Anomaly

4.4.2.2 Gradiometer

In the case of the gradiometer, IDA correctly identified three targets, though the location accuracy of the fitting algorithm was outside the 1-m halo. In addition, one 155-mm item was not detected because part of its dipole signature extended into an unsurveyed area (see Table 4-11).

4.4.2.3 EMI

As expected, the EMI system had difficulty fitting those ordnance items emplaced at greater depths. Table 4-12 lists the ordnance detected by only one group. All three ordnance items were deeper than 2 m.

Table 4-11. Ordnance Found by Only One Group Using the Magnetic Gradiometer Data

Ordnance	Depth (m)	Missed By	Refit Comment
8 in.	1.83	IDA	Weak Anomaly
8 in.	2.32	NRL	Faint Signature
60 mm	0.30	IDA	Faint signature
155 mm	1.04	NRL	Weak Anomaly
155 mm	1.19	IDA	Near unsurveyed area
250 lb	2.38	NRL	Faint signature
500 lb	3.66	IDA	Refit outside 1-m halo
500 lb	3.96	IDA	Refit outside 1-m halo
500 lb	2.23	IDA	Refit outside 1-m halo
750 lb	3.96	IDA	Faint signature

Table 4-12. Ordnance Found by Only One Group Using the EMI Data

Ordnance	Depth (m)	Missed By
8 in.	2.32	IDA
8 in.	2.74	NRL
250 lb	3.11	IDA

4.5 FALSE ALARMS UNIQUE TO EACH SENSOR

Exploiting characteristics of the false alarms unique to each sensor is a potential avenue for improved overall detection performance. For the EMI and magnetometer data, we parse the full set of false alarms to provide a list of false alarms not within the 1-m false-alarm critical radius (see Section 4.3.2). Comparing the fitted parameters for the unique and common false alarms, we conclude that there are no compelling trends to differentiate false alarms identified by both the magnetometer and the EMI from those that are only found by a single detector.

Figures 4-20(a) and (b) show the depth of the false alarms for the magnetometer and EMI system, respectively. Here, the number of false alarms in each depth bin is normalized to the total number of false alarms for the sensor (either unique or common). Table 4-13 lists the mean and standard deviation for the depths. For the magnetometer, the mean common false-alarm depth is slightly less than that of the unique false alarms. That difference is a result of the insensitivity of the EMI system to deeper objects.

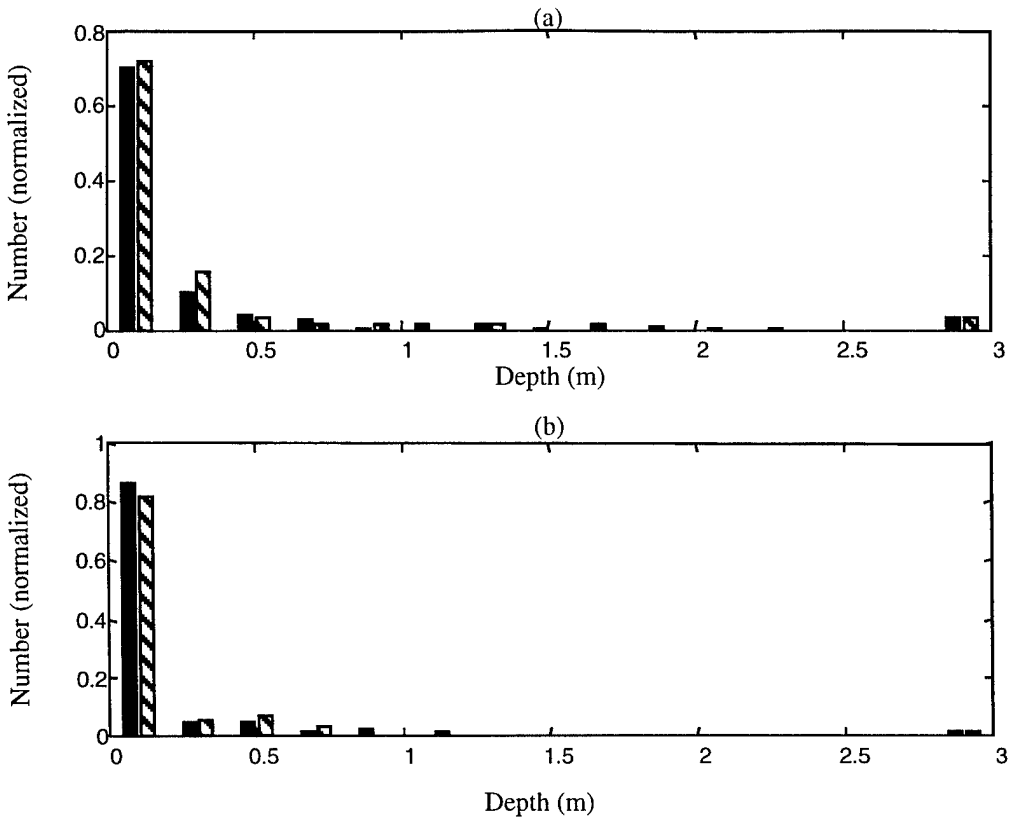

Figure 4-20. A Comparison of the Distribution of Depths for Unique (Solid) and Common (Hashed) False Alarms. (a) Magnetometer. (b) EMI.

Table 4-13. Comparison of Fitted Parameters for Common and Unique False Alarms

	Mean Depth (m)	STD+ Depth (m)	Mean Size (cm)	STD Size (cm)	Mean Rel. Inclination (deg)	STD Inclination (deg)
Unique Magnetometer	0.43	0.96	8.1	9.6	31.8	42.2
Common Magnetometer	0.31	0.69	8.6	9.0	47.8	34.5
Unique EMI	0.12	0.54	3.3	4.7	—	—
Common EMI	0.16	0.49	3.8	5.1	—	—

+ STD is standard deviation.

Figures 4-21(a) and (b) show the estimated ferrous size of the source of the signature measured by the sensors. For both sensors, the average size of the common false alarms is slightly larger than that of the unique false alarms, but given the variance of the size for these sets, the difference is statistically insignificant. As is the case with ordnance, the size estimated from the EMI data is smaller than that estimated from the magnetometer data.

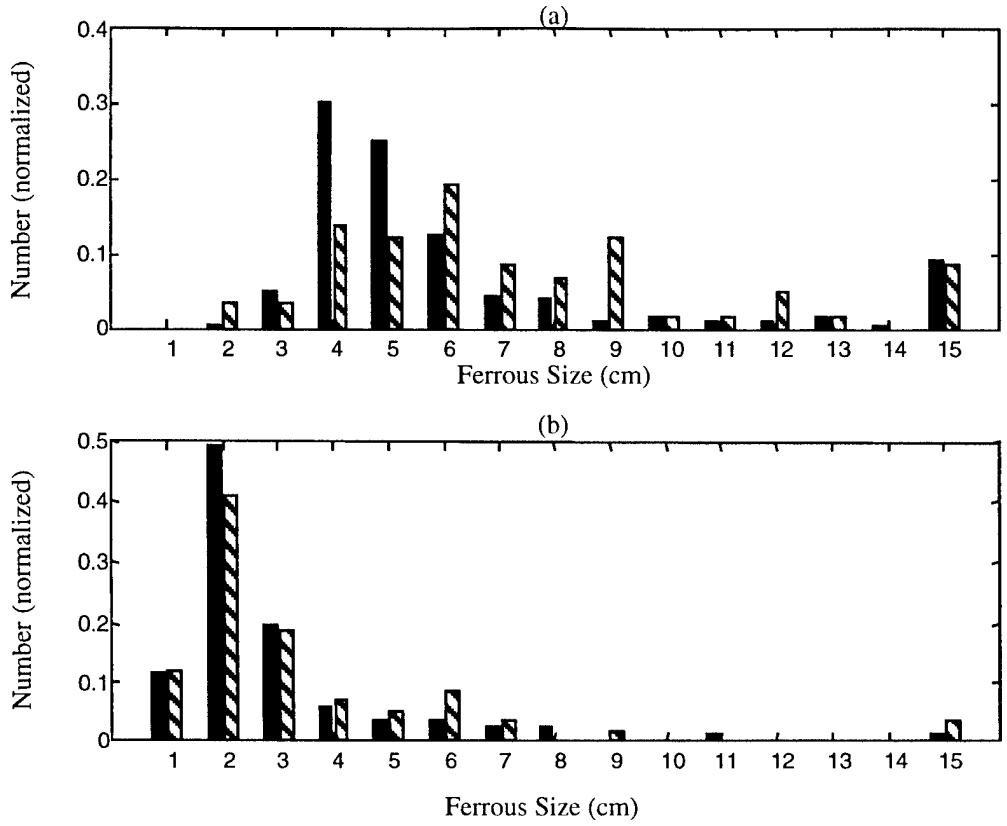

Figure 4-21. A Comparison of the Distribution of Sizes for Unique (Solid) and Common (Hashed) False Alarms. (a) Magnetometer. (b) EMI.

The relative inclination, which is used in Chapter 3 to sort ordnance from clutter, shows a slight trend towards higher values for common false alarms relative to unique false alarms for the magnetometer. Figure 4-22 shows the relative inclination for the two classes of false alarms. Table 4-13 lists the mean and the standard deviation of the relative inclination. It should be noted that 40 percent of the false alarms unique to the magnetometer have a relative inclination less than the 30-deg cutoff used in the analysis presented in Section 4.1.1. This compares to only 18 percent for the common false alarms. It should also be noted that none of the unique magnetometer detections had a relative inclination below 39 deg. The difference in the distribution of the relative inclination for the two classes of false alarms suggests that this feature might be employed in conjunction with simple and/or logical data features.

4.6 SIMPLE AND/OR SENSOR FUSION

The simplest method for data fusion is to use a simple logic gate (AND or OR). This decision-based fusion can lead to higher detection rates (the OR process) or lower

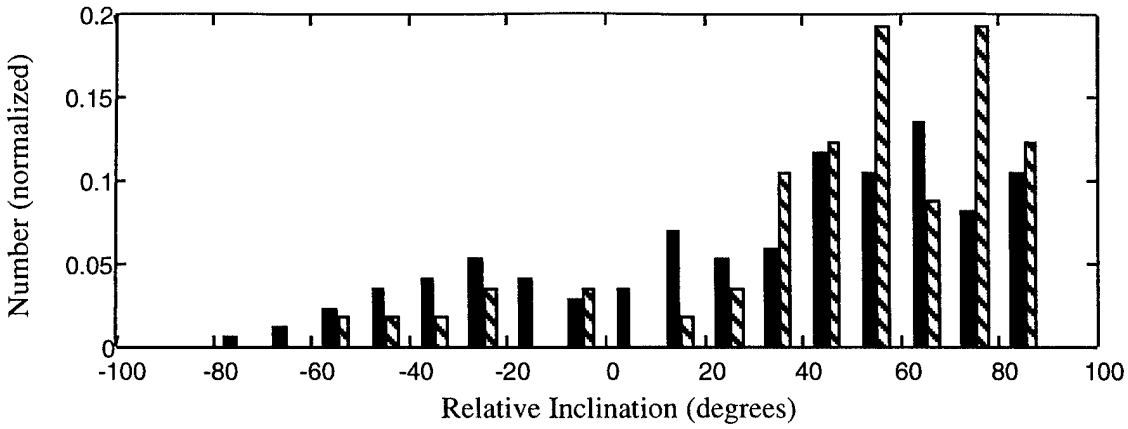

Figure 4-22. A Comparison of the Relative Inclination for the Magnetometer for Unique (Solid) and Common (Hashed) False Alarms

false-alarm rates (the AND process). It is valuable to assess the overall performance of the *MTADS* using the simple decision-based data fusion. Figure 4-23 shows the probability of detection and the probability of false alarm for the individual sensors and the fused data. Table 4-14 lists the detection performance for the sensors and the fusion methods. Neither the AND nor the OR fusion is better (within the statistical error) than the best sensor, the EMI.

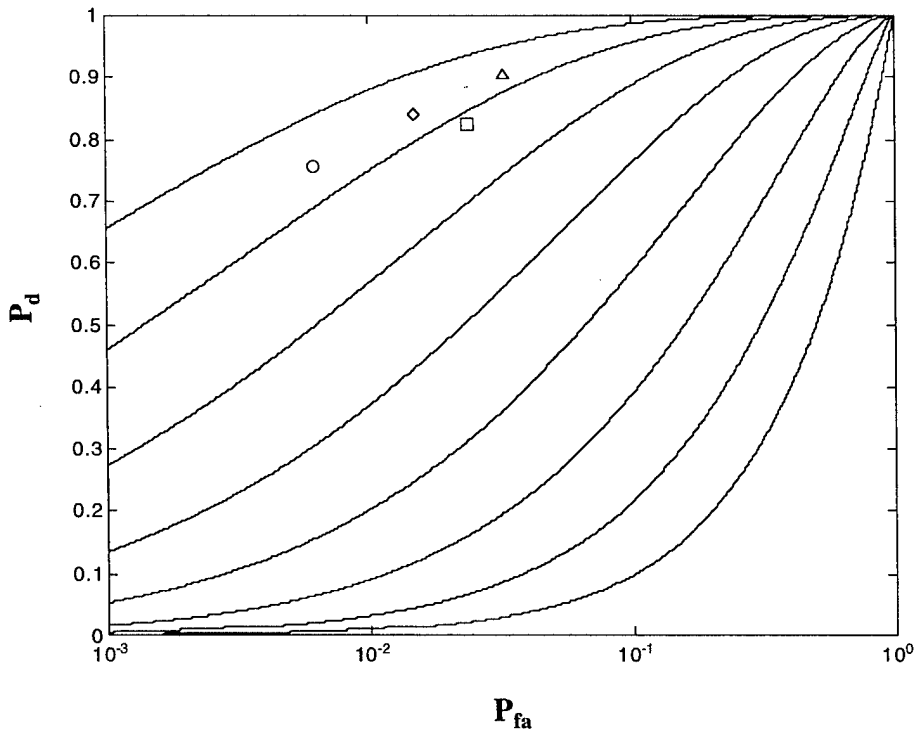

Figure 4-23. P_d versus P_{fa} for the Magnetometer (Square), EMI (Diamond), Sensor AND (Circle), and Sensor OR (Triangle)

Table 4-14. Detection Performance for the Sensors and Fusion Methods

	P_d	P_{fa}	d
Magnetometer	0.823	0.024	2.90
EMI	0.839	0.015	3.16
Sensor AND	0.758	0.006	3.21
Sensor OR	0.903	0.033	3.14

To improve performance, feature-level fusion must employed. That is, the two sets of features from sensors should have a measurable degree of orthogonality. As shown in Section 4.3.1, the magnetometer and the EMI have a slightly different list of ordnance detected on the MTR. The EMI has a very robust detection rate for small, shallow ordnance (and the magnetometer does not); the magnetometer has better performance for large, deep ordnance. Still, this type of orthogonality is not enough, since some features are needed for false-alarm mitigation. In addition, highly cluttered environments will lead to undetected ordnance, even within the set of ordnance best detected by the sensor. Table 4-15 lists the ordnance missed by both the magnetometer and the EMI at the MTR. All these ordnance items were deeply emplaced bombs obscured in some manner by the cluttered environment.

Table 4-15. Ordnance Missed by Magnetometer and EMI

Ordnance Type	Depth (m)
2,000-lb Bomb	4.88
1,000-lb Bomb	5.09
500-lb Bomb	4.42
500-lb Bomb	3.87
250-lb Bomb	3.08

REFRENCES

Altshuler, T. W., A. M. Andrews, R. E. Dugan, V. George, M. P. Mulqueen, and D. A. Sparrow, *Demonstrator Performance at the Unexploded Ordnance Advanced Technology Demonstration at Jefferson Proving Ground (Phase I) and Implications for UXO Clearance,* IDA Paper P-3114, October 1995.

Altshuler, T. W., "Shape and Orientation Effects on Magnetic Signature Prediction for Unexploded Ordnance," *UXO Forum 1996,* p. 282, 1996.

Altshuler, T.W., A. M. Andrews, and D. A. Sparrow, "Mine and UXO Detection: Measures of Performance and Their Implications in Real-World Scenarios," *Proceedings of SPIE,* Volume 3079, p. 284, April 1997.

Andrews, A. M., V. George, T. W. Altshuler, and M. P. Mulqueen, *Results of the Countermine Task Force Mine Detection Technology Demonstrations at Fort A.P. Hill, Virginia, March 18–22, 1996,* IDA Paper P-3192, July 1996.

Van Trees, H. L., *Detection, Estimation and Modulation Theory,* Part 1, 1968.

McDonald, J. R., H. H Nelson, R. A. Jeffries, and R. Robertson, "Results of the *MTADS* Technology Demonstration #2," NRL/PU/6110–97–349, 1997.

Nelson, H. H., T. W. Altshuler, E. M. Rosen, J. R. McDonald, B. Barrow, and N. Khadr, "Magnetic Modeling of UXO and UXO-like Targets and Comparison with Signature Measurements by MTADS," *UXO Forum 1998,* 1998.

Nelson, H. H., J. R. McDonald, and R. Robertson, *"MTADS* TECHEVAL Demonstration, October 1996," NRL/PU/6110–97–348, 1997.

Simonson, K. H., "Statistical Considerations in Designing Tests of Mine Detection Systems, I—Measures Related to Probability of Detection," Sandia National Laboratory, 1998, forthcoming.

GLOSSARY

DAQ	data acquisition system
DAS	data analysis system
EMI	electromagnetic induction
ESTCP	Environmental Security Technology Certification Program
FAR	false-alarm rate
GoF	goodness of fit
IDA	Institute for Defense Analyses
MCAGCC	Marine Corps Air Ground Combat Center
ME	magnetometer and EMI pair of sensors
MTADS	Multi-sensor Towed Array Detection System
MTR	Magnetic Test Range
NRL	Naval Research Laboratory
ROC	Receiver Operating Characteristic
RTK-DGPS	real-time kinematic differential global position system
UXO	unexploded ordnance

APPENDIX A

MODELED MAGNETIC SIGNATURES OF EMPLACED ORDNANCE

APPENDIX A

MODELED MAGNETIC SIGNATURES OF EMPLACED ORDNANCE

The magnetic dipole moment of each ordnance item emplaced and used as part of the baseline (see Chapter 3) at the Magnetic Test Range has been modeled assuming a purely induced magnetic signature. Table A-1 presents the modeled magnetic dipole moments for 62 ordnance items emplaced, as well as the modeled maximum magnetic signature. For this calculation the ordnance is assumed to be solid.

Table A-1. Modeled Magnetic Moments for Ordnance at the MTR

Ordnance ID	Ordnance Type	Modeled Moment Magnitude ($A\text{-}m^2$)	Modeled Inclination (deg)	Modeled Declination (deg)	Maximum Magnetic Signature (γ)
MK84	2,000 lb	109.5	10.9	0.0	69.0
MK83	1,000 lb	30.7	9.6	0.0	16.7
MK117	750 lb	32.3	18.3	–8.1	42.5
A1	500 lb	29.1	22.4	–22.7	33.5
A2	500 lb	26.5	76.0	180.0	47.7
A3	500 lb	37.8	86.1	0.0	378.6
A4	500 lb	37.7	47.8	40.8	79.0
A5	500 lb	22.2	11.7	0.0	32.2
A6	500 lb	42.1	46.8	0.0	81.7
A7	500 lb	27.0	51.5	81.1	409.5
A8	500 lb	26.5	76.0	180.0	1,526.2
A9	500 lb	27.0	51.5	81.1	275.1
A10	500 lb	26.5	76.0	180.0	249.4
B1	250 lb	17.2	66.0	0.0	78.6
B2	250 lb	17.2	66.0	0.0	76.5
B3	250 lb	6.57	19.3	36.8	36.1
B4	250 lb	15.0	48.4	39.9	93.6
B5	250 lb	15.1	85.2	0.0	92.9
B6	250 lb	15.1	85.2	0.0	108.9
B7	250 lb	15.1	34.8	0.0	400.1
B8	250 lb	6.57	19.3	–36.8	31.3
B9	250 lb	6.57	19.3	36.8	46.9
B10	250 lb	8.94	14.1	0.0	62.4
C1	8 in.	7.52	65.7	0.0	74.5
C2	8 in.	4.70	81.0	180.0	32.3
C3	8 in.	2.34	31.8	41.9	22.8
C4	8 in.	6.57	49.3	38.2	66.4
C5	8 in.	3.98	18.1	0.0	43.1
C6	8 in.	2.99	24.4	34.3	36.1
C7	8 in.	2.99	24.4	–34.3	26.5

Ordnance ID	Ordnance Type	Modeled Moment Magnitude ($A\text{-}m^2$)	Modeled Inclination (deg)	Modeled Declination (deg)	Maximum Magnetic Signature (γ)
C8	8 in.	3.98	18.1	0.0	36.4
C9	8 in.	6.60	83.8	0.0	81.3
C10	8 in.	6.60	83.8	0.0	81.3
D2	155 mm	2.23	80.5	180.0	70.1
D3	155 mm	0.653	60.0	0.0	35.3
D4	155 mm	3.13	49.2	–38.5	148.1
D7	155 mm	3.13	49.2	38.5	216.0
D8	155 mm	0.653	60.0	0.0	79.2
D9	155 mm	1.41	23.6	34.7	146.8
D10	155 mm	2.27	54.4	75.7	557.2
E2	105 mm	0.600	81.8	180.0	54.4
E3	105 mm	0.190	60.0	0.0	23.1
E4	105 mm	0.829	49.6	37.8	79.0
E7	105 mm	0.833	83.5	0.0	235.0
E8	105 mm	0.505	19.0	0.0	78.0
E9	105 mm	0.833	83.5	0.0	419.8
E10	105 mm	0.190	60.0	0.0	59.9
F1	81 mm	0.427	65.6	0.0	69.0
F2	81 mm	0.268	82.0	180.0	47.6
F3	81 mm	0.375	83.4	0.0	105.6
F4	81 mm	0.373	49.6	–37.7	87.7
F7	81 mm	0.373	49.6	37.7	155.5
G1	60 mm	0.109	65.1	0.0	50.9
G2	60 mm	0.070	86.3	180.0	35.9
G3	60 mm	0.029	60.0	0.0	18.7
G4	60 mm	0.096	50.9	35.2	176.8
G5	60 mm	0.029	60.0	0.0	27.6
G6	60 mm	0.029	60.0	0.0	27.6
G7	60 mm	0.097	81.3	0.0	69.3
G8	60 mm	0.061	24.6	0.0	39.0
G9	60 mm	0.029	60.0	0.0	27.6
G10	60 mm	0.029	60.0	0.0	73.5

REPORT DOCUMENTATION PAGE

Form Approved
OMB No. 0704-0188

Public Reporting burden for this collection of information is estimated to average 1 hour per response, including the time for reviewing instructions, searching existing data sources, gathering and maintaining the data needed, and completing and reviewing the collection of information. Send comments regarding this burden estimate or any other aspect of this collection of information, including suggestions for reducing this burden, to Washington Headquarters Services, Directorate for Information Operations and Reports, 1215 Jefferson Davis Highway, Suite 1204, Arlington, VA 22202-4302, and to the Office of Management and Budget, Paperwork Reduction Project (0704-0188), Washington, DC 20503.

1. AGENCY USE ONLY *(Leave blank)*	2. REPORT DATE	3. REPORT TYPE AND DATES COVERED
	September 1998	Final—December 1996–July 1998

4. TITLE AND SUBTITLE
Evaluation of the Multi-Sensor Towed Array Detection System (MTADS) Performance at the Marine Corps Air Ground Combat Center (MCAGCC), Twentynine Palms, California

5. FUNDING NUMBERS
DASW01 94 C 0054
T-AM2-1528.1

6. AUTHOR(S)
Thomas W. Altshuler, Marc Mander

7. PERFORMING ORGANIZATION NAME(S) AND ADDRESS(ES)
Institute for Defense Analyses
1801 N. Beauregard St.
Alexandria, VA 22311-1772

8. PERFORMING ORGANIZATION REPORT NUMBER
IDA Document D-2161

9. SPONSORING/MONITORING AGENCY NAME(S) AND ADDRESS(ES)
ESTCP Program Office
901 N. Stuart Street, Suite 303
Arlington, VA 22203

10. SPONSORING/MONITORING AGENCY REPORT NUMBER

11. SUPPLEMENTARY NOTES

12a. DISTRIBUTION/AVAILABILITY STATEMENT
Approved for Public Release: distribution unlimited (June 22, 2000)

12b. DISTRIBUTION CODE

13. ABSTRACT ***(Maximum 180 words)***

In December 1996, on the Magnetic Test Range at the Marine Corps Air Ground Combat Center, Twentynine Palms, California, the Multisensor Towed Array Detection System *(MTADS)* underwent its first semi-blind field test. After completing the data acquisition and determining the location of potential ordnance, the Institute for Defense Analyses performed an assessment to determine overall detection performance and unique characteristics of the *MTADS*. The detection rates for both the magnetometer and the electromagnetic induction system exceeded 80 percent with approximately 30 and 20 false alarms per acre, respectively, for the two detection systems. The magnetic gradiometer exhibited somewhat poorer detection performance than the other two sensor systems. The *MTADS* also demonstrated excellent accuracy when determining the location and depth of the ordnance. All three sensor arrays exhibited better than 40 cm mean location error and less than 20 cm mean depth error. The data collected at Twentynine Palms was also used to test a magnetic clutter discrimination algorithm based on the relative contribution of induced and remanent magnetization. Employing this algorithm resulted in at least 30 percent fewer false alarms, with minimal loss of unexploded ordnance detection capability when using the magnetometer.

14. SUBJECT TERMS
Unexploded Ordnance, UXO, the Multisensor Towed Array Detection System, *MTADS*, magnetometer, magnetic gradiometers, electromagnetic induction, false alarm reduction

15. NUMBER OF PAGES
108

16. PRICE CODE

17. SECURITY CLASSIFICATION OF REPORT	18. SECURITY CLASSIFICATION OF THIS PAGE	19. SECURITY CLASSIFICATION OF ABSTRACT	20. LIMITATION OF ABSTRACT
UNCLASSIFIED	UNCLASSIFIED	UNCLASSIFIED	SAR